COMPENSATION OF MODEL UNCERTAINTIES IN DAMAGE IDENTIFICATION BY MEANS OF THE APPROXIMATION ERROR APPROACH

Gabriel Lucas Sousa da Silva

Dissertação de Mestrado apresentada ao Programa de Pós-graduação em Engenharia Mecânica, COPPE, da Universidade Federal do Rio de Janeiro, como parte dos requisitos necessários à obtenção do título de Mestre em Engenharia Mecânica.

Orientador: Daniel Alves Castello

Rio de Janeiro
Fevereiro de 2018

COMPENSATION OF MODEL UNCERTAINTIES IN DAMAGE IDENTIFICATION BY MEANS OF THE APPROXIMATION ERROR APPROACH

Gabriel Lucas Sousa da Silva

DISSERTAÇÃO SUBMETIDA AO CORPO DOCENTE DO INSTITUTO ALBERTO LUIZ COIMBRA DE PÓS-GRADUAÇÃO E PESQUISA DE ENGENHARIA (COPPE) DA UNIVERSIDADE FEDERAL DO RIO DE JANEIRO COMO PARTE DOS REQUISITOS NECESSÁRIOS PARA A OBTENÇÃO DO GRAU DE MESTRE EM CIÊNCIAS EM ENGENHARIA MECÂNICA.

Examinada por:

Prof. Daniel Alves Castello, D.Sc.

Prof. Fernando Alves Rochinha, D.Sc.

Prof. Franciane Conceição Peters, D.Sc.

RIO DE JANEIRO, RJ – BRASIL
FEVEREIRO DE 2018

Silva, Gabriel Lucas Sousa da

Compensation of model uncertainties in damage identification by means of the approximation error approach/Gabriel Lucas Sousa da Silva. – Rio de Janeiro: UFRJ/COPPE, 2018.

IX, 109 p.: il.; 29, 7cm.

Orientador: Daniel Alves Castello

Dissertação (mestrado) – UFRJ/COPPE/Programa de Engenharia Mecânica, 2018.

Referências Bibliográficas: p. 68 – 75.

1. Approximation Error. 2. Structural Health Monitoring. I. Castello, Daniel Alves. II. Universidade Federal do Rio de Janeiro, COPPE, Programa de Engenharia Mecânica. III. Título.

Resumo da Dissertação apresentada à COPPE/UFRJ como parte dos requisitos necessários para a obtenção do grau de Mestre em Ciências (M.Sc.)

COMPENSAÇÃO DE INCERTEZAS DE MODELAGEM EM ESTIMAÇÃO DE DANO POR ABORDAGEM BAYESIANA

Gabriel Lucas Sousa da Silva

Fevereiro/2018

Orientador: Daniel Alves Castello

Programa: Engenharia Mecânica

Esta dissertação apresenta uma aplicação do *Approximation Error Approach* (AEA), no contexto de *Structural Health Monitoring* (SHM). A abordagem proposta baseia-se na aplicação da Teoria Bayesiana de probabilidade na solução de problemas inversos. Tal abordagem permite corrigir a resposta prevista por um modelo através da compensação por um erro de modelagem associado usando uma formulação matemática que é relativamente simples.

A aplicação de diferentes distribuições *a priori* para os parâmetros considerados nas simulações necessárias para o AEA é investigada. Resultados obtidos utilizando-se AEA e uma abordagem de mínimos quadrados são comparados.

Abstract of Dissertation presented to COPPE/UFRJ as a partial fulfillment of the requirements for the degree of Master of Science (M.Sc.)

COMPENSATION OF MODEL UNCERTAINTIES IN DAMAGE IDENTIFICATION BY MEANS OF THE APPROXIMATION ERROR APPROACH

Gabriel Lucas Sousa da Silva

February/2018

Advisor: Daniel Alves Castello

Department: Mechanical Engineering

This work presents an application of the Approximation Error Approach (AEA) in the context of Structural Health Monitoring (SHM). Based on the Bayesian framework of statistical inversion, this approach allows one to compensate for errors caused by incorrect modeling of a physical system while still providing a relatively simple mathematical formulation. The application of different prior distributions of the unknown parameters is investigated. The AEA is compared to a traditional least-squares approach consisting of a forward model unable to compensate for modeling related errors.

Contents

List of Figures

Chapter 1

Introduction

1.1 Motivation

There is a consensus among authors (see Section 7 of reference [2] and references therein) that model uncertainties can successfully hinder identification strategies, thus leading to the need for means to counteract their effects.

In the context of Structural Dynamics, one can talk about the concept of resonance frequency of a system. Here we use this concept to exemplify and make a brief discussion about the effects of uncertainties in inverse analysis.

For a damage state characterized by a reduction in stiffness, a *damaged* structure will have lower frequencies associated with it than those correspondent to an undamaged one.

We refer to Fig. 1.1 for this discussion. Consider that, for the inversion, one uses a model that is *believed to be an exact representation of reality* in every aspect other than an uncertain parameter, and that the *only free parameter* is the one related to the damage state of the structure, or simply the *damage* parameter. Therefore this model is unable to capture the differences in frequency caused by the uncertainties. Clearly, under these conditions, even this model with only one source of uncertainty is unable to produce consistent results: the model is only able to identify correctly two states (the undamaged blue and damaged red lines), for a reference value of this *unknown* variable, and since the *damage* is the only free variable, in order to match the measured features, in this case the frequency, it must find a specific, not necessarily correct, damage state.

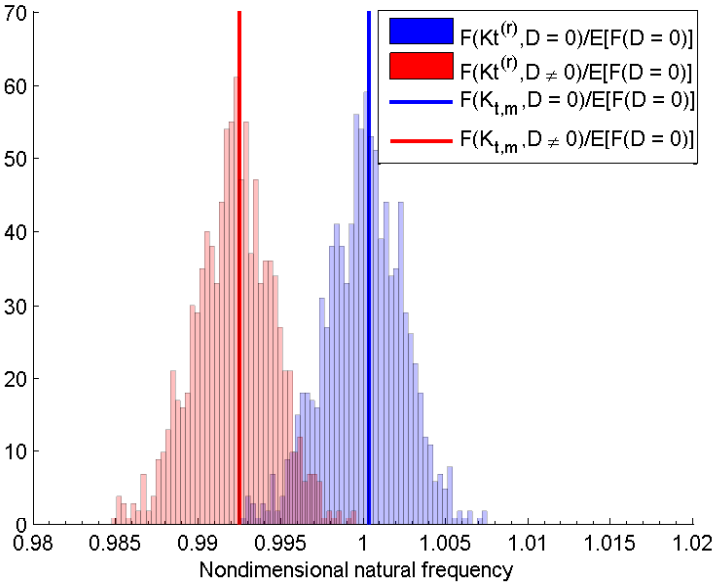

Figure 1.1: The effects of uncertainties in the 5th resonance frequency of a plate are illustrated by means of overlapping histograms: the blue bars represent the undamaged structure and the red bars, the damaged one.

Fig. 1.1 presents the change in (the 5th) resonance frequency due to damage and compares it to that caused by *unknown* boundary conditions – *unknown* in this context refers to what is modeled incorrectly (but assumed right) versus what is actually present.

The key concept of this discussion is that the features used in the inversion process might contain corrupted information (with respect to the model) due to some uncertainties, thus leading to erroneous identification of the damage state.

1.2 Objetives

This work is concerned with the handling of model uncertainties in *Structural Health Monitoring* (SHM). It is not concerned, however, with the elaboration of identification strategies nor with comparison between different strategies presented in literature.

With the intent of mitigating the effects caused by modeling errors, we explore the application of a technique known as *Approximation Error Approach* (AEA) [1]. This technique has been shown to be a feasible way to compensate for discretization errors, uncertain boundary data and geometry, as well as physical modeling errors in a complex set of problems (see Section 1.3.3). It is relatively simple when compared to other strategies to compensate for modeling errors.

1.3 Literature Review

In this section, a brief literature review on vibration based techniques is presented. For a more comprehensive review, we refer to the works by FRISWELL [2], SIMOEN *et al.* [3], FARRAR and WORDEN[4], FARRAR *et al.* [5], CARDEN and FANNING [6], MONTALVÃO *et al.* [7], DOEBLING *et al.* [8].

1.3.1 An Introduction

In this work, we chose to follow the definition given by FARRAR and WORDEN [4], that is to say *damage* can be defined as changes introduced into a system that adversely affect its performance. Implicit in this definition is the existence of a reference state of the system, often its undamaged one, to which comparisons can be drawn. Therefore, changes in material properties and/or geometry as well as boundary conditions fall into this definition.

Damage is, in anyway, a defect that originates at the *material level* and grows at different rates depending on the operational conditions – corrosion, impacts, etc. – leading to a defect at the *component level*, and finally *system* (structural) level.

The implementation of processes to identify and monitor the health of a structure is known as *Structural Health Monitoring* (SHM) [4]. It consists of extracting pertinent data from the structure and posterior identification of its current state, often related to answering questions such as "Is it necessary to perform maintenance ahead of schedule?" or " Is the structure currently capable of continued operation?". In this sense, it is clear the need for monitoring in various industrial applications in to order determine the safety and reliability of their systems.

In the context of SHM there are four major concepts: *operation evaluation; feature selection; data acquisition and analysis* and *model development*.

Briefly speaking, *operation evaluation* concerns itself with the prior evaluation of possible implementation issues, one needs to answer questions like: "Is it worth to implement SHM?", "What needs to be monitored and how?", "Are there limitations to online data acquisition?", "Is there a scenario that is of major concern?", etc.

Feature selection is the stage in which characteristics of the structure are selected to be measured in order to estimate damage: vibration data, frequency response, etc. *Data acquisition* is closely related to feature selection: excitation methods, number of sensors, their types and locations, and all the remaining necessary hardware.

Finally, *model development*: the *development* of algorithms that utilize the selected features in order to differentiate between damaged and undamaged states of a structure. FARRAR *et al.* [5] point out that most of the works in literature do not make use of *statistical models* to asses if changes in the selected features are statistically significant to imply damage, and such is the case of this dissertation. One should seek reference [5] for a more in depth discussion.

RYTTER [9] proposed a leveled approach to damage assessment: *detection* or *identification*; *localization*; *extension* or *severity*; and *prognosis*. Following this order, increased knowledge of the damage state. The application of finite element model based approaches allows for the assessment of presence of damage, location and quantification of its extent. Prognosis requires the damage mechanism to be determined, which might be possible using hypothesis testing among candidate mechanisms [2]. For more on damage prognosis, see reference [10].

The damage identification problem fits in the broader category known as *inverse problems*. Due to the ill-posed character of inverse problems, they are usually recast as optimization problems by which one aims to find an appropriate estimate of the desired parameters that best fits the data, usually in a least squares sense [2, 11–15]. The "data" stands for measurements of the selected features.

FRISWELL [2] presents a review of the inverse methods commonly used in damage identification. For a general review of optimization techniques used in inverse problems of parameter estimation and function estimation, as well as regularization techniques, see the review by COLAÇO *et al.* [15].

Most works in literature are found in the framework of *Finite Element Model Updating* (FEMU), which can use either *parametric* or *direct* methods [2]. Model updating is the process by which one adjusts the parameters of some model. In *direct methods*, the goal is to reproduce the measured data by controlled chances to the stiffness matrix; while in *parametric based methods* a set of physically meaningful parameters can be selected and then estimated. Such approaches are suited for

dealing with erroneous assumptions for model parameters, however other typical modeling errors such that idealizations of the physical system and those caused by numerical discretization cannot be addressed [16].

In contrast, there are techniques that do not necessarily require the use of computational models, such as those based on the use of Neural Networks [6]. Although such techniques require vast amounts of data to be available for the training of the Network, in order to allow it to recognize and distinguish between damaged and undamaged states. In this dissertation, we consider the use of a model based approach.

Most works in literature are based on the use of *modal features*, such as resonance frequencies, mode shapes and/or their derivatives (mode shape curvature), in particular see references [17–27]. Other methods include energy based indexes (strain energy) and the use of Wavelet Transforms [6].

However, there are relatively few works concerning the use of temporal data for damage identification, a fact that is recognized by some authors such as LINK and WEILAND [28]. They point out that the use of data from impact testing carries high-frequency information, which enhances the estimation of even localized damage. FRISWELL [2] further elaborates that the problem with low frequency data is relative size difference between the excited modes's spatial wavelengths and the extension of damage itself.

FU *et al.* [29], in their work concerning the use of time series as a feature for the identification, studied the collocation of sensors, total time and time of excitation. They found out that an increased number of measurement points and longer measurement time improves the damage identification. Tests performed prior to setting up the damage identification inverse problem presented in this dissertation are in agreement with the findings of FU *et al.* [29]. In other words, this is the *optimal experiment setup* [13, 14] that must be performed (*feature selection* and *data acquisition*) in order to create conditions that allow for the identification of the structure's integrity state.

Other works where the use of time series data was considered are those by PEREIRA *et al.* [30], CASTELLO *et al.* [31].

In [28, 29], sensitivity based techniques were used in order to drive an iterative procedure to solve the inverse problem. In regards to regularization techniques, both works used Tikhonov regularization.

GRIP *et al.* [27] used Total Variation (TV) regularization, which is an edge-preserving method with many applications in image processing techniques. They [27] compared the use of TV regularization with use of damage functions proposed by TEUGHELS and ROECK [22], and presented formulas for a second-order differentiable approximation of the TV regularization.

While TEUGHELS and ROECK [22] use a Gauss–Newton method with trust region to solve the minimization problem, in fact this, in conjunction with the use of the proposed *damage functions*, which effectively reduces the number of unknown parameters, provides an alternative to classical regularization methods. They also mention the possibility of using a two stage procedure to identify damage.

An analogous multi-stage procedure is presented by LEE and SHIN [26], who proposed to iteratively remove undamaged areas from the identification process as an alternative to regularization. Another interesting aspect of their investigations was the use of an analytical model for the dynamics of the damaged plate. Such mode is based on series expansion into an orthogonal functions and defines a damage parameter dependent on the mode shapes.

The success of model updating techniques is strongly based on the quality of the *damage model* used and its ability to describe the changes due to damage [2, 25, 28], for this same reason, knowledge of the damage mechanism is specially critical to *prognosis*. Thus a key aspect of the application of inverse methods is the model used to described the damage.

A commonly used model is a damage state characterized by a reduction in stiffness of the structure, such as in the works of CHOI *et al.* [17], MOAVENI and BEHMANESH [24], LEE and SHIN [26], FU *et al.* [29], who directly relate this to changes in the Young's Modulus. In other works, such as those by CORRÊA *et al.* [18], CASTELLO *et al.* [19], STUTZ *et al.* [20], PEREIRA *et al.* [30] and CASTELLO *et al.* [31], a "global cohesion" variable, which affects the whole of what can be classified as *stiffness*, is defined. For FE models this cohesion variable quantifies the structural integrity by directly modifying the FE stiffness matrices.

To summarize, most of the found literature consists of works in the FEMU framework, and among them most consider the use of modal features to identify the damage state. In this dissertation, the selected procedure was to use time series data in conjunction with a parametric based approach to estimate a continuous damage field such as in references [18–22, 24, 29–31], even though in this work the damage field is simplified (*localized*), thus allowing for a limited set of parameters to be used in the identification problem.

As mentioned by FU *et al.* [29], the problem of damage identification in plates is relatively new, with few works still found in literature. Between these, there are those cited directly in [29], as well as references [17, 18, 25, 26] of this work. For this reason, we also consider the inverse problem of damage identification with uncertainties in plates.

1.3.2 Dealing with Uncertainties

BOLLER [32] mentions it is not necessary to localize and estimate damage with a high level of accuracy (specially because such an accurate description would require knowledge of the damage mechanism [2]), he states that a better approach is to roughly locate the damage and with the help of traditional Non Destructive Testing (NDT) techniques one may perform a closer analysis.

In practice, however, the reliance on models to predict the behavior of the monitored system is one of the major drawbacks of model based approaches as stated by FRISWELL [2] and DOEBLING *et al.* [8]. There are always errors related to measurement data and physical/mathematical modeling of a system, and so it happens that many times these modeling errors can cause changes to the predicted features that are of an equal or greater order of magnitude than those changes caused by damage, which in turn make the solution of the inverse problem more difficult and can even render the estimated results useless, this statement is corroborated by findings such as those in references [3, 24, 25] (see Section 1.1, for an example).

Modeling errors include (but are not limited to) environmental and other non-stationary effects (such as temperature, humidity, etc), unmodeled nonlinear behavior, incorrect material properties, discretization errors, geometry approximation, etc. There is still the matter of the damage mechanism itself [2, 25], for example composite materials can experience many different modes of structural damage, such as delamination, fiber matrix debonding, fiber breakage, fiber pull-out and matrix cracking, which further complicates the damage identification problem when in conjunction with the structural response scatter caused by uncertainties in material properties.

Different methods were considered in literature to deal with some of these errors. SIMOEN *et al.* [3] wrote an extensive review paper showcasing the two most common approaches to compensate for modeling errors in the FEMU framework: the non-probabilistic fuzzy approach and the probabilistic one, based on the Bayesian framework. The sources of modeling errors are discussed and examples are worked out comparing both approaches to the traditional (deterministic) FEMU.

Most of the first works concerning the Bayesian approach for FEMU stems from the works by BECK and KATAFYGIOTIS [23] and by VANIK *et al.* [33] who showed that the Bayesian approach allows for updated probabilities of model parameters and damage measures. To exemplify other methodologies for dealing with model uncertainty, consider the following works by CHANDRASHEKHAR and GANGULI [25], MOAVENI and BEHMANESH [24, 34], BEHMANESH *et al.* [35], NANDAN and SINGH [36, 37] and LEE *et al.* [38].

MOAVENI and BEHMANESH [24] applied the concepts of SHM to the Dowling Hall Footbridge, located at the Tufts University campus in Medford, Massachusetts. Modal data was utilized to feed the FEMU algorithm, to deal with data variability caused by fluctuating temperatures, a static polynomial model was used to compensate the effects in the measured natural frequencies.

BEHMANESH *et al.* [35] presented the mathematical background for the Hierarchical Bayesian Model Framework for dealing with modeling errors in FEMU, and a simple example is considered: the approach is tested for uncertainty quantification of model updating parameters and probabilistic damage identification. This approach is similar to the one presented in this text, in the sense that a large number of numerical simulations is necessary and a modified likelihood metric is constructed.

BEHMANESH and MOAVENI [34] continued the work on the Dowling Footbridge now considering both ambient temperature and excitation amplitude in a Hierarchical Bayesian model framework.

In their two-part paper, NANDAN and SINGH [36, 37] performed a series of numerical simulations concerning the Thermoelasticity problem to evaluate the changes in modal features caused by seasonal temperature variations, solar irradiance and wind speed (convection boundary condition), considering changes in material property due to temperature and thermal gradients. These experiments are based on environmental data recorded at a site in North Carolina, USA, with strong seasonal and diurnal trends in temperature. They found out that these variations caused significant changes to the observed modal features, therefore to compensate the errors due to environment modeling they applied a filter to capture the low-frequency seasonal trends and a subspace system identification approach. Their main concern was to establish an approach to relate modal frequency and bridge body temperature.

CHANDRASHEKHAR and GANGULI [25] performed a study of the uncertainty effects on damage parameter (delamination) and selected feature, thus observing their negative impact on damage assessment. In order to deal with it, a fuzzy logic based methodology was applied to deal with the uncertainties in material properties. Fuzzy approaches have the advantage of not needing to be trained with vast amounts of data such as Neural Network approaches.

LEE *et al.* [38] used Neural Networks to compensate for modeling errors. A set of modal variables with low sensitivity to modeling errors was selected to train the algorithm and reduce the effects of errors in the baseline finite element model used to generate the training patterns. An algorithm to compensate for measurement errors was also considered. The method was tested in a lab environment with good results, and then in a real life scenario with satisfactory results.

1.3.3 The Approximation Error Approach

This work's goal is to introduce to the SHM community a tool for dealing with modeling errors in general: the Approximation Error Approach (AEA), which was developed originally by KAIPIO and SOMERSALO [1] to handle model reduction errors. Mostly used in clinical applications as tomography, where the use of approximate models is desirable to reduce the computational burden necessary, while a reliable and fast diagnosis is still required. Given the extent of this author's knowledge, thus far this approach has not been applied to SHM.

KOLEHMAINEN *et al.* [39] used this approach to rule out the influence of a distributed parameter that appears in Diffuse Optical Tomography that is uninteresting, even though it is of consequence when considering the inverse problem. In this paper, a considerably reduced numerical model was also considered.

NISSINEN *et al.* [40] adapted the AEA to compensate for the modeling errors caused by unknown body shape in Electrical Impedance Tomography, that is the error caused by having to map the thoracic cavity cross section to a reference domain, without actually knowing the original cross section. While in [41], the AEA was applied to compensate for unknown contact impedance of the utilized sensors.

MOZUMDER *et al.* [42] applied the same method for the Optical Tomography problem, compensating for the modeling errors caused by considering a reference cranial cross section, while KOULOURI *et al.* [43] used this approach to alleviate the errors present in the solution for the source problem of the Poison Equation when an approximate model for the domain is employed.

TARVAINEN *et al.* [44] used the AEA to compensate modeling errors stemming from the use of a qualitatively incorrect physical model, while also using a highly reduced forward model for the inverse problem.

Applications similar to that of reference [44] are found in the works by COTTA [45], ORLANDE *et al.* [46] and LAMIEN and ORLANDE [47], all of which considered the application of the AEA to the Markov Chain Monte Carlo (MCMC) technique. For large scale problems, limitations are imposed to the number of states of the Markov Chain in order to obtain results in a feasible time, thus the need for surrogate or reduced models. In the aforementioned works, the particularities of associating the AEA with MCMC technique.

COTTA [45] was concerned with the use of waste heat to enhance the production of biodiesel. In terms of the inverse problem, the estimation of the kinetic constants of the biodiesiel synthesis reaction, which is modeled as a reaction-convection-diffusion equation, was considered using 3D, 2D and 1D models for the forward model. In addition to a considerable time reduction, the AEA furnished better estimates of the parameters as well as better predictions than simply using the reduced models.

ORLANDE *et al.* [46] considered the inverse problem of estimating the heat flux at the boundaries of a plate. A reduced model consisting of a one-dimensional approximation of the heat conduction problem with an improved lumped formulation (that takes into account gradients across the thickness of the plate) and constant properties is used instead of a complete three-dimensional one. The authors found that the AEA outperformed the Delayed Acceptance Metropolis-Hastings (DAMH) algorithm, which is one technique used to deal with reduced models in MCMC, in terms of computational time required. However, an increase in time was observed when compared to the case where only the reduced model was used. Also, the AEA produced lower mean square error of the estimated field in comparison with the DAMH, which *does use* the complete model at some point.

LAMIEN and ORLANDE [47] considered the inverse problem of estimating thermal conductivity and volumetric heat capacity of a fluid using a standard probe technique. The AEA was used to compensate for model errors caused by the use of a purely *conductive* model for the fluid domain instead of a *convective* one.

This idea that some variability can be accounted for is of interest for scenarios where practically the same problem needs to be solved many times, with slight variations, such as in the medical field, with the Optical Tomography problem, or in the context of mechanics with the inspection of pipe assemblies or trusses, where every part is similar, except for variations in their fixations that could be substantial, or with composite plates and the fluctuation of material properties therein.

The approximation error approach was shown to be a feasible way to compensate for discretization errors, uncertain boundary data and geometry, as well as physical modeling errors in a complex set of problems. Due to its theoretical simplicity and computational cost reduction (when compared to other approaches to compensate for modeling errors) we were motivated to apply it to SHM.

1.4 Outline

This text is organized as follows:

In Chapter 2, the mathematical formulation of the Approximation Error Approach is presented in parallel with the Bayesian framework for inverse problems. Computational considerations for the implementation of the method are also presented.

In Chapter 3, a case study consisting of estimating parametric damage field is presented. The general concept of direct problem is briefly discussed, and the particular directly problem of this chapter is presented. Next, the general concept of inverse problem is briefly described, and the particular inverse problem of this chapter is presented. At the end of the chapter, the details of how data is collected for the inverse problem are discussed.

In Chapter 4, the First Order Shear Deformation Theory for plates is briefly presented. The direct and inverse problems for damage identification in plate structures are described. At the end of the chapter, the details of how data is collected for the inverse problem are discussed.

In Chapter 5, the inverse problem is solved by both the "Traditional" least squares parameter estimation approach (see [13]) and the AEA. This chapter describes the general aspects of setting the parameters for the AEA and calculating its statistics for the problems discussed in Chapters 3 and 4.

In Chapter 6, the Adjoint Formulation is applied to the damage identification problem of a plate structure to efficiently calculate the gradient used in gradient-based minimization techniques. However, due to the characteristics of the of the AEA, we were unable at this time to construct an adjoint problem that preserves the correlation structure between different measurements in the AEA, thus only a benchmark problem *without modeling errors* is presented.

In Chapter 7, concluding remarks and ideas for further developments are presented.

After, relevant appendices are included. These are as follows: A - The finite element discretization for the FSDT; B - The improved reduced system model reduction; C - The generation of random fields for distributed paramaters; D - The Gaussian approximation for the posterior estimated probability distribution and; E - The adjoint formulation and details on how to obtain the derivatives of the forward model.

Chapter 2

Approximation Error Approach

2.1 Basic Concepts

The Approximation Error Approach was introduced by KAIPIO and SOMERSALO [1] originally to handle model reduction errors. This approach was extended to nonstationary inverse problems by HUTTUNEN and KAIPIO [48], although the problem is not formulated as such in this text.

The AEA is based on the Bayesian framework of inverse problems, in which all unknowns are modeled as random variables (see [11, 12]). Let $\boldsymbol{\theta}$ be a vector of unknowns and $\bar{\mathbf{y}}$ a vector containing measurements of some feature related to the system being identified. Once probabilistic models for $\boldsymbol{\theta}$ and $\bar{\mathbf{y}}$ are constructed, the *Posterior* probability distribution function (PDF) $\pi(\mathbf{x}|\bar{\mathbf{y}})$ can be assessed through the use of Bayes' Formula, eq. (2.1.1). The *posterior* PDF reflects the uncertainty of the unknowns $\boldsymbol{\theta}$ given the measurements $\bar{\mathbf{y}}$, given any *prior information* available.

$$\pi(\boldsymbol{\theta}|\bar{\mathbf{y}}) = \frac{\pi(\bar{\mathbf{y}}|\boldsymbol{\theta})\pi(\boldsymbol{\theta})}{\pi(\bar{\mathbf{y}})} \tag{2.1.1}$$

In eq.(2.1.1), $\pi(\bar{\mathbf{y}}|\boldsymbol{\theta})$ is the *Likelihood function* of the measurements $\bar{\mathbf{y}}$ given the unknown parameters $\boldsymbol{\theta}$. This function associates a probability to the occurrence of a given measurement realization to a realization of the parameters. $\pi(\boldsymbol{\theta})$ is the *Prior* PDF of the unknowns $\boldsymbol{\theta}$, this function allows for any current knowledge regarding the possible values of $\boldsymbol{\theta}$ to be taken into account. $\pi(\bar{\mathbf{y}})$ is the PDF for the measurements, and once a realization of $\bar{\mathbf{y}}$ is drawn, that is to say an experiment is made, the value of $\pi(\bar{\mathbf{y}})$ is simply a scaling constant.

The *maximum a posteriori* (MAP) of $\pi(\boldsymbol{\theta}|\bar{\mathbf{y}})$ is a commonly used (point) estimate for the unknowns:

$$\boldsymbol{\theta}' = arg\max_{\boldsymbol{\theta}} \pi(\boldsymbol{\theta}|\bar{\mathbf{y}}) \tag{2.1.2}$$

This chapter starts with a brief review of the traditional Bayesian approach.

2.2 Classical Bayesian Framework for Statistical Inversion

Let $\mathcal{A}_c(\boldsymbol{\theta})$ be a deterministic *accurate forward model* without any uncertainties or other model errors, i.e., the map $\boldsymbol{\theta} \mapsto \mathcal{A}_c(\boldsymbol{\theta})$ provides accurate predictions whose differences from measured data $\bar{\mathbf{y}}$ are basically due to the measurement noise $\mathbf{e}$, which is a vector of additive errors related to the measurement process [13, 14]. Then the observation model is given by:

$$\bar{\mathbf{y}} = \mathcal{A}_c(\boldsymbol{\theta}) + \mathbf{e} \tag{2.2.1}$$

Let $\pi(\boldsymbol{\theta}, \bar{\mathbf{y}}, \mathbf{e})$ be the *joint* PDF of the unknowns $\boldsymbol{\theta}$, measurements $\bar{\mathbf{y}}$ and measurement errors $\mathbf{e}$. Then:

$$\pi(\boldsymbol{\theta}, \bar{\mathbf{y}}, \mathbf{e}) = \pi(\bar{\mathbf{y}}|\boldsymbol{\theta}, \mathbf{e})\pi(\mathbf{e}|\boldsymbol{\theta})\pi(\boldsymbol{\theta}) \tag{2.2.2}$$

$$= \pi(\bar{\mathbf{y}}, \mathbf{e}|\boldsymbol{\theta})\pi(\boldsymbol{\theta}) \tag{2.2.3}$$

Since eq.(2.2.1) is valid, $\pi(\bar{\mathbf{y}}|\boldsymbol{\theta}, \mathbf{e})$ can be expressed as:

$$\pi(\bar{\mathbf{y}}|\boldsymbol{\theta}, \mathbf{e}) = \delta(\bar{\mathbf{y}} - (\mathcal{A}_c(\boldsymbol{\theta}) + \mathbf{e}))$$

Therefore marginalizing with respect to the measurement additive errors $\mathbf{e}$ yields the following *Likelihood* distribution:

$$\begin{aligned}
\pi(\bar{\mathbf{y}}|\boldsymbol{\theta}) &= \int \pi(\bar{\mathbf{y}}, \mathbf{e}|\boldsymbol{\theta}) d\mathbf{e} \\
&= \int \pi(\bar{\mathbf{y}}|\boldsymbol{\theta}, \mathbf{e})\pi(\mathbf{e}|\boldsymbol{\theta}) d\mathbf{e} \\
&= \int \delta(\bar{\mathbf{y}} - (\mathcal{A}_c(\boldsymbol{\theta}) + \mathbf{e}))\pi(\mathbf{e}|\boldsymbol{\theta}) d\mathbf{e} \\
&= \pi_{\mathbf{e}|\boldsymbol{\theta}}(\bar{\mathbf{y}} - \mathcal{A}_c(\boldsymbol{\theta})|\boldsymbol{\theta})
\end{aligned}$$

where $\pi_{\mathbf{e}|\boldsymbol{\theta}}(\bar{\mathbf{y}} - \mathcal{A}_c(\boldsymbol{\theta})|\boldsymbol{\theta})$ is the PDF of $\mathbf{e}$ given $\boldsymbol{\theta}$, $\pi(\mathbf{e}|\boldsymbol{\theta})$, evaluated at the residue $\mathbf{e} = \bar{\mathbf{y}} - \mathcal{A}_c(\boldsymbol{\theta})$.

Applying Bayes's Formula, eq.(2.1.1):

$$\pi(\boldsymbol{\theta}|\bar{\mathbf{y}}) \propto \pi(\bar{\mathbf{y}}|\boldsymbol{\theta})\pi(\boldsymbol{\theta}) = \pi_{\mathbf{e}|\boldsymbol{\theta}}(\bar{\mathbf{y}} - \mathcal{A}_c(\boldsymbol{\theta})|\boldsymbol{\theta})\pi(\boldsymbol{\theta}) \tag{2.2.4}$$

If $\mathbf{e}$ and $\boldsymbol{\theta}$ are assumed to be mutually independent, we have $\pi_{\mathbf{e}|\boldsymbol{\theta}}(\mathbf{e}|\boldsymbol{\theta}) = \pi_{\mathbf{e}}(\mathbf{e}) \equiv \pi(\mathbf{e})$. Furthermore, if $\mathbf{e}$ and $\boldsymbol{\theta}$ are both normally distributed, $\mathbf{e} \sim \mathcal{N}(\mathbf{e}_*, \boldsymbol{\Sigma}_e)$ and $\boldsymbol{\theta} \sim \mathcal{N}(\boldsymbol{\theta}_*, \boldsymbol{\Sigma}_{\boldsymbol{\theta}})$, the prior distribution of $\boldsymbol{\theta}$, we get:

$$\pi(\boldsymbol{\theta}|\bar{\mathbf{y}}) \propto \exp\left\{-\frac{1}{2}(\bar{\mathbf{y}} - \mathcal{A}_c(\boldsymbol{\theta}) - \mathbf{e}_*)^T \boldsymbol{\Sigma}_e^{-1}(\bar{\mathbf{y}} - \mathcal{A}_c(\boldsymbol{\theta}) - \mathbf{e}_*) - \frac{1}{2}(\boldsymbol{\theta} - \boldsymbol{\theta}_*)^T \boldsymbol{\Sigma}_{\boldsymbol{\theta}}^{-1}(\boldsymbol{\theta} - \boldsymbol{\theta}_*)\right\} \tag{2.2.5}$$

Therefore, a MAP estimate of $\boldsymbol{\theta}$ is the solution of the following problem:

$$\boldsymbol{\theta}' = arg\min_{\boldsymbol{\theta}} V(\boldsymbol{\theta}) \tag{2.2.6a}$$

$$V(\boldsymbol{\theta}) = \|\boldsymbol{\Gamma}_e(\bar{\mathbf{y}} - \mathcal{A}_c(\boldsymbol{\theta}) - \mathbf{e}_*)\|^2 + \|\boldsymbol{\Gamma}_{\boldsymbol{\theta}}(\boldsymbol{\theta} - \boldsymbol{\theta}_*)\|^2 \tag{2.2.6b}$$

where $\boldsymbol{\Gamma}_e^T \boldsymbol{\Gamma}_e = \boldsymbol{\Sigma}_e^{-1}$ and $\boldsymbol{\Gamma}_{\boldsymbol{\theta}}^T \boldsymbol{\Gamma}_{\boldsymbol{\theta}} = \boldsymbol{\Sigma}_{\boldsymbol{\theta}}^{-1}$.

In the absence of prior information, an observation model with additive Gaussian noise with mean $\mathbf{e}_*$ and covariance $\boldsymbol{\Sigma}_e$ leads to the *Traditional Least Squares* functional [13, 14].

$$V(\boldsymbol{\theta}) = \|\boldsymbol{\Gamma}_e(\bar{\mathbf{y}} - \mathcal{A}_c(\boldsymbol{\theta}) - \mathbf{e}_*)\|^2 \tag{2.2.7}$$

where $\boldsymbol{\Gamma}_e^T \boldsymbol{\Gamma}_e = \boldsymbol{\Sigma}_e^{-1}$.

2.3 Approximation Error and Premarginalization

In order to obtain eq.(2.2.4), it is practically always necessary to marginalize with respect to the unknown but uninteresting measurement related errors $\mathbf{e}$, that is to say "before" the estimation process. The problem here is that generally we cannot perform premarginalization with all uninteresting unknowns as we did for $\mathbf{e}$ because their effect on the response is not additive. Let these auxiliary but uninteresting unknowns be denoted by the vector $\boldsymbol{\xi}$. If premarginalization cannot be performed, perhaps one solution could be to estimate both $\boldsymbol{\theta}$ and $\boldsymbol{\xi}$: for example, if a Markov Chain Monte Carlo (MCMC) approach were used, the marginalization over $\boldsymbol{\xi}$ can only be done after running the chain for parameters (as described in [40, 42]). However this is computationally much more expensive than estimating $\boldsymbol{\theta}$ when $\boldsymbol{\xi}$ is known.

That is the key feature of the AEA: to perform premarginalization *approximately*, in a computationally feasible way. To that end some assumptions have to be made regarding some of the distributions that appear during the development of this approach.

Let $(\bar{\boldsymbol{\theta}}, \mathbf{z}, \boldsymbol{\xi}, \mathbf{e})$ be our set of unknowns. Where $\mathbf{e}$ represents additive errors, $\boldsymbol{\xi}$ represents auxiliary uncertainties such as unknown boundary data and/or geometry, and $(\bar{\boldsymbol{\theta}}, \mathbf{z})$ are two parameters of which only $\bar{\boldsymbol{\theta}}$ is of interest. Let an accurate forward model be given by:

$$(\bar{\boldsymbol{\theta}}, \mathbf{z}, \boldsymbol{\xi}) \mapsto \mathcal{A}_c(\bar{\boldsymbol{\theta}}, \mathbf{z}, \boldsymbol{\xi})$$

The unknowns $(\bar{\boldsymbol{\theta}}, \mathbf{z}, \boldsymbol{\xi})$ are not necessarily mutually independent. However, let $\mathbf{e}$ be mutually independent with $(\bar{\boldsymbol{\theta}}, \mathbf{z}, \boldsymbol{\xi})$. Then the observation model can be written as:

$$\bar{\mathbf{y}} = \mathcal{A}_c(\bar{\boldsymbol{\theta}}, \mathbf{z}, \boldsymbol{\xi}) + \mathbf{e} \tag{2.3.1}$$

In the following, let $\boldsymbol{\theta}$ be an approximation of the primary unknown $\bar{\boldsymbol{\theta}}$, where $\bar{\boldsymbol{\theta}}$ and $\boldsymbol{\theta}$ can be related by some sort of projection operator $\mathbf{P}$, $\boldsymbol{\theta} = \mathbf{P}\bar{\boldsymbol{\theta}}$[1]. This distinction allows for different levels of discretization to be used, but also allows one to set $\mathbf{P} = \mathbf{I}$, where $\mathbf{I}$ is the identity matrix. Such transformation is heavily featured in references [40, 42], where mapping between two difference sets of domain was necessary.

[1] This projection can be the result of an averaging operation or some homogenization technique.

Proceed by setting $(\mathbf{z}, \boldsymbol{\xi}) \rightarrow (\mathbf{z}_0, \boldsymbol{\xi}_0)$, and substituting the accurate forward model by a much simpler one[2].

$$\boldsymbol{\theta} \mapsto A(\boldsymbol{\theta}, \mathbf{z}_0, \boldsymbol{\xi}_0)$$

Thus, we rewrite the observation model as:

$$\begin{aligned}\bar{\mathbf{y}} &= \mathcal{A}_c(\bar{\boldsymbol{\theta}}, \mathbf{z}, \boldsymbol{\xi}) + \mathbf{e} \\ &= A(\boldsymbol{\theta}, \mathbf{z}_0, \boldsymbol{\xi}_0) + [\mathcal{A}_c(\bar{\boldsymbol{\theta}}, \mathbf{z}, \boldsymbol{\xi}) - A(\boldsymbol{\theta}, \mathbf{z}_0, \boldsymbol{\xi}_0)] + \mathbf{e} \\ &= A(\boldsymbol{\theta}, \mathbf{z}_0, \boldsymbol{\xi}_0) + \boldsymbol{\epsilon} + \mathbf{e}\end{aligned}$$

Where

$$\boldsymbol{\epsilon} = \boldsymbol{\epsilon}(\bar{\boldsymbol{\theta}}, \mathbf{z}, \boldsymbol{\xi}) = \mathcal{A}_c(\bar{\boldsymbol{\theta}}, \mathbf{z}, \boldsymbol{\xi}) - A(\boldsymbol{\theta}, \mathbf{z}_0, \boldsymbol{\xi}_0) \tag{2.3.2}$$

is defined to be the *approximation error* that arises when using a simplified model. Once both A and $\mathcal{A}_c$ are fixed we have $\pi(\boldsymbol{\epsilon}|\bar{\boldsymbol{\theta}}, \mathbf{z}, \boldsymbol{\xi}) = \delta(\boldsymbol{\epsilon} - \boldsymbol{\epsilon}(\bar{\boldsymbol{\theta}}, \mathbf{z}, \boldsymbol{\xi}))$, where $\delta(\cdot)$ is the Dirac's Delta distribution.

In order to carry out the marginalization, the first approximation is to assume that the model predictions and thus the approximation error are essentially the same for $\bar{\boldsymbol{\theta}}$ and $\boldsymbol{\theta}$ [39]: $\boldsymbol{\epsilon}(\bar{\boldsymbol{\theta}}, \mathbf{z}, \boldsymbol{\xi}) \approx \boldsymbol{\epsilon}(\boldsymbol{\theta}, \mathbf{z}, \boldsymbol{\xi})$ and thus $\pi(\boldsymbol{\epsilon}|\bar{\boldsymbol{\theta}}, \mathbf{z}, \boldsymbol{\xi}) \approx \pi(\boldsymbol{\epsilon}|\boldsymbol{\theta}, \mathbf{z}, \boldsymbol{\xi})$.

Applying Baeys' Formula:

$$\begin{aligned}\pi(\bar{\mathbf{y}}, \boldsymbol{\theta}, \mathbf{z}, \boldsymbol{\xi}, \mathbf{e}, \boldsymbol{\epsilon}) &= \pi(\bar{\mathbf{y}}|\boldsymbol{\theta}, \mathbf{z}, \boldsymbol{\xi}, \mathbf{e}, \boldsymbol{\epsilon})\, \pi(\boldsymbol{\theta}, \mathbf{z}, \boldsymbol{\xi}, \mathbf{e}, \boldsymbol{\epsilon}) \\ &= \delta(\bar{\mathbf{y}} - A(\boldsymbol{\theta}, \mathbf{z}_0, \boldsymbol{\xi}_0) - \mathbf{e} - \boldsymbol{\epsilon}(\boldsymbol{\theta}, \mathbf{z}, \boldsymbol{\xi}))\, \pi(\boldsymbol{\theta}, \mathbf{z}, \boldsymbol{\xi}, \mathbf{e}, \boldsymbol{\epsilon}) \\ &= \delta(\bar{\mathbf{y}} - A(\boldsymbol{\theta}, \mathbf{z}_0, \boldsymbol{\xi}_0) - \mathbf{e} - \boldsymbol{\epsilon}(\boldsymbol{\theta}, \mathbf{z}, \boldsymbol{\xi}))\, \pi(\mathbf{e}, \boldsymbol{\epsilon}|\boldsymbol{\xi}, \boldsymbol{\theta}, \mathbf{z})\, \pi(\mathbf{z}, \boldsymbol{\xi}|\boldsymbol{\theta})\, \pi(\boldsymbol{\theta}) \\ &= \pi(\bar{\mathbf{y}}, \mathbf{z}, \boldsymbol{\xi}, \mathbf{e}, \boldsymbol{\epsilon}|\boldsymbol{\theta})\, \pi(\boldsymbol{\theta})\end{aligned}$$

Therefore

$$\pi(\bar{\mathbf{y}}|\boldsymbol{\theta}) = \int_{\Omega} \pi(\bar{\mathbf{y}}, \mathbf{z}, \boldsymbol{\xi}, \mathbf{e}, \boldsymbol{\epsilon}|\boldsymbol{\theta}) d\Omega \tag{2.3.3}$$

[2] This simplicity may result from using a drastically reduced computational model or a simplified physics model, see references [39, 44, 45, 47].

Where $\Omega = \mathbb{D}\mathbf{z} \times \mathbb{D}\xi \times \mathbb{D}\mathbf{e} \times \mathbb{D}\epsilon$, and $\mathbb{D}(\cdot)$ denotes the vector space containing the variable $(\cdot)$. Carrying out the integration:

$$\begin{aligned}
\pi(\bar{\mathbf{y}}|\boldsymbol{\theta}) &= \int_{\Omega} \pi(\bar{\mathbf{y}}, \mathbf{z}, \boldsymbol{\xi}, \mathbf{e}, \boldsymbol{\epsilon}|\boldsymbol{\theta}) d\Omega \\
&= \int\limits_{\mathbb{D}\mathbf{e} \times \mathbb{D}\epsilon} \delta(\bar{\mathbf{y}} - A(\boldsymbol{\theta}, \mathbf{z}_0, \boldsymbol{\xi}_0) - \boldsymbol{\epsilon} - \mathbf{e}) \left[\int\limits_{\mathbb{D}\mathbf{z} \times \mathbb{D}\xi} \pi(\boldsymbol{\epsilon}, \mathbf{e}|\mathbf{z}, \boldsymbol{\xi}, \boldsymbol{\theta}) \pi(\boldsymbol{\xi}, \mathbf{z}|\boldsymbol{\theta}) d\mathbf{z} d\xi \right] d\mathbf{e} d\boldsymbol{\epsilon} \\
&= \int\limits_{\mathbb{D}\mathbf{e} \times \mathbb{D}\epsilon} \delta(\bar{\mathbf{y}} - A(\boldsymbol{\theta}, \mathbf{z}_0, \boldsymbol{\xi}_0) - \boldsymbol{\epsilon} - \mathbf{e}) \pi(\boldsymbol{\epsilon}, \mathbf{e}|\boldsymbol{\theta}) d\mathbf{e} d\boldsymbol{\epsilon} \\
&= \int\limits_{\mathbb{D}\mathbf{e} \times \mathbb{D}\epsilon} \delta(\bar{\mathbf{y}} - A(\boldsymbol{\theta}, \mathbf{z}_0, \boldsymbol{\xi}_0) - \boldsymbol{\epsilon} - \mathbf{e}) \pi(\boldsymbol{\epsilon}|\boldsymbol{\theta}) \underbrace{\pi(\mathbf{e}|\boldsymbol{\epsilon}, \boldsymbol{\theta})}_{=\pi(\mathbf{e})} d\mathbf{e} d\boldsymbol{\epsilon} \\
&= \int\limits_{\mathbb{D}\epsilon} \pi_{\mathbf{e}}(\bar{\mathbf{y}} - A(\boldsymbol{\theta}, \mathbf{z}_0, \boldsymbol{\xi}_0) - \boldsymbol{\epsilon}) \pi_{\boldsymbol{\epsilon}|\boldsymbol{\theta}}(\boldsymbol{\epsilon}|\boldsymbol{\theta}) d\boldsymbol{\epsilon}
\end{aligned}$$

Now let both $\pi_{\epsilon|\boldsymbol{\theta}}$ and $\pi_{\mathbf{e}}$ be approximated by normal distributions and the normal approximation for the joint PDF $\pi(\boldsymbol{\epsilon}, \boldsymbol{\theta})$ be written as:

$$\pi(\boldsymbol{\epsilon}, \boldsymbol{\theta}) \propto \exp\left\{ -\frac{1}{2} \begin{pmatrix} \boldsymbol{\epsilon} - \boldsymbol{\epsilon}_* \\ \boldsymbol{\theta} - \boldsymbol{\theta}_* \end{pmatrix}^T \begin{pmatrix} \boldsymbol{\Sigma}_{\epsilon\epsilon} & \boldsymbol{\Sigma}_{\epsilon\boldsymbol{\theta}} \\ \boldsymbol{\Sigma}_{\boldsymbol{\theta}\epsilon} & \boldsymbol{\Sigma}_{\boldsymbol{\theta}\boldsymbol{\theta}} \end{pmatrix}^{-1} \begin{pmatrix} \boldsymbol{\epsilon} - \boldsymbol{\epsilon}_* \\ \boldsymbol{\theta} - \boldsymbol{\theta}_* \end{pmatrix} \right\} \tag{2.3.4}$$

This a key step: by making a Gaussian approximation for these PDFs one wishes to gain in computational efficiency by simplifying the resulting expressions for the optimization problem. Following this assumption, one can write from eq.(2.3.4) the conditioned random variables:

$$\mathbf{e} \sim \mathcal{N}(\mathbf{e}_*, \boldsymbol{\Sigma}_{\mathbf{e}}), \quad \boldsymbol{\epsilon}|\boldsymbol{\theta} \sim \mathcal{N}(\boldsymbol{\epsilon}_*|\boldsymbol{\theta}, \boldsymbol{\Sigma}_{\epsilon|\boldsymbol{\theta}})$$

Where

$$\boldsymbol{\epsilon}_*|\boldsymbol{\theta} = \boldsymbol{\epsilon}_* + \boldsymbol{\Sigma}_{\epsilon\boldsymbol{\theta}} \boldsymbol{\Sigma}_{\boldsymbol{\theta}\boldsymbol{\theta}}^{-1} (\boldsymbol{\theta} - \boldsymbol{\theta}_*)$$

$$\boldsymbol{\Sigma}_{\epsilon|\boldsymbol{\theta}} = \boldsymbol{\Sigma}_{\epsilon\epsilon} - \boldsymbol{\Sigma}_{\epsilon\boldsymbol{\theta}} \boldsymbol{\Sigma}_{\boldsymbol{\theta}\boldsymbol{\theta}}^{-1} \boldsymbol{\Sigma}_{\boldsymbol{\theta}\epsilon}$$

Now let us define the normal variable $\boldsymbol{\nu}|\boldsymbol{\theta}$ as the sum of measurement and model related errors:

$$\boldsymbol{\nu}|\boldsymbol{\theta} = \mathbf{e} + \boldsymbol{\epsilon}|\boldsymbol{\theta} \tag{2.3.6}$$

Therefore $\boldsymbol{\nu}|\boldsymbol{\theta} \sim \mathcal{N}(\boldsymbol{\nu}_{*|\boldsymbol{\theta}}, \boldsymbol{\Sigma}_{\nu|\boldsymbol{\theta}})$. Where:

$$\boldsymbol{\nu}_{*|\boldsymbol{\theta}} = \mathbf{e}_* + \boldsymbol{\epsilon}_* + \boldsymbol{\Sigma}_{\epsilon\boldsymbol{\theta}} \boldsymbol{\Sigma}_{\boldsymbol{\theta}\boldsymbol{\theta}}^{-1} (\boldsymbol{\theta} - \boldsymbol{\theta}_*) \tag{2.3.7a}$$

$$\boldsymbol{\Sigma}_{\nu|\boldsymbol{\theta}} = \boldsymbol{\Sigma}_e + \boldsymbol{\Sigma}_{\epsilon\epsilon} - \boldsymbol{\Sigma}_{\epsilon\boldsymbol{\theta}} \boldsymbol{\Sigma}_{\boldsymbol{\theta}\boldsymbol{\theta}}^{-1} \boldsymbol{\Sigma}_{\boldsymbol{\theta}\epsilon} \tag{2.3.7b}$$

Thus eq.(2.3.3) leads to an approximate Gaussian distribution:

$$\bar{\mathbf{y}}|\boldsymbol{\theta} \sim \mathcal{N}(\bar{\mathbf{y}} - A(\boldsymbol{\theta}, \mathbf{z}_0, \boldsymbol{\xi}_0), \boldsymbol{\Sigma}_{\nu|\boldsymbol{\theta}})$$

Now assume that the *prior* model for $\boldsymbol{\theta}$ is also Gaussian, $\boldsymbol{\theta} \sim \mathcal{N}(\boldsymbol{\theta}_*, \boldsymbol{\Sigma}_{\boldsymbol{\theta}\boldsymbol{\theta}})$. Finally, we obtain an approximation for the posterior distribution:

$$\begin{aligned}\pi(\boldsymbol{\theta}|\bar{\mathbf{y}}) \propto \exp\Big\{ &-\frac{1}{2}(\bar{\mathbf{y}} - A(\boldsymbol{\theta}, \mathbf{z}_0, \xi_0) - \boldsymbol{\nu}_{*|\boldsymbol{\theta}})^T \boldsymbol{\Sigma}_{\nu|\boldsymbol{\theta}}^{-1} (\bar{\mathbf{y}} - A(\boldsymbol{\theta}, \mathbf{z}_0, \xi_0) - \boldsymbol{\nu}_{*|\boldsymbol{\theta}}) + \\ &-\frac{1}{2}(\boldsymbol{\theta} - \boldsymbol{\theta}_*)^T \boldsymbol{\Sigma}_{\boldsymbol{\theta}}^{-1} (\boldsymbol{\theta} - \boldsymbol{\theta}_*) \Big\}\end{aligned} \tag{2.3.8}$$

Therefore a MAP estimate of $\boldsymbol{\theta}$ is the solution of the following problem:

$$\boldsymbol{\theta}' = arg\min_{\boldsymbol{\theta}} V(\boldsymbol{\theta}) \tag{2.3.9a}$$

$$V(\boldsymbol{\theta}) = \|\boldsymbol{\Gamma}_{\nu|\boldsymbol{\theta}}(\bar{\mathbf{y}} - A(\boldsymbol{\theta}, \mathbf{z}_0, \xi_0) - \boldsymbol{\nu}_{*|x})\|^2 + \|\boldsymbol{\Gamma}_{\boldsymbol{\theta}}(\boldsymbol{\theta} - \boldsymbol{\theta}_*)\|^2 \tag{2.3.9b}$$

$$\boldsymbol{\nu}_{*|\boldsymbol{\theta}} = \mathbf{e}_* + \boldsymbol{\epsilon}_* + \boldsymbol{\Sigma}_{\epsilon\boldsymbol{\theta}} \boldsymbol{\Sigma}_{\boldsymbol{\theta}\boldsymbol{\theta}}^{-1} (\boldsymbol{\theta} - \boldsymbol{\theta}_*) \tag{2.3.9c}$$

$$\boldsymbol{\Sigma}_{\nu|\boldsymbol{\theta}} = \boldsymbol{\Sigma}_e + \boldsymbol{\Sigma}_{\epsilon\epsilon} - \boldsymbol{\Sigma}_{\epsilon\boldsymbol{\theta}} \boldsymbol{\Sigma}_{\boldsymbol{\theta}\boldsymbol{\theta}}^{-1} \boldsymbol{\Sigma}_{\boldsymbol{\theta}\epsilon} \tag{2.3.9d}$$

Where $\boldsymbol{\Gamma}_{\nu|\boldsymbol{\theta}}$ and $\boldsymbol{\Gamma}_{\boldsymbol{\theta}}$ are the Cholesky factors of $\boldsymbol{\Sigma}_{\nu|\boldsymbol{\theta}}^{-1}$ and $\boldsymbol{\Sigma}_{\boldsymbol{\theta}}^{-1}$, respectively, such that $\boldsymbol{\Gamma}_{\nu|\boldsymbol{\theta}}^T \boldsymbol{\Gamma}_{\nu|\boldsymbol{\theta}} = \boldsymbol{\Sigma}_{\nu|\boldsymbol{\theta}}^{-1}$ and $\boldsymbol{\Gamma}_{\boldsymbol{\theta}}^T \boldsymbol{\Gamma}_{\boldsymbol{\theta}} = \boldsymbol{\Sigma}_{\boldsymbol{\theta}}^{-1}$.

Since the problem (2.3.9) is, in essence, a well defined modification of the traditional least squares problem, eq.(2.2.7), it can be solved by traditional algorithms [39, 42].

In addition, if one assumes that $\boldsymbol{\theta}$ and $\boldsymbol{\epsilon}$ are mutually independent, that is, if $\boldsymbol{\Sigma}_{\epsilon\boldsymbol{\theta}}$ is neglected[3], it is possible to construct the so called *enhanced approximation error model* [1, 12, 39, 42, 46].

Therefore a MAP estimate of $\boldsymbol{\theta}$ would consider the following equations

$$\boldsymbol{\nu}_{*|\boldsymbol{\theta}} = \mathbf{e}_* + \boldsymbol{\epsilon}_* \tag{2.3.10a}$$

$$\boldsymbol{\Sigma}_{\nu|\boldsymbol{\theta}} = \boldsymbol{\Sigma}_e + \boldsymbol{\Sigma}_{\epsilon\epsilon} \tag{2.3.10b}$$

instead of eq.(2.3.9c-2.3.9d).

[3] In this work, it was observed that the entries of $\boldsymbol{\Sigma}_{\epsilon\boldsymbol{\theta}}$ were in average 10 orders of magnitude smaller than those of $\boldsymbol{\Sigma}_{\epsilon\epsilon}$. However we still considered the complete AE model.

2.4 Computational Considerations

In Section 2.2 a quick reminder of Bayesian Framework of inverse problems was given in order to justify the mathematical approach used in Section 2.3. Here it is discussed how one goes about gathering the necessary statistics in order to perform a MAP estimation using the Approxiation Error Approach.

Firstly, it is interesting to note that the prior model $\pi(\boldsymbol{\theta}, \mathbf{z}, \boldsymbol{\xi})$ does not have to be jointly normal, and neither does the marginal prior model $\pi(\boldsymbol{\theta})$ [39]. In practice, whatever the prior model $\pi(\boldsymbol{\theta}, \mathbf{z}, \boldsymbol{\xi})$ is, a set of samples $(\boldsymbol{\theta}^{(l)}, \mathbf{z}^{(l)}, \boldsymbol{\xi}^{(l)})$ is to be drawn and the approximation error computed:

$$\boldsymbol{\epsilon}^{(l)} = \mathcal{A}_c(\bar{\boldsymbol{\theta}}^{(l)}, \mathbf{z}^{(l)}, \boldsymbol{\xi}^{(l)}) - A(\boldsymbol{\theta}^{(l)}, \mathbf{z}_0, \boldsymbol{\xi}_0),\ l = 1, 2, ..., N_{mc} \tag{2.4.1a}$$

$$\boldsymbol{\epsilon}^{(l)} = A(\boldsymbol{\theta}^{(l)}, \mathbf{z}^{(l)}, \boldsymbol{\xi}^{(l)}) - A(\boldsymbol{\theta}^{(l)}, \mathbf{z}_0, \boldsymbol{\xi}_0),\ l = 1, 2, ..., N_{mc} \tag{2.4.1b}$$

One should use eq.(2.4.1a) if discretization errors are to be considered, and eq.(2.4.1b) if not. Notice that, when no discretization errors are accounted for, the only distinction between models is how the distributed parameters are treated. The same can be said about using models with different physics behind them.

Finally, define $\mathbf{r}^{(l)} = [\boldsymbol{\epsilon}^{(l)}, \boldsymbol{\theta}^{(l)}]^T \in \mathbb{R}^{N_p+N_m}$, where N_p is the dimension of the parameter space and N_m is the total number of measurements. Then necessary statistics can be computed from:

$$\mathbf{r}_* = \begin{pmatrix} \boldsymbol{\epsilon}_* \\ \boldsymbol{\theta}_* \end{pmatrix} = \mathbb{E}\left[\begin{pmatrix} \boldsymbol{\epsilon} \\ \boldsymbol{\theta} \end{pmatrix}\right] \approx \frac{1}{N_{mc}} \sum_{l=1}^{N_{mc}} \mathbf{r}^{(l)} \tag{2.4.2}$$

$$\boldsymbol{\Sigma} = \begin{pmatrix} \boldsymbol{\Sigma}_{\epsilon\epsilon} & \boldsymbol{\Sigma}_{\epsilon\boldsymbol{\theta}} \\ \boldsymbol{\Sigma}_{\boldsymbol{\theta}\epsilon} & \boldsymbol{\Sigma}_{\boldsymbol{\theta}\boldsymbol{\theta}} \end{pmatrix} = \mathbb{E}\left[(\mathbf{r} - \mathbf{r}_*)(\mathbf{r} - \mathbf{r}_*)^T\right] \approx \frac{1}{N_{mc} - 1} \sum_{l=1}^{N_{mc}} (\mathbf{r}^{(l)} - \mathbf{r}_*)(\mathbf{r}^{(l)} - \mathbf{r}_*)^T \tag{2.4.3}$$

where N_{mc} is the number of Monte Carlo simulations necessary to obtain convergence[4]. For more details on Monte Carlo simulations, see reference [49].

Figure 2.1 depicts a flowchart for the general application of AEA. The upper half of the flowchart, hereby denominated *Training stage*, consists of draws of the random variables and computation of the corresponding statistics, eq.(2.4.2 - 2.4.3). This stage is done prior to actual solution procedure and, given its nature, can take advantage from parallel computation.

The *Solution stage* consists of constructing the Likelihood function, eq.(2.3.9), and solving the optimization problem for $\boldsymbol{\theta}'$.

[4] In order to guarantee a non singular sample covariance matrix: $N_{mc} > N_p + N_m$.

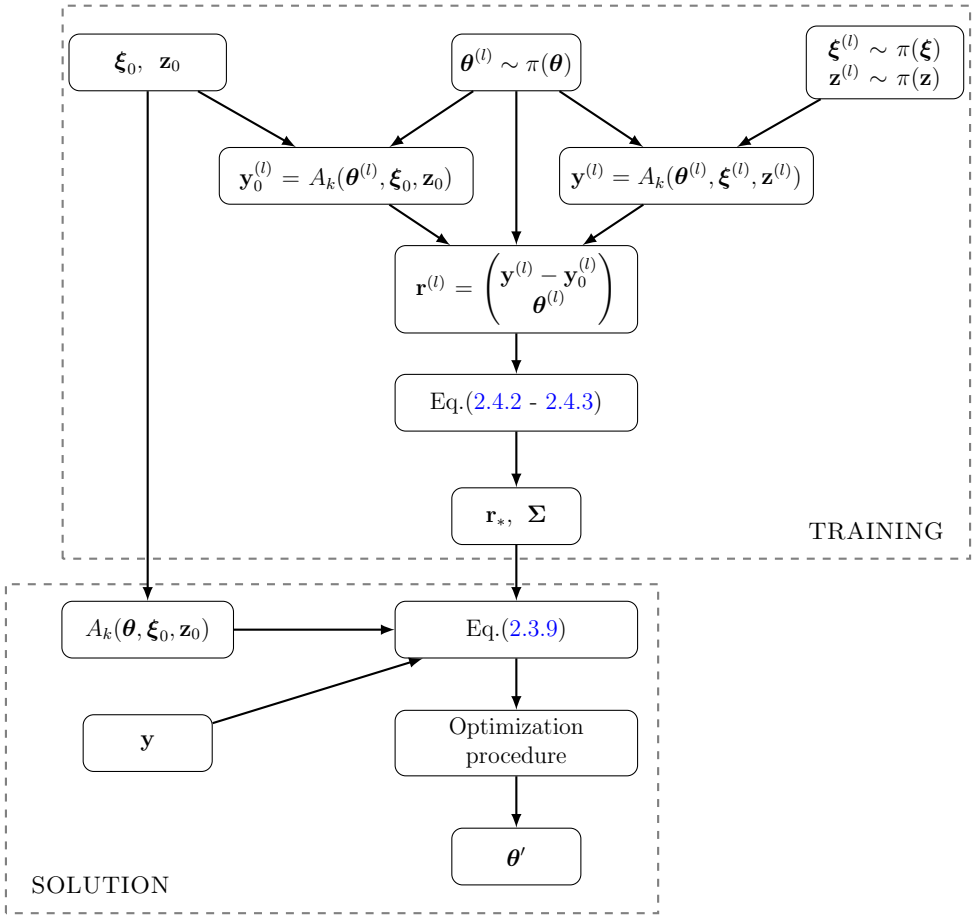

Figure 2.1: Application of the Approximation Error Approach.

Chapter 3

Case Study 1: Beam

In this chapter, the Approximation Error Approach is applied to the damage identification problem of a clamped-free beam. The inverse problem consists of identifying the distributed damage given a set of scenarios with varying degrees of stiffness of the clamped side. In this chapter, therefore, we describe some of the necessary aspects concerning the estimation problem.

We primarily chose the system proposed by RITTO *et al.* [50] due to the availability of experimental results concerning the stiffness of the clamped side. In their paper, to represent the decreasing stiffness of the clamped side, an experimental test rig was constructed where the interface between the beam and the support at the clamped side was filled with several layers of rubber patches. While RITTO *et al.* [50] did this to model deterioration of the boundary condition and subsequently identify it, the goal of this section is to use one single (not necessarily the best) forward model to identify damage given a set of *unknown* boundary conditions.

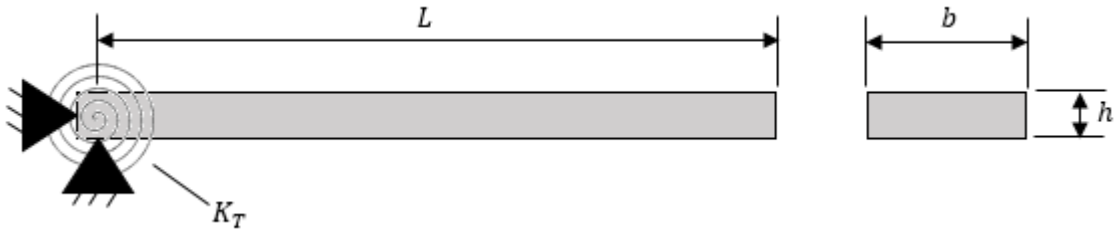

Figure 3.1: Physical model: Pinned-free beam with torsion spring.

3.1 The System

The system is modeled as shown in Fig. 3.1: assuming that one cannot ensure the clamped boundary condition in practice, the system is modeled as a beam pinned at the left side, with a torsion spring attached to the pinned end in such a way that, when taking the limit $K_t \to \infty$, the system behaves like a clamped-free beam, K_t being the torsional stiffness constant of the spring.

The beam properties and stiffness parameter, K_t, identified in [50] are given in Table 3.1.

Table 3.1: Beam Properties and identified stiffness parameter.

$L(m)$	$b(mm)$	$h(mm)$	$E_0(GPa)$	$\rho(kg/m^3)$	$K_{t,max}(Nm/rad)$
0.511	30.7	3.04	200	7850	3.8×10^3

In Table 3.1, L is the beam's length, b and h are the cross section's dimensions, E_0 and ρ are the Young's Modulus and specific mass of the material

The maximum angle of rotation caused by a bending moment M_B at the end of the beam is given by $\phi_{max} = M_B L/2EI$ [51], which results in the corresponding torsional stiffness of the beam being

$$K_{t,B} = \frac{2E_0 I}{L} \tag{3.1.1}$$

where I is the moment of inertia, which is orientation dependent.

For this system, $K_{t,B} \approx 56.3\, Nm/rad$. Therefore the identified stiffness is $K_{t,max} \approx 67.5\, K_{t,B}$. This value is not that high, which may explain why, in the next sections, both the approximation error and traditional approaches falter when $K_{t,True}$ is low – the structure should present a very low frequency first mode akin to a rigid body motion.

3.2 Direct Problem

Generally speaking, the *Direct Problem* consists of predicting system response $\mathbf{y}$ (displacements, accelerations, modal data, etc), given a set of *known* input variables $\mathbf{u}$ (prescribed displacement, external excitation, etc) and/or state variables $\mathbf{q}$ and parameters/boundary conditions $\boldsymbol{\theta}$. This is accomplished through the use of a *forward model*:

$$\mathbf{y} = \mathcal{A}_c(\mathbf{u}, \mathbf{q}, \boldsymbol{\theta})$$

In our case, given system presented in Fig. 3.1, which is modeled as an *Euler-Bernoulli* beam, with properties defined in Table 3.1, torsion spring with constant K_t fixed at some value $K_{t,True}$ or $K_{t,REF}$ and damage field model given by eq.(3.2.1), one wishes to predict its dynamic behavior $\mathbf{y}$ given an excitation $\mathbf{u}$.

Damage is assumed to be the cause of a local reduction in stiffness, this is modeled as a change in the elastic parameter E_0, at some position x along the length of the beam [17, 24, 26, 29]. It is further assumed that the damage state does not evolve during the vibration tests, thus it can be modeled as a field independent of time, as given by eq.(3.2.1). This is, in fact, an assumption about the damage mechanism.

$$E(x) = (1 - d(x))E_0 \tag{3.2.1}$$

where $d(x) : [0, L] \mapsto [0, 1]$ determines the intensity of the damage at the position x, and E_0, given in Table 3.1, is the *undamaged* value of the Young's Modulus.

In other words, one wishes to solve eq.(3.2.2) subjected to the boundary conditions eq.(3.2.3) for the displacement field $w(x,t)$ and/or its derivatives at given positions along the beam [52]. In eq.(3.2.2), inertial effects concerning rotation are not considered.

$$\rho A\ddot{w} + (EIw'')'' = F(t)\delta(x - x_F), \quad \forall t > 0, x \in (0, L) \tag{3.2.2}$$

$$w(0,t) = 0, \ -EIw''(0,t) = -K_t w'(0,t), \quad \forall t > 0 \tag{3.2.3a}$$

$$-EIw''(L,t) = 0, \ -EIw'''(L,t) = 0, \quad \forall t > 0 \tag{3.2.3b}$$

$$w(x,0) = \dot{w}(x,0) = 0, \quad \forall x \in [0, L] \tag{3.2.3c}$$

where $(\cdot)'$ and $\dot{(\cdot)}$ represent respectively the spacial and time derivatives of a given variable. The term $\delta(x - x_F)$ denotes that the force $F(t)$ acts at $x = x_F$. The force excitation present in eq.(3.2.2) is a chirp given by:

$$F(t) = F_0 sin\left(2\pi\left(\frac{t}{T_f}\Delta\omega + \omega_0\right)t\right) \tag{3.2.4}$$

where $\omega_0 = 1500\,Hz$, $\Delta\omega = 500\,Hz$, $F_0 = 1\,N$ and $T_f = 0.025\,s$. With this *linear* frequency sweep the 8th, 9th and 10th resonance frequencies and modes are excited.

Equations (3.2.2-3.2.3)are discretized using the Finite Element Method (see [53, 54]). The resulting system of ordinary differential equations (ODEs) is integrated in time using a Newmark-β Method (see reference [52]) with the appropriate time step $\Delta t = 10^{-5}\,s$. The algorithm is reproduced in Fig. 3.2.

The Rayleigh model was used to construct the damping matrix, that is

$$\mathbf{D} = c_1\mathbf{M} + c_2\mathbf{K} \tag{3.2.5}$$

where $\mathbf{M}$ and $\mathbf{K}$ are respectively the mass and stiffness matrices obtained from the FE model and the proportionality constants are set as $c_1 = 10^{-4}s^{-1}$ and $c_2 = 10^{-8}s$.

This sequence of operations defines the *forward model* $A(\cdot)$, and any corresponding accurate ones, denoted by $\mathcal{A}_c(\cdot)$.

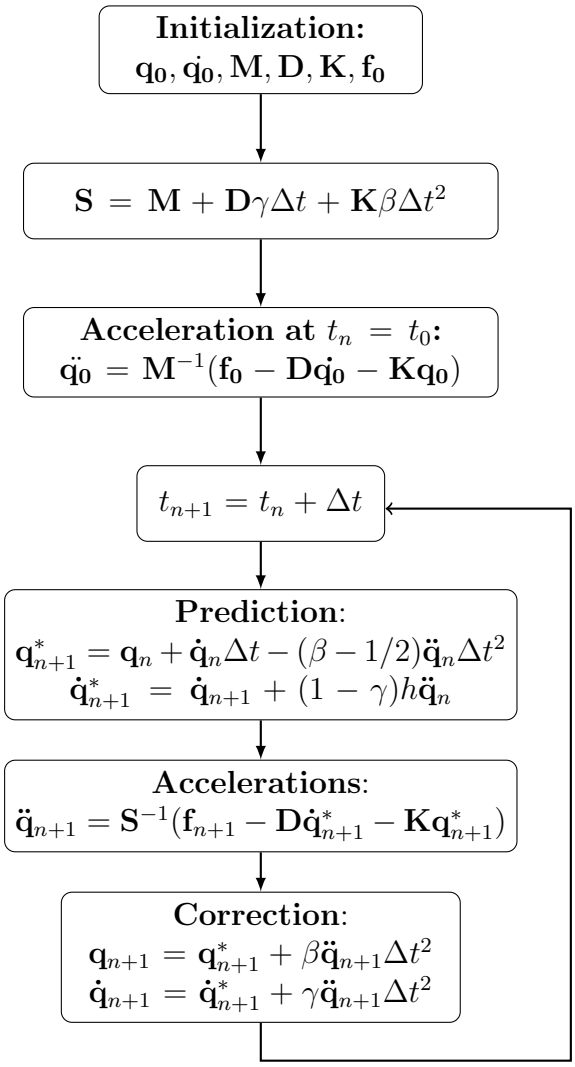

Figure 3.2: Flowchart: Newmark Integration Scheme for Linear Time Invariant (LTI) System. For LTI systems integrated using constant time step Δt, $\mathbf{S}$ is constant, thus its inverse $\mathbf{S}^{-1}$ can be stored to save time. In particular, the method was programmed considering the average acceleration ($\gamma = 1/2$ and $\beta = 1/4$) over the time interval $[t_n, t_{n+1}]$. The method is based upon the solution of three coupled equations for $\ddot{\mathbf{q}}_{n+1}$, $\dot{\mathbf{q}}_{n+1}$ and $\mathbf{q}_{n+1}$, and for efficiency the algorithm is organized in two steps, where the prediction step consists of an extrapolation of the solution at t_n when the acceleration at t_{n+1} is zero, $\ddot{\mathbf{q}}_{n+1} = \mathbf{0}$ [52].

3.3 Inverse Problem

As for the *Inverse Problem*, given a set of measurement data $\bar{\mathbf{y}}$ and input variables $\mathbf{u}$, one seeks information about *unknown* parameters and/or boundary conditions $\boldsymbol{\theta}$. Given the ill-posedness of the inverse problem, one usually seeks to find the set estimate $\boldsymbol{\theta}'$ that minimizes the discrepancy between the experimental data and the predicted response.

In our case, the measurement set $\bar{\mathbf{y}}$ consists of acceleration data gathered with an array of sensors distributed uniformly along the beam. Given this data, we seek to estimate the damage field $d(x)$ given by eq.(3.2.1) using a forward model that is *not necessarily correct* in terms of its boundary conditions.

The field $d(x)$ is a function defined along the length of the beam which can assume a wide variety of shapes. In this text, however, a *localized* damage is estimated and for such a specific parametrization is proposed, eq.(3.3.1), in order to reduce the dimension of the parameter space. The proposed bell shaped curve is a continuous unimodal damage field. We are well aware of the limitations imposed by this parametrization in regard to damage estimation, however this dissertation's goal is to present the Approximation Error Approach in the SHM context. This strategy was proved amenable for our applications.

$$d(x) = dam \exp\left\{ -\left(\frac{x_a - x_c}{2s} \right)^2 \right\};\ x_a = x/L; \tag{3.3.1}$$

The parameters to be estimated are

- x_c is the dimensionless position at which the damage intensity is maximum
- $dL = 6s$, the support of the field such that $d(x_c \pm 3s) \approx 0.01\, dam$
- dam, maximum intensity of damage

where s is a dummy parameter that relates dL to the dispersion of the bell function.

Following these definitions, the parameter space is the subset of $\mathbb{R}^3$ given by the cube $\Omega_P = [0,1] \times [0,1] \times [0,1]$[1]. The inverse problem is then solved by finding the set of parameters $\boldsymbol{\theta}' = (x_c', dL', dam')^T$ that is the solution of the minimization problem:

$$\boldsymbol{\theta}' = arg\min_{\boldsymbol{\theta} \in \Omega_P} V(\boldsymbol{\theta}) \tag{3.3.2}$$

where $V(\boldsymbol{\theta})$ is some functional, given either by equations (2.2.7) or (2.3.9b-2.3.9d), that is, Least Squares or AEA.

[1] There is no practical advantage to search for $dL \in \mathbb{R}^+$, thus the search space for $d\ell$ is such that $dL \in [0,1]$

Chapter 4

Case Study 2: Plate

In this chapter, we aim to apply both the Traditional Least-Squares and Approximation Error approaches to the problem of a simply supported aluminum plate under various conditions. Therefore, we describe some of the necessary aspects concerning the estimation problem.

4.1 The System

The computational model presented here mimics an experimental assembly,found at the *Laboratório de Análise Dinâmica e Processamento de Imagens e Sinais* (LADEPIS) located within the *Laboratório de Estruturas e Materiais Professor Lobo Carneiro* (LABEST/COPPE) at the Universidade Federal do Rio de Janeiro (UFRJ), in Rio de Janeiro, Brazil. The isotropic aluminum plate has properties given in Table 4.1.

Table 4.1: Plate Properties.

$L_X(m)$	$L_Y(m)$	$h(mm)$	$E_0(GPa)$	ν	$G_0(GPa)$	$\rho_0(kg/m^3)$
2.25	1.65	5.0	69	0.33	$0.5\,E_0/(1+\nu)$	2725

In Table 4.1, L_X and L_Y are the plate's dimensions, h is its thickness, E_0, G_0, ν are its material's elastic parameters and ρ the specific mass.

This assembly was used by DA COSTA [55] in an investigation on passive damping systems.

Given the slight differences between in pressure from one screw to the next, it is possible for an effectively non-uniform distribution of stiffness to arise in this assembly. Although the characterization of this *field* of distributed stiffness is not of interest, knowledge of its structure is essential to the inverse problem when this is solved by the traditional approach (to be seen in Section 5.3.3).

4.2 First Order Shear Deformation Theory

The plate is modeled following the Mindlin–Reissner Plate Theory, also known as First Order Shear Deformation Plate Theory (FSDT) (see [56]), which takes into account shear deformations through the thickness of the plate.

According to this theory, the equations of motion of a plate subjected to a load q, resting over an elastic bedding with elastic constant k, for all $\mathbf{x} \in \Omega$, are:

$$0 = N_{xx,x} + N_{xy,y} - I_0\ddot{u}_0 - I_1\ddot{\phi}_x \tag{4.2.1a}$$

$$0 = N_{xy,x} + N_{yy,y} - I_0\ddot{v}_0 - I_1\ddot{\phi}_y \tag{4.2.1b}$$

$$0 = Q_{x,x} + Q_{y,y} - kw_0 + \mathcal{N} + q - I_0\ddot{w}_0 \tag{4.2.1c}$$

$$0 = M_{xx,x} + M_{xy,y} - Q_x - I_2\ddot{\phi}_x - I_1\ddot{u}_0 \tag{4.2.1d}$$

$$0 = M_{xy,x} + M_{yy,y} - Q_y - I_2\ddot{\phi}_y - I_1\ddot{v}_0 \tag{4.2.1e}$$

$$\mathcal{N} = \partial_x(N_{xx}\partial_x w_0 + N_{xy}\partial_y w_0) + \partial_y(N_{xy}\partial_x w_0 + N_{yy}\partial_y w_0) \tag{4.2.1f}$$

Whose *Essential Boundary Conditions* are, for all $\mathbf{x} \in \Gamma_u$:

$$u_0 - \hat{u}_0 = 0,\ v_0 - \hat{v}_0 = 0,\ w_0 - \hat{w}_0 = 0,\ \phi_x - \hat{\phi}_x = 0,\ \phi_y - \hat{\phi}_y = 0 \tag{4.2.2}$$

And the *Natural Boundary Conditions* are, for all $\mathbf{x} \in \Gamma_t$:

$$N_{nn} - \hat{N}_{nn} = 0,\ N_{ns} - \hat{N}_{ns} = 0,\ Q_n - \hat{Q}_n = 0,\ M_{nn} - \hat{M}_{nn} = 0,\ M_{ns} - \hat{M}_{ns} = 0 \tag{4.2.3}$$

where Ω, Γ_u and Γ_t denote respectively the domains corresponding to the plate's middle plane ($z = 0$) and the different (non intersecting) boundaries of the plate at which essential and natural boundary conditions are applied, $\partial\Omega = \Gamma$, $\Gamma_u \cup \Gamma_t = \Gamma$ and $\Gamma_u \cap \Gamma_t = \{\varnothing\}$.

In equations (4.2.1-4.2.3), u_0, v_0 and w_0 denote the displacements in the x-, y- and z- directions of a point at the middle plane, and $\phi_x = \partial_z u$ and $\phi_y = \partial_z v$ are the rotations of a transverse normal about the y- and x- axes such that the shear deformations are $\gamma_{\alpha z} = \partial_\alpha w_0 + \phi_\alpha$, see Fig. 4.1.

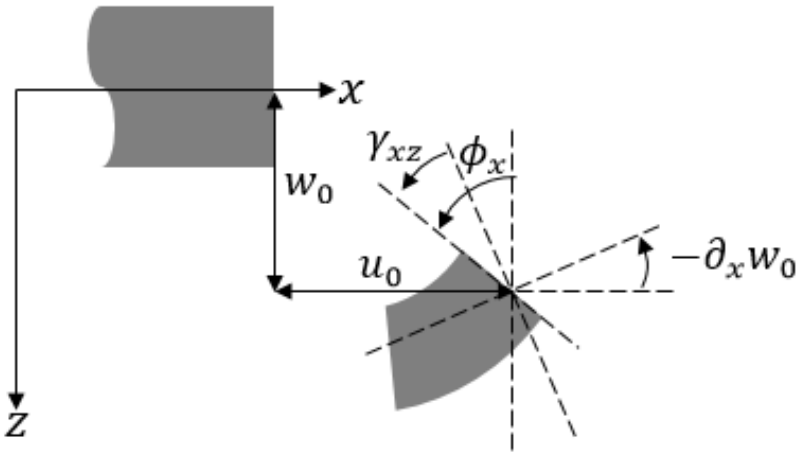

Figure 4.1: Undeformed and deformed geometries of an edge under the assumptions of the FSDT.

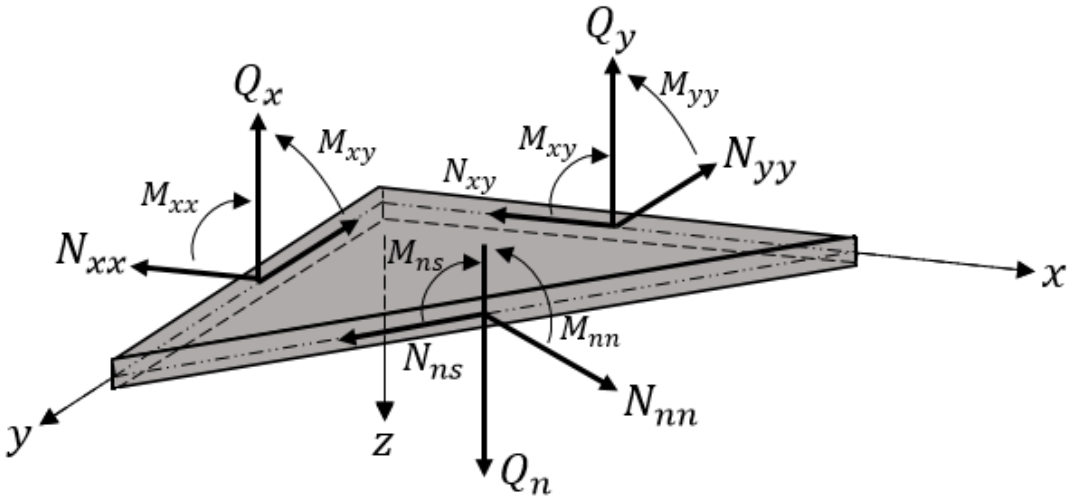

Figure 4.2: Thickness-integrated forces and moments.

$M_{\alpha\beta}$, $N_{\alpha\beta}$ and $Q_{\alpha\beta}$ are the thickness-integrated forces and moments, defined in eq.(4.2.4), that result from internal stresses $\bar{\sigma}_{xx}$, $\bar{\sigma}_{yy}$, $\bar{\sigma}_{xz}$, $\bar{\sigma}_{yz}$ and $\bar{\sigma}_{xy}$, see Fig. 4.2. Prescribed values of these quantities are denoted by $(\hat{\bullet})$.

$$\begin{pmatrix} N_{xx} \\ N_{yy} \\ N_{xy} \end{pmatrix} = \int_{-h/2}^{h/2} \begin{pmatrix} \bar{\sigma}_{xx} \\ \bar{\sigma}_{yy} \\ \bar{\sigma}_{xy} \end{pmatrix} dz \tag{4.2.4a}$$

$$\begin{pmatrix} M_{xx} \\ M_{yy} \\ M_{xy} \end{pmatrix} = \int_{-h/2}^{h/2} \begin{pmatrix} \bar{\sigma}_{xx} \\ \bar{\sigma}_{yy} \\ \bar{\sigma}_{xy} \end{pmatrix} z dz \tag{4.2.4b}$$

$$\begin{pmatrix} Q_x \\ Q_y \end{pmatrix} = K_s \int_{-h/2}^{h/2} \begin{pmatrix} \bar{\sigma}_{xz} \\ \bar{\sigma}_{yz} \end{pmatrix} dz \tag{4.2.4c}$$

I_0, I_1 and I_2 are thickness integrated inertia parameters. It follows, from eq.(4.2.5), that for a symmetric distribution of ρ with respect to the $x-y$ plane $I_1 = 0$, and thus the equations of motion for u_0 and v_0 are decoupled from those of w_0, ϕ_x and ϕ_y.

$$\begin{pmatrix} I_0, & I_1, & I_2 \end{pmatrix} = \int_{-h/2}^{h/2} \begin{pmatrix} 1, & z, & z^2 \end{pmatrix} \rho(x,y,z) dz \tag{4.2.5}$$

The values in local and global coordinates are related through:

$$Q_n = n_x Q_x + n_y Q_y + (\hat{N}_{xx}\partial_x w_0 + \hat{N}_{xy}\partial_y w_0) n_x + (\hat{N}_{xy}\partial_x w_0 + \hat{N}_{yy}\partial_y w_0) n_y \tag{4.2.6a}$$

$$\begin{pmatrix} \phi_x \\ \phi_y \end{pmatrix} = \begin{pmatrix} n_x & -n_y \\ n_y & n_x \end{pmatrix} \begin{pmatrix} \phi_n \\ \phi_s \end{pmatrix}, \tag{4.2.6b}$$

$$\begin{pmatrix} N_{nn} & M_{nn} \\ N_{ns} & M_{ns} \end{pmatrix} = \begin{pmatrix} n_x^2 & n_y^2 & 2n_x n_y \\ -n_x n_y & n_x n_y & n_x^2 - n_y^2 \end{pmatrix} \begin{pmatrix} N_{xx} & M_{xx} \\ N_{yy} & M_{yy} \\ N_{xy} & M_{xy} \end{pmatrix} \tag{4.2.6c}$$

where n_x and n_y are the components of the outward unity normal $\mathbf{n}$ to the boundary in the x- and y- positive directions, and n- and s- are local coordinates such that the positive direction of $\mathbf{n}$ is n-, and s- is the tangential direction following the right-hand rule.

$M_{\alpha\beta}$, $N_{\alpha\beta}$ and $Q_{\alpha\beta}$ are related to the displacements through the constitutive equations

$$\begin{pmatrix} Q_x \\ Q_y \end{pmatrix} = K_s \begin{pmatrix} A_{55} & 0 \\ 0 & A_{44} \end{pmatrix} \begin{pmatrix} w_{0,x} + \phi_x \\ w_{0,y} + \phi_y \end{pmatrix} \tag{4.2.7a}$$

$$\begin{pmatrix} N_x \\ N_y \\ N_{xy} \end{pmatrix} = \begin{pmatrix} A_{11} & A_{12} & 0 \\ A_{12} & A_{22} & 0 \\ 0 & 0 & A_{66} \end{pmatrix} \begin{pmatrix} u_{0,x} + \frac{1}{2}(w_{0,x})^2 \\ v_{0,y} + \frac{1}{2}(w_{0,y})^2 \\ u_{0,y} + v_{0,x} + w_{0,x}w_{0,y} \end{pmatrix} \tag{4.2.7b}$$

$$\begin{pmatrix} M_x \\ M_y \\ M_{xy} \end{pmatrix} = \begin{pmatrix} D_{11} & D_{12} & 0 \\ D_{12} & D_{22} & 0 \\ 0 & 0 & D_{66} \end{pmatrix} \begin{pmatrix} \phi_{x,x} \\ \phi_{y,y} \\ \phi_{x,y} + \phi_{y,x} \end{pmatrix} \tag{4.2.7c}$$

which are the constitutive equations for an orthotropic material with principal materials axes (x_1, x_2, x_3) coinciding with the plate coordinates (x, y, z).

For a plate made up of *only one layer*, we have:

$$A_{11} = \frac{E_1 h}{1 - \nu_{12}\nu_{21}}, \qquad A_{22} = \frac{E_2 h}{1 - \nu_{12}\nu_{21}}, \qquad A_{12} = A_{21} = \nu_{12} A_{22} \tag{4.2.8a}$$

$$D_{11} = A_{11}\frac{h^2}{12}, \qquad D_{22} = A_{22}\frac{h^2}{12}, \qquad D_{12} = D_{21} = A_{12}\frac{h^2}{12} \tag{4.2.8b}$$

$$A_{55} = G_{13} h, \qquad A_{44} = G_{23} h \tag{4.2.8c}$$

$$A_{66} = G_{12} h \qquad D_{66} = A_{66}\frac{h^2}{12} \tag{4.2.8d}$$

where K_s is the shear correction factor used to corrected the strain energy predicted from the FSDT. The value of $K_s = 5/6$ proposed by Reissner was chosen.

4.3 Direct Problem

Given an isotropic aluminum plate with properties and dimensions defined in Table 4.1, one wishes to find the acceleration response $\mathbf{y}$ given an excitation $\mathbf{u}$, which corresponds to the two consecutive impacts, and auxiliary parameters $\boldsymbol{\theta}$, which correspond to the damage field $d(\mathbf{x})$.

Damage is assumed to be the cause of a local reduction in stiffness, this is modeled as a change in the elastic parameter, E_0, at some position $\mathbf{x}$ over the area of the plate [17, 24, 26, 29]. It is further assumed that the damage state does not evolve during the vibration tests, thus it can be modeled as a field independent of time, as given by eq.(4.3.1).

$$E(\mathbf{x}) = (1 - d(\mathbf{x}))E_0 \tag{4.3.1}$$

The function $d(\mathbf{x}) : \mathbf{x} \in \Omega \subseteq \mathbb{R}^2 \mapsto [0, 1]$ determines the intensity of the damage at the position $\mathbf{x} = (x, y) \in \Omega$, where Ω is the domain of the plate and E_0, given in Table 4.1, is the *undamaged* value of the Young's Modulus.

The *decoupled* system of equations (4.2.1c-4.2.1e) is solved using the Finite Element Method [53, 56], considering only linear terms and no axial loads ($\mathcal{N} = 0$). The discretization used was a mesh composed of quadrilateral linear elements with linear interpolation of geometry, each element with 4 nodes and 3 degrees of freedom per node (see Appendix A for details about Neumann boundary conditions). The resulting system of ODEs is integrated using a Newmark-β Method with the appropriate time step $\Delta t = 10^{-5}\, s$ (see Fig. 3.2 and referece [52] for details).

The damping matrix is constructed in accordance to eq.(3.2.5), with proportionality constants $c_1 = 10^{-3}\, s^{-1}$ and $c_2 = 10^{-6}\, s$.

To sum up, the forward model is the solution of the computational model correspondent to the finite element discretization of eq.(4.2.1), with constitutive properties equations given by eq.(4.2.7-4.2.8) for an isotropic aluminum plate with properties given in Table 4.1, subjected to boundary conditions given by eq.(4.2.2-4.2.3) for a simply supported case[1], given a particular excitation (input data) of the correspondent physical system.

The selected feature is the acceleration response collected for $T = 0.050\, s$, the excitation being two consecutive impacts, similar to what is found in reference [29], occurring at $t = 0.0\, s$ and $t = 0.025\, s$[2].

[1] With the addition of torsional springs to simulate the boundary fixation.

[2] There's marginal improvement in comparison with results obtained using a single impact. Most of the improvement in the inverse solution was due to an increased time interval.

4.4 Inverse Problem

As for the *Inverse Problem*, given a set of acceleration measurements $\mathbf{y}$ and input variables $\mathbf{u}$, one seeks information about *unknown* parameters $\boldsymbol{\theta}$ corresponding to the structure's damage field $d(\mathbf{x})$ given by eq.(4.3.1) using the forward model previously described.

The field $d(\mathbf{x})$ is a function defined over the area of the plate which can assume a wide variety of shapes. In this chapter, however, a *localized* damage is estimated and for such the procedure given in Chapter 3 is followed, that is, the field is parameterized in order to reduce the dimension of the parameter space. The proposed bell shaped curve, given in eq.(4.4.1), is a continuous unimodal damage field. We are well aware of the limitations imposed by this parametrization in regard to damage estimation, however this strategy was proved amenable for our applications.

$$a = \cos(\theta)^2/(2\sigma_x^2) + \sin(\theta)^2/(2\sigma_y^2) \tag{4.4.1a}$$

$$b = \sin(2\theta)/(4\sigma_y^2) - \sin(2\theta)/(4\sigma_x^2) \tag{4.4.1b}$$

$$c = \sin(\theta)^2/(2\sigma_x^2) + \cos(\theta)^2/(2\sigma_y^2) \tag{4.4.1c}$$

$$d(\mathbf{x}, \boldsymbol{\theta}) = D \exp\left\{ - \left[a(x - x_0)^2 + 2b(x - x_0)(y - y_0) + c(y - y_0)^2 \right] \right\} \tag{4.4.1d}$$

Where the parameters $\boldsymbol{\theta}$ are

- D is the maximum intensity of damage
- x_0 and y_0 are the coordinates at which the damage intensity is maximum
- σ_x and σ_y are related to the support of the field
- θ is related to the correlation between x- and y- directions, measured from $+y$

Following these definitions, the parameter space is the set $\Omega_P \subset \mathbb{R}^6$, with $\Omega_P = \{\boldsymbol{\theta} \in \mathbb{R}^6 \,|\, \boldsymbol{\theta} \in [0, 1] \times [0, L_X] \times [0, L_Y] \times [0, L_X] \times [0, L_Y] \times [0, \pi/2]\}$[3].

The inverse problem is then solved by finding the set of parameters $\boldsymbol{\theta}' = (D', x_0', y_0', \sigma_x', \sigma_y', \theta')^T$ that is the solution of a minimization problem similar to (3.3.2), here repeated for convenience:

$$\boldsymbol{\theta}' = arg\min_{\boldsymbol{\theta} \in \Omega_P} V(\boldsymbol{\theta})$$

Where $V(\boldsymbol{\theta})$ is some functional relating the parameters to the measurement data.

[3] There is no practical reason to set $(\sigma_x, \sigma_y) \in \mathbb{R}^+ \times \mathbb{R}^+$, thus they are limited to $(\sigma_x, \sigma_y) \in [0, L_X] \times [0, L_Y]$ instead.

Chapter 5

Results

This chapter consists of a series of numerical experiments regarding the application of the Approximation Error Approach in comparison with the Traditional Least Squares. In all of these experiments, the approximation error is calculated in accordance with eq.(2.4.1b) and the related statistics are calculated as indicated in eq.(2.4.2-2.4.3).

All dimensional quantities are in their respective SI units.

5.1 Particularities of The Inverse Problem

The output of a forward model is collected at specific nodes and concatenated in a column-stack fashion to construct $\mathbf{y}$, the output vector. The output data of the model at the nodes corresponding to positions x_S from the N_s sensors are concatenated vertically: $\mathbf{y} \in \mathbb{R}^{N_m \times 1}$, $N_m = \sum_{i=1}^{N_s} N_i$.

$$\mathbf{y} = (\mathbf{y}_1^T, \cdots, \mathbf{y}_i^T, \cdots, \mathbf{y}_{N_s}^T)^T, \quad \mathbf{y}_i = (y_{i,1}, \cdots, y_{i,j}, \cdots, y_{i,N_i})^T$$

where every sensor i provides a vector $\mathbf{y}_i$ containing N_i measurements.

Concerning the *synthetic* measurement data, $\bar{\mathbf{y}}$ is generated by adding uncorrelated Gaussian noise with zero mean to an ideal response $\mathbf{y}^{ideal}$, which is obtained integrating the resulting system ODEs of a reference structure, with a given damage profile, specified by different scenarios within Sections 5.2 and 5.3.

For each sensor i an ideal response $\mathbf{y}_i^{ideal}$ is polluted as follows:

$$\bar{\mathbf{y}}_i = \mathbf{y}_i^{ideal} + \mathbf{e}_i, \quad \mathbf{e}_i \sim \mathcal{N}(\mathbf{0}, \sigma_i^2 \mathbf{I}_{N_i \times N_i}), \quad \sigma_i = 0.05 \max(\mathbf{y}_i^{ideal}).$$

The measurement covariance matrix is

$$\mathbf{W}_e = \mathrm{diag}(\boldsymbol{s});$$

where $\mathbf{s}$ is constructed in accordance to $\mathbf{y}$:

$$\sigma_i = 0.05 \max_j ((\mathbf{y}_i^{ideal})_j) \rightarrow \boldsymbol{s}_i = \sigma_i^2 \underbrace{(1, \cdots, 1)}_{1 \times N_i} \rightarrow \boldsymbol{s} = \underbrace{(\boldsymbol{s}_1, \cdots, \boldsymbol{s}_{N_s})}_{1 \times N_m \text{ vectors}}.$$

5.1.1 Beam Structure

Eight acceleration sensors are placed over the beam, each sensor collecting $N_i = 251$ measurements at a sampling frequency $f_s = 10^4\ Hz$, resulting in a total of $N_m = 2008$ measurements. Sensors are placed at the following positions:

$$x_S = (0.125, 0.250, 0.375, 0.500, 0.625, 0.750, 0.875, 1)\ L.$$

Figure 5.1 presents both a typical set of synthetic measurements corresponding to the sensor at $x_S = L$ and ideal responses of the correspondent damaged and undamaged structures for a beam with a free end and $K_{t,True} = K_{t,max}$ being excited by a chirp at $x_F = 0.95\,L$. For the damaged structure the parameters used to build the damage field, eq.(3.2.1), are $x_c = 0.5$, $dL = 0.1$ and $dam = 0.2$.

The measurements are compared to the true response of the damaged structure and to the response of an undamaged structure. Notice how, for (relatively) low frequencies ($t < 0.005\,s$), there is little to no difference between the acceleration responses of both structures, this is consistent with what is found in literature regarding the effects of damage being only truly important at high frequencies.

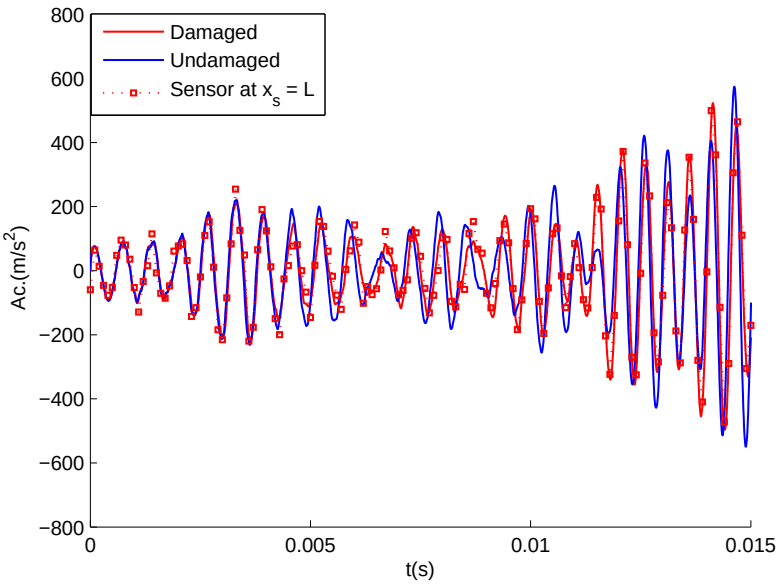

Figure 5.1: Ideal excitation response at $x_S = L$ of damaged and undamaged structures and synthetic measurements corresponding to the damaged case.

5.1.2 Plate Structure

Four acceleration sensors are placed at uniformly spaced locations over the plate, Fig. 5.2. Where every sensor provides a vector containing $N_i = 501$ measurements over a period of $T = 0.050\,s$, which is consistent with the sampling frequency $f_s = 10^4\ Hz$, resulting in a total of $N_m = 2004$ measurements. The system of ODEs resulting from the FE discretization is integrated using a time step $\Delta t = 10^{-5} s$.

For convenience, define a variable $\ell_{\min}$ which is the minimum length of the plate: $\ell_{\min} \equiv \min(L_X, L_Y)$.

The optimization problems using a Particle Swarm Optimization algorithm (see [15, 57–59]). Results are obtained from an *ad hoc* strategy, in order to improve the estimation process of the parameters with lower sensitivity, $(\sigma_x, \sigma_y, \theta)$, which are related to the support of the damage field. The estimation process consists of firstly identifying the damage's central position, then correcting intensity and support, while allowing small variations on the position. The strategy is divided in two steps as follows:

1 Identify location – search for $\boldsymbol{\theta}'_1 = (D', x'_{0,1}, y'_{0,1})$ with $\boldsymbol{\theta}_2 = (\sigma_x, \sigma_y, \theta)$ fixed at $\boldsymbol{\theta}'_2 = (0.05\ell_{\min}, 0.05\ell_{\min}, 0)$.

2 Reinitialize – search for $\boldsymbol{\theta}'$ while limiting the parameter space for (x_0, y_0): $(x'_0, y'_0) \in [x'_{0,1} - 0.05\ell_{\min}, x'_{0,1} + 0.05\ell_{\min}] \times [y'_{0,1} - 0.05\ell_{\min}, y'_{0,1} + 0.05\ell_{\min}]$

In doing this, we are able to establish a baseline with which to compare the performance of the AEA.

Also, in order to obtain results in a timely manner, model reduction was implemented. The Improved Reduced System (IRS) method[1] was used in *all* of the inverse analyses presented in the next section. See reference [60] or Appendix B for details. Figure 5.2 shows a mesh of 20×20 elements, this mesh contains a total of 1323 degrees of freedom, while the reduced one has 558, a reduction of almost 60%.

[1] This technique was chosen due to the fact that it produces better results when compared to *Static Condensation*, with the advantage of *not being* an iterative procedure.

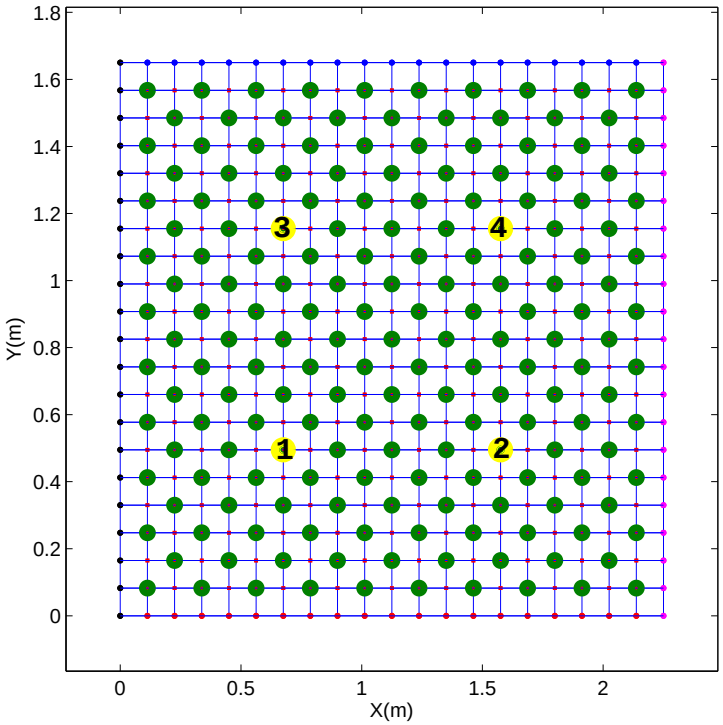

Figure 5.2: Mesh (20×20): nodes for model reduction and sensors. Sensors are presented in yellow. Primary nodes are colored green. Number of degrees of freedom: 1323 without model reduction, 558 with model reduction.

5.1.3 Concerning the Solution of the Inverse Problem

The optimization problems are solved by means of Particle Swarm Optimization [15, 57–59], which is a global search heuristic algorithm. In the definition of this algorithm, there are parameters related to the total number of global iterations, the *number of generations*, and the number of evaluations of the objective function per iteration, the *number of particles*. At each generation, the parameter space is surveyed by the particles, and the best one is chosen, which carries a weight that influences the behavior of the others.

The classic implementation of the PSO allows one to specify the parameter space by defining lower and upper boundaries for parameter values, thus the parameter constraints defined in Sections 3.3 and 4.4 can be easily introduced in the optimization algorithm.

The implemented scheme of PSO is based upon the one described by NAPOLES *et al.* [58], whose proposed algorithm uses techniques to detect and deal with premature convergence. In regards to the specifics of the execution, a maximum of 80 generations was set. Each generation used a total of 47 particles[2].

[2] Value found by means of meta-optimization of the PSO algorithm by PEDERSEN [59].

5.2 Results 1: Beam Structure

Within this section, different scenarios are specified by the believed quality of the fixation on the clamped side, determined by the value of the spring's stiffness coefficient $K_t = K_{t,True}$. For each of these scenarios, synthetic measurement data is generated from an ideal structure with given $K_t = K_{t,True}$ and the inverse problem is solved for the identification of the damage field using both the AEA and the Traditional Least Squares.

5.2.1 Benchmark Problem

Figure 5.3 shows a rectangular damage field (with dimensions $dL \times dam$, centered at x_c) and estimated fields using both approaches without any sort of modeling errors associated. This rectangular field was chosen in order to avoid an inverse crime, and, while the proposed parametrization is unable to to recover the actual field, notice that both approaches give similarly satisfactory results, in the absence of modeling errors.

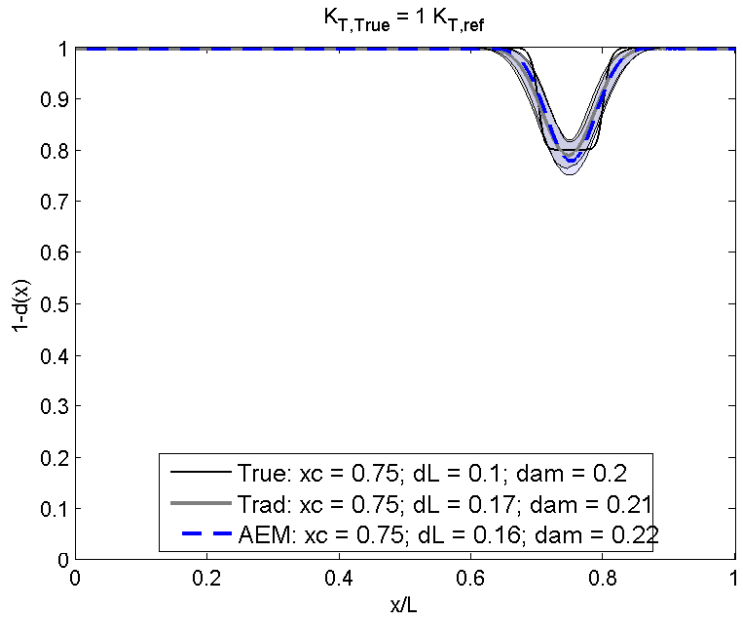

Figure 5.3: Damage field estimated both the AEA and least-squares approach when no sources of error are included, that is $K_{t,True} = K_{t,REF}$ and $x_{F,True} = x_{F,REF}$.

5.2.2 Parameters for the AEA

Going forward, we associate the parameters x_c, dL, dam to their respective random variables X_c, $d\mathcal{L}$, $\mathcal{D}$.

In order to apply the AEA, the necessary statistics of the approximation error have to be computed. To that end, consider $N_{mc} = 10^4$ samples of $\boldsymbol{\theta}^{(l)} = (X_c^{(l)}, d\mathcal{L}^{(l)}, \mathcal{D}^{(l)})^T$ drawn from the following distributions:

- $X_c \sim \mathcal{U}[0.1, 0.9]$
- $d\mathcal{L} \sim \mathcal{U}[0.1, 0.25]$
- With 20% probability: generate an undamaged structure, $D = 0$. Otherwise $D \neq 0$, drawn $\mathcal{D}$ from $\mathcal{D} \sim \mathcal{U}[0.05, 0.4]$.

where $\mathcal{U}[a, b]$ denotes the uniform distribution with non-zero support in $[a, b]$.

This value of 20% was completely arbitrary. No further investigations about how different ratios of undamaged to damage training data can affect the AEA.

Statistics concerning the parameter $\boldsymbol{\xi}^{(l)}$ to be premarginalized, whether it represents either the torsional constant $K_t^{(l)}$ or the position of applied excitation $X_F^{(l)}$ or both, must also be computed.

In Section 5.2.3 we consider the effects of errors due only to incorrect modeling of K_t, in Section 5.2.4 only errors due to the position of applied excitation are considered, and finally in Section 5.2.5 both errors are considered. Reference values for K_t and x_F are $K_{t,REF} = 3800\,Nm/rad = 67.5\,K_{t,B}$ and $x_{F,REF} = 0.95L$, respectively. Samples of the corresponding random variables are drawn from:

- $K_t \sim \mathcal{N}(\mu_K = K_{t,REF}, \sigma_K^2) \times \mathbb{1}_{\mathbb{R}^+}[Nm/rad]$
- $X_F \sim \mathcal{N}(\mu_F = x_{F,REF}, \sigma_F^2) \times \mathbb{1}_{[0,L]}[m]$

where $\mathbb{1}_\Omega$ indicates the distribution's non-zero probability support is the domain Ω.

Where $\sigma_K = 0.0834\,\mu_K$ is such that $P(0.75\mu_K < K_t < 1.25\mu_K) > 99\%$[3]. Figure 5.4 shows the proposed gaussian PDF for K_t as well as the tested values of K_t presented in Section 5.2.3.

Analogously, $P(|X_F - \mu_F| < 3\sigma_F) > 99\%$[4]. That is, there is an envelope of $6\sigma_F \approx 5.2mm$ in length ($\approx 1\%L$) in which the chirp, eq.(3.2.4), can be applied. Equivalently, $\sigma_F = 0.0017L = 0.87mm$.

[3] The value of σ_K was chosen based on a Gaussian distribution with support $\mathbb{R}$.
[4] The value of σ_F was chosen based on a Gaussian distribution with support $\mathbb{R}$.

The term $\|\boldsymbol{\Gamma}_{\boldsymbol{\theta}}(\boldsymbol{\theta}-\boldsymbol{\theta}_*)\|^2$ in eq.(2.3.9b) is related to the *prior* distribution of the parameters, acting as a regularization term for the solution of the inverse problem. If this term is large compared to $\|\boldsymbol{\Gamma}_{\nu|\boldsymbol{\theta}}(\mathbf{y} - A(\boldsymbol{\theta}, \mathbf{z}_0, \xi_0) - \boldsymbol{\nu}_{*|\boldsymbol{\theta}})\|^2$, the solution to the minimization problem will seek to satisfy $\boldsymbol{\theta}' \to \boldsymbol{\theta}_*$, which is the effect of prior information on the parameters. Therefore, in the following sections, the parameters related to the definition of the *prior* in the AEA are fixed to

$$\boldsymbol{\theta}_* = (0.5, 0.5, 0.5)^T, \quad \boldsymbol{\Sigma}_{\boldsymbol{\theta}\boldsymbol{\theta}} = 0.75\ \mathbf{I}_{3\times 3}$$

in order to ***reproduce*** a non informative prior (see [11, 12]). In doing this, we hope to not give any unfair advantages to the AEA in comparison with the Traditional least squares, which ***does not*** benefit from prior information.

Although one could include in the present analysis variations from the reference values of the Young's modulus E_0, the specific mass ρ, the dimensions of the beam L, h, b, etc., in this section, there are no parameters corresponding to $\mathbf{z}^{(l)}$ or $\mathbf{z}_0$[5], eq.(2.3.2). In Section 5.3.4 we consider such application.

It should be noted that, while using the simplified model $A(\cdot)$ in *conjunction with* the AEA for the inversion process may at times be advantageous, this model is still an erroneous one. The AEA is expected to correct model predictions for the situations considered in the training stage, however outside such conditions it should have no effect over the predictions of $A(\cdot)$.

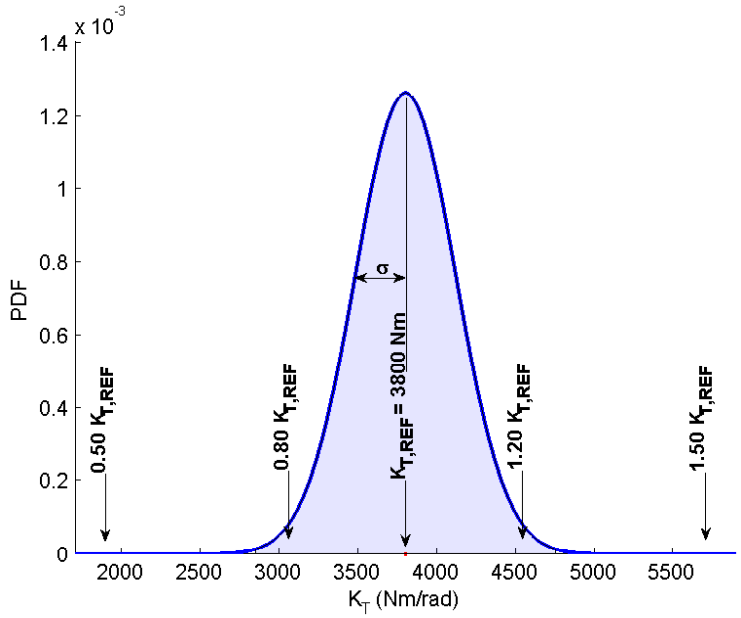

Figure 5.4: Proposed PDF for marginalization of K_t. The values of $K_{t,True}$ tested in Section 5.2.3 are indicated by arrows.

[5] Alternatively speaking, setting a reference value $\mathbf{z}_0$ is equivalent to sample $\mathbf{z}^{(l)} \sim \delta(\mathbf{z} - \mathbf{z}_0)$.

5.2.3 Uncertain Torsional Stiffness

This section presents results concerning the solution of the inverse problem, that is, the estimated damage field, in a scenario with unknown boundary conditions corresponding to the quality of "clamped" side – simulated by different values of $K_{t,True}$. The modeling error arises from an erroneous assumption on a model parameter, in this case such parameter could have been introduced in the estimation process as well, in order to be updated in conjunction with the damage field. We do not consider such application, instead the proposed scenario is one in which accurate knowledge of such parameter is not of interest.

Figure 5.5 shows the estimated damage field with increasing values of $K_{t,True}$ compared to $K_{t,REF}$. There is a series of results in the range $K_{t,True} \in [0.9, 1.1] \times K_{t,REF}$ considering a fine discretization in values of $K_{t,True}$, however the results are not shown due to great similarity with Fig. 5.3.

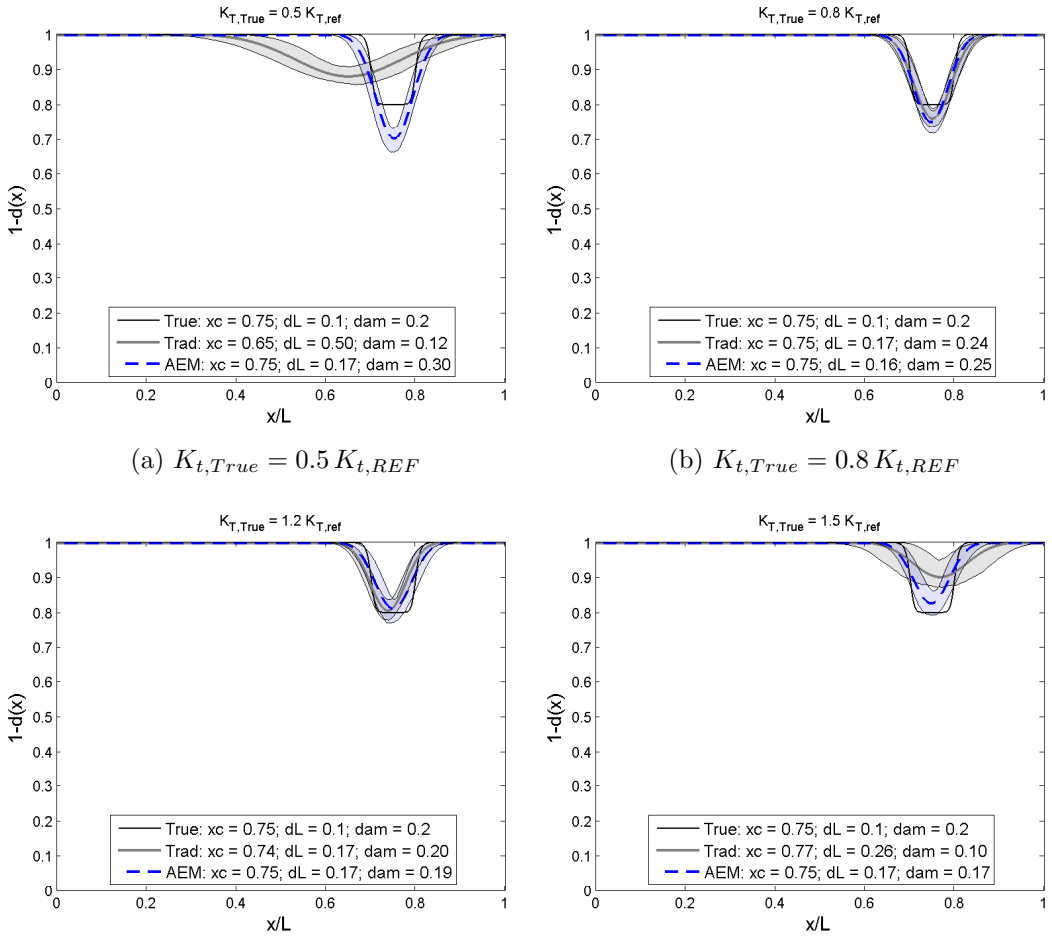

(a) $K_{t,True} = 0.5\,K_{t,REF}$ (b) $K_{t,True} = 0.8\,K_{t,REF}$

(c) $K_{t,True} = 1.2\,K_{t,REF}$ (d) $K_{t,True} = 1.5\,K_{t,REF}$

Figure 5.5: Damage field estimated for different values of $K_{t,True}$ using the same forward model with $K_t = K_{t,REF}$ for both the AEA and least-squares approach. All cases consider $x_F = x_{F,REF}$.

5.2.4 Uncertain Excitation Point

This section presents results concerning the solution of the inverse problem, that is, the estimated damage field, in a scenario with unknown parameters corresponding to the position at which the excitation is applied to the structure. As in the previous section, the modeling error arises from an erroneous assumption on a model parameter, which could have been considered in the estimation process.

A particularity of this analysis was the use of a finer mesh over the 99% probability support of X_F. The effective sampling procedure consists of choosing node points over this support following the PDF of X_F.

As observed from Fig. 5.6, the AEA was able to produce more consistent results in comparison with the Traditional approach. Results contained within this range are not shown due to the similarity to Fig. 5.6. However, it should be noted that the Traditional Approach produced consistent results for the range $x_{F,True} \geq x_{F,True}$.

It is interesting to take this opportunity to compare the predicted time responses of both estimates. Figure 5.7 shows the predicted responses compared to synthetic data used in the inversion generated for $x_{F,True} = 0.955\, x_{F,REF}$, data is presented for the sensor placed at $x = L$.

It should be noted that, while both approaches produced good estimates of the position, the slight overestimation of the intensity in the case using only a traditional least squares lead to a time prediction that "escapes" the $\pm 3\sigma$ boundaries of the *modeling error*. In contrast, note that such boundaries enclosure the measured data and the predicted response using the Approximation Error model $A(\cdot)$ (AEM, model that uses prediction from the AEA results).

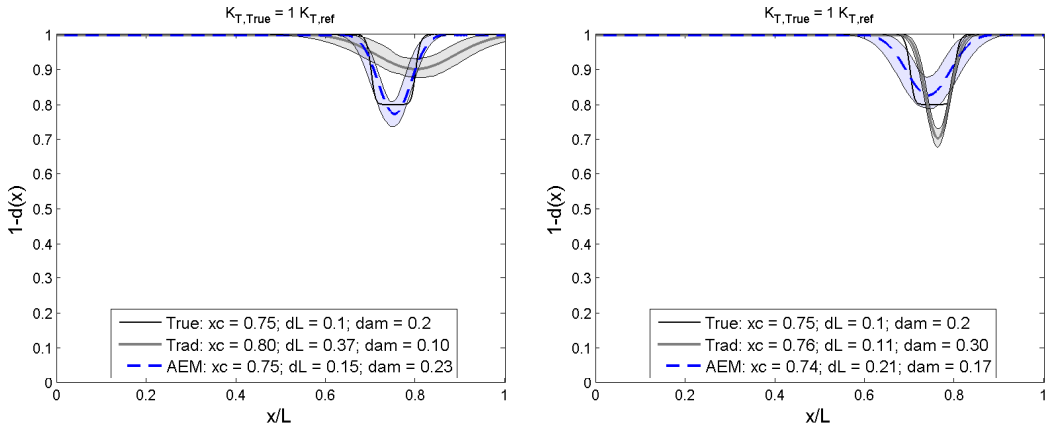

(a) $x_{F,True} = 0.945L$ (b) $x_{F,True} = 0.955L$

Figure 5.6: Damage field estimated for different values of $x_{F,True}$ using the same forward model with $x_F = x_{F,REF}$ for both the Approximation error and least-squares approaches. All cases consider $K_{t,True} = K_{t,REF}$.

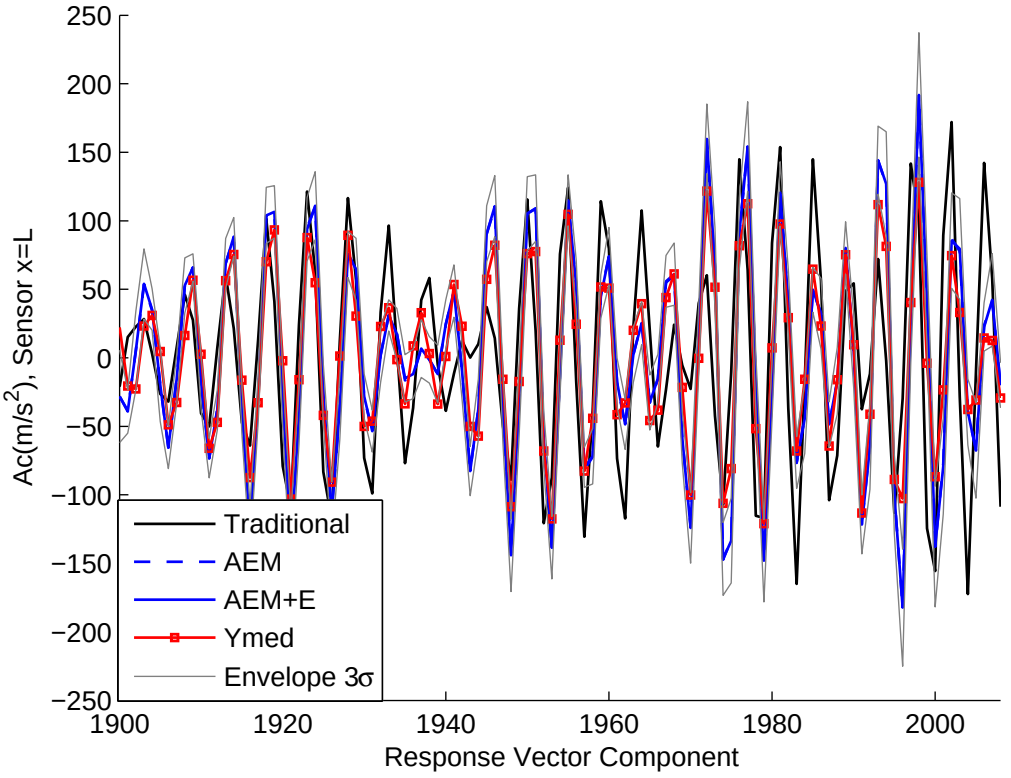

Figure 5.7: Comparison of time responses with measurements. Predicted responses for damage fields estimated with Approximation Error and Traditional Least Squares, for $x_{F,True} = 0.955\, x_{F,REF}$ and $K_{t,True} = K_{t,REF}$.

5.2.5 Uncertainties in both Force Application and Fixation

This section presents results concerning the solution of the inverse problem, that is, the estimated damage field, in a scenario with unknown boundary conditions corresponding to the position at which the excitation is applied to the structure as well as the quality of the clamp – simulated by different values of $K_{t,True}$.

As observed from Fig. 5.8, for values of $K_{t,True}$ at the lower range, none of the approaches was able to produce adequate and consistent results in the presence of the two types of uncertainty combined.

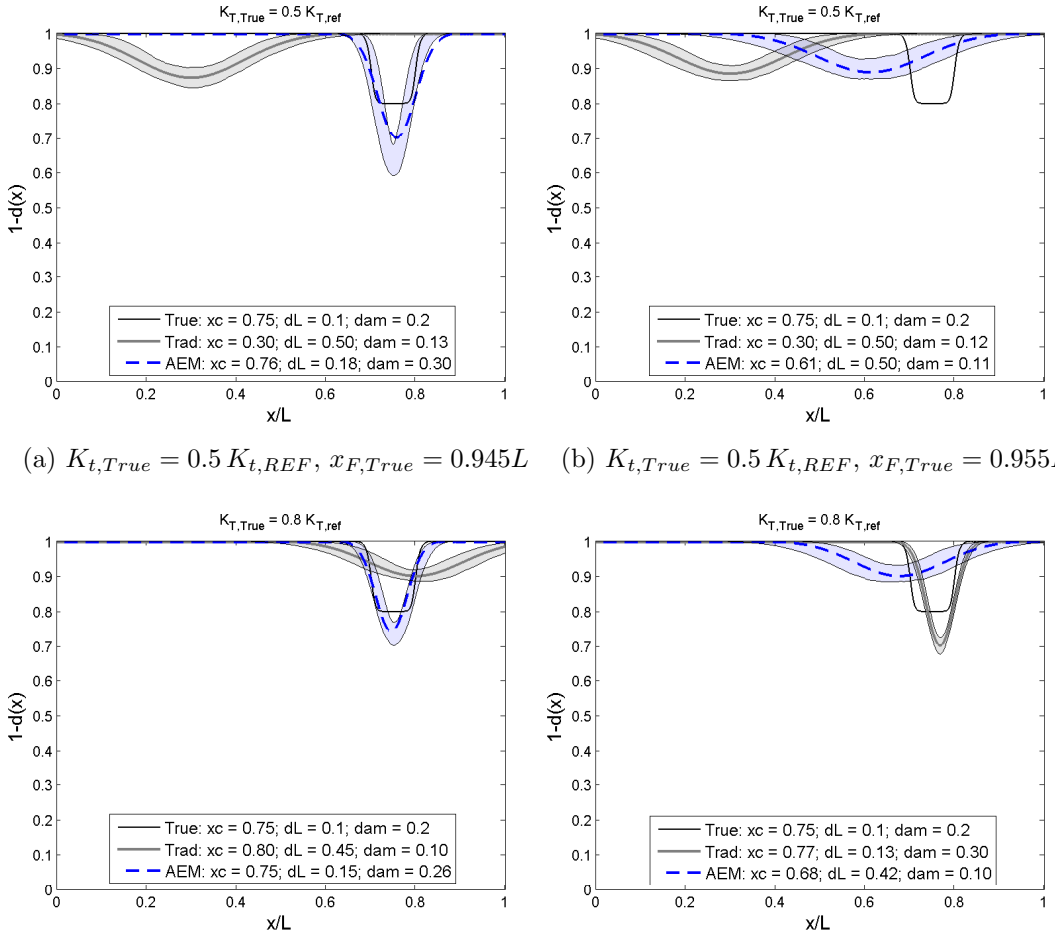

(a) $K_{t,True} = 0.5\,K_{t,REF}$, $x_{F,True} = 0.945L$ (b) $K_{t,True} = 0.5\,K_{t,REF}$, $x_{F,True} = 0.955L$

(c) $K_{t,True} = 0.8\,K_{t,REF}$, $x_{F,True} = 0.945L$ (d) $K_{t,True} = 0.8\,K_{t,REF}$, $x_{F,True} = 0.955L$

Figure 5.8: Damage field estimated for different combinations of $x_{F,True}$ and $K_{t,True}$ using the same forward model for both the AEA and least-squares approach.

As observed from Fig. 5.9, for values of $K_{t,True}$ at the upper range, the AEA was able to produce more consistent results in the presence of the two types of uncertainty combined.

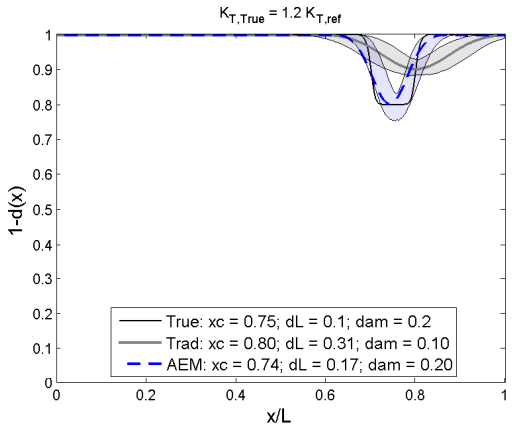

(a) $K_{t,True} = 1.2\,K_{t,REF}$, $x_{F,True} = 0.945L$

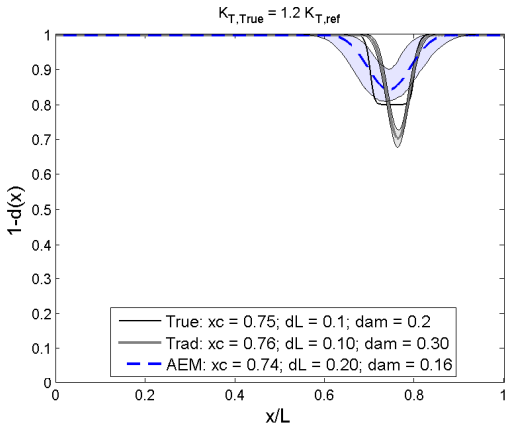

(b) $K_{t,True} = 1.2\,K_{t,REF}$, $x_{F,True} = 0.955L$

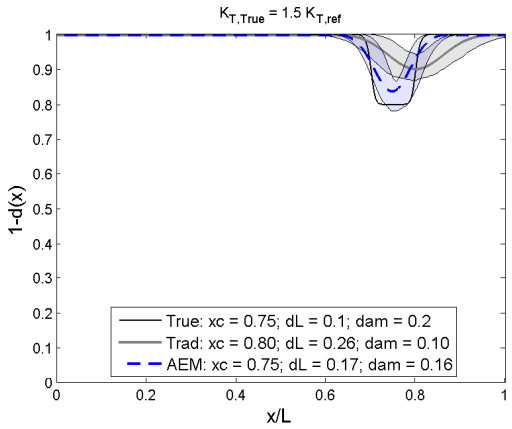

(c) $K_{t,True} = 1.5\,K_{t,REF}$, $x_{F,True} = 0.945L$

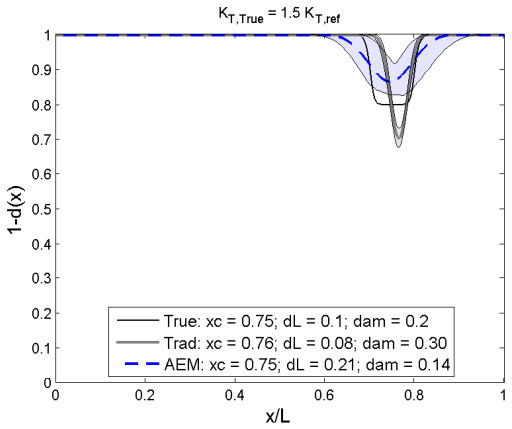

(d) $K_{t,True} = 1.5\,K_{t,REF}$, $x_{F,True} = 0.955L$

Figure 5.9: Damage field estimated for different combinations of $x_{F,True}$ and $K_{t,True}$ using the same forward model for both the AEA and least-squares approach.

5.3 Results 2: Plate Structure

Within this section, different scenarios are specified by the different sources of modeling errors. For each of these scenarios, synthetic measurement data is generated from an ideal structure, whose specificities are disregarded at some point by the simplified model, such as the variation of the distributed stiffness at the boundaries, in Section 5.3.3. The inverse problem is solved for the identification of the damage field using both the AEA and the Traditional Least Squares.

5.3.1 Benchmark Problem

First and foremost, we present the results of the estimated damage field for a simply supported plate configuration, *without* any uncertainties associated using the procedure described at Section 5.1.2.

The chosen values to generate synthetic data were $\boldsymbol{\theta} = (D, x_0, y_0, \sigma_x, \sigma_y, \theta) = (0.2, 0.5\,L_X, 0.75\,L_Y, 0.06\,L_X, 0.12\,L_Y, \pi/3)$.

Figure 5.11 presents the evolution of the objective function corresponding to the Traditional Least-Squares, eq.(2.2.7), through the different generations of the PSO algorithm (here counted cumulatively). The onset of the 2nd step of the proposed two-steps procedure is characterized by an entirely *new swarm*, and thus a possible increase in the objective function.

As it can be seen by analyzing Fig. 5.12, there is good agreement between the predicted response and the actual ideal response used to generate the synthetic data.

Given the relatively good agreement between all predicted *time response* and their respective measurements, even when the traditional approach faltered, in the next sections we refrain from showing comparisons of in the time domain, instead using modal response for comparison between both approaches.

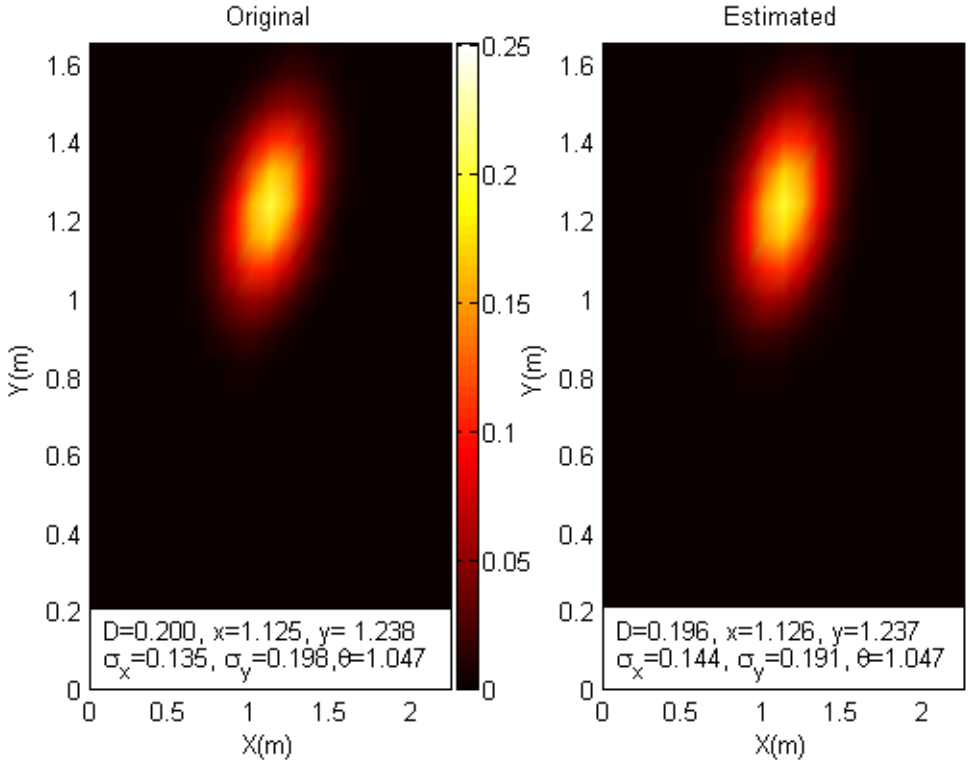

Figure 5.10: True damage field and estimated damage field.

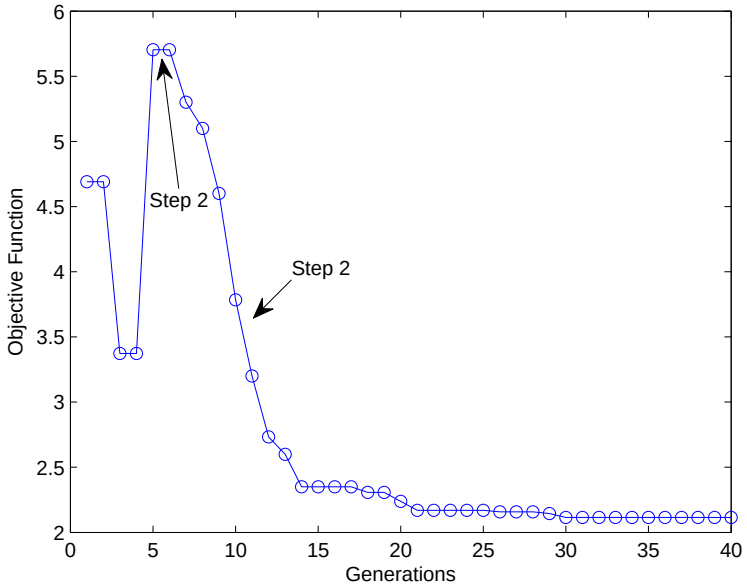

Figure 5.11: Evolution of the Least-Squares Objective Function through generations. Note that due to the way eq.(2.2.7) is stated, the objective function has a nondimensional output.

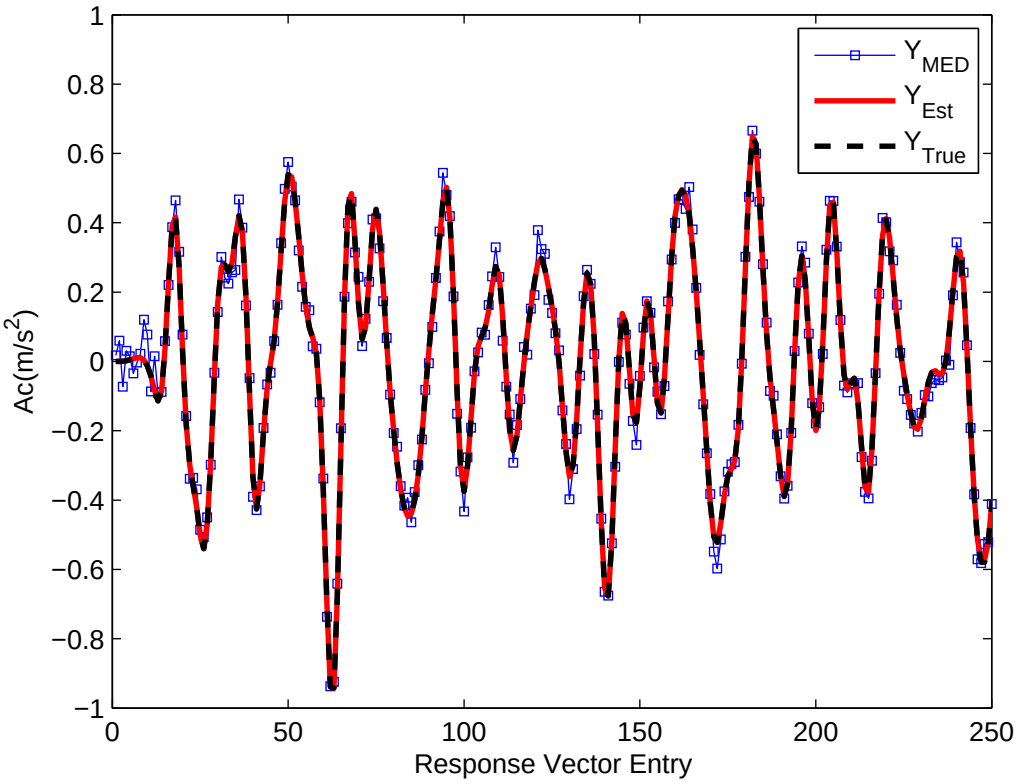

(a) Sensor 1, $0\,s < t \leq 0.025\,s$

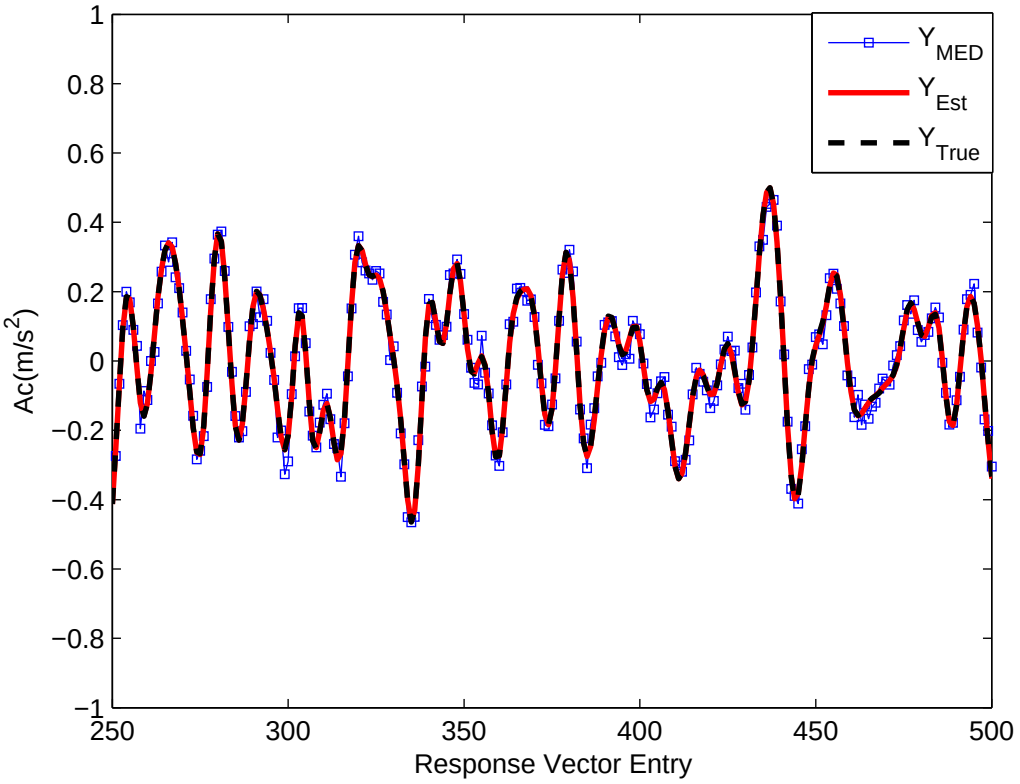

(b) Sensor 1, $0.025\,s < t \leq 0.050\,s$

Figure 5.12: Measurement (Y_{MED}) vs Predicted (Y_{EST}) vs Actual (Y_{TRUE}) data, for sensor 1. Results obtained from *one* impact.

5.3.2 Parameters for the AEA

Going forward, we associate the parameters D, x_0, y_0, σ_x, σ_y and θ to their respective random variables counterparts: $\mathcal{D}$, X_0, Y_0, σ_X, σ_Y and Θ.

In order to apply the AEA, the necessary statistics of the approximation error have to be computed. To that end, consider $N_{mc} = 10^4$ realizations of $\boldsymbol{\theta}^{(l)} = (\mathcal{D}^{(l)}, X_0^{(l)}, Y_0^{(l)}, \sigma_X^{(l)}, \sigma_Y^{(l)}, \Theta^{(l)})^T$ sampled as follows:

- $X_0 \sim \mathcal{U}[0, L_X]$
- $Y_0 \sim \mathcal{U}[0, L_Y]$
- $\sigma_X \sim \mathcal{U}[0.05, 0.25] \times L_X$
- $\sigma_Y \sim \mathcal{U}[0.05, 0.25] \times L_Y$
- $\Theta \sim \mathcal{U}[0, \pi/4]$
- With 20% probability: generate an undamaged structure, $D = 0$. Otherwise $D \neq 0$, drawn $\mathcal{D}$ from $\mathcal{D} \sim \mathcal{U}[0.05, 0.60]$.

where X_0, Y_0, σ_X and σ_Y are in meters, Θ is in radians and D is nondimensional.

In this Section, random fields (RF) are used in the training stage of the AEA to generate distributed parameters $\boldsymbol{\xi}^{(l)}$ and $\mathbf{z}^{(l)}$ to be premarginalized. Concerning the generation of RF, there are two important parameters: *correlation length* L_C, which measures the degree of correlation between field values at different points in space, and the *standard-deviation* σ, which defines the deviation of different realizations of the RF at a point in space. For more on this subject, we refer to appendix Appendix C and references therein.

Samples of the random variables corresponding to the parameters to be premarginalized are drawn from:

- $\boldsymbol{\xi}^{(l)} \sim \mathcal{N}(\mu_K = K_{t,REF} \times \mathbf{1}, \mathbb{C}_K) \times \mathbb{1}_{\mathbb{R}^+}[Nm/rad/m]$, in Section 5.3.3.
- $\mathbf{z}^{(l)} \sim \mathcal{N}(\mu_\rho = \rho_{F,REF} \times \mathbf{1}, \mathbb{C}_\rho) \times \mathbb{1}_{\mathbb{R}^+}[kg/m^3]$, in Section 5.3.4.

where $\mathbb{1}_\Omega$ indicates the distribution's non-zero probability support is the domain Ω and $\mathbf{1}$ indicates the vector of ones, $\mathbf{1} = (1, \cdots, 1)^T$, with the appropriate dimensions. Covariance matrices $\mathbb{C}_K$ and $\mathbb{C}_\rho$ are functions of the correlation length and standard-deviation, as defined in Appendix C.

The correlation length L_C is defined in terms of the minimum length of the plate $\ell_{\min}$. Its value was chosen such that the effects of the unknown distributed parameters on the measured features would mask those of the damage at the considered frequency range, thus hindering the estimation process, in both cases this value was set to $L_C = 0.4\,\ell_{\min}$.

For the study presented in Section 5.3.3, samples for the torsional stiffness distribution at each side of the plate are generated using a Gaussian RF with mean $K_{t,REF} = 12.8 \times 10^3\, Nm/rad/m$ and standard-deviation $\sigma = 0.10\, K_{t,REF}$. One such field used to generate the synthetic measurements is shown in Fig. 5.13, where sides are named following a counter-clockwise spiral: left, bottom, right and top edges are respectively labeled L1, L2, L3 and L4. The reference value assumed is $\boldsymbol{\xi}_0 = K_{t,REF}$.

For the study presented in Section 5.3.4, samples for the distribution of mass are generated using a Gaussian RF with mean $\rho_{REF} = \rho_0$ and standard-deviation $\sigma = 0.01\, \rho_{REF}$. Section 5.3.4 presents a study that is consistent with the problem of a field $\mathbf{z}$ that is absolutely necessary for the formulation but not of interest as a solution of the inverse problem, thus assuming a reference value $\mathbf{z}_0$, more specifically $\mathbf{z}_0 = \rho_0 = 2725 kg/m^3$.

The parameters related to the definition of the *priors* in all the AEA cases are fixed to

$$\boldsymbol{\theta}_* = \mathbb{E}[\boldsymbol{\theta}^{(l)}], \quad \boldsymbol{\Sigma}_{\boldsymbol{\theta}\boldsymbol{\theta}} = \mathrm{diag}([1, L_X, L_Y, L_X/2, L_Y/2, \pi/4])$$

in order to ***reproduce*** a non informative prior (see [11, 12]).

We consider the Frequency Response Function (FRF) of the accelerations collected at sensor 4 (unless stated otherwise) in order to compare the results from the Approximation Error and Traditional approaches.

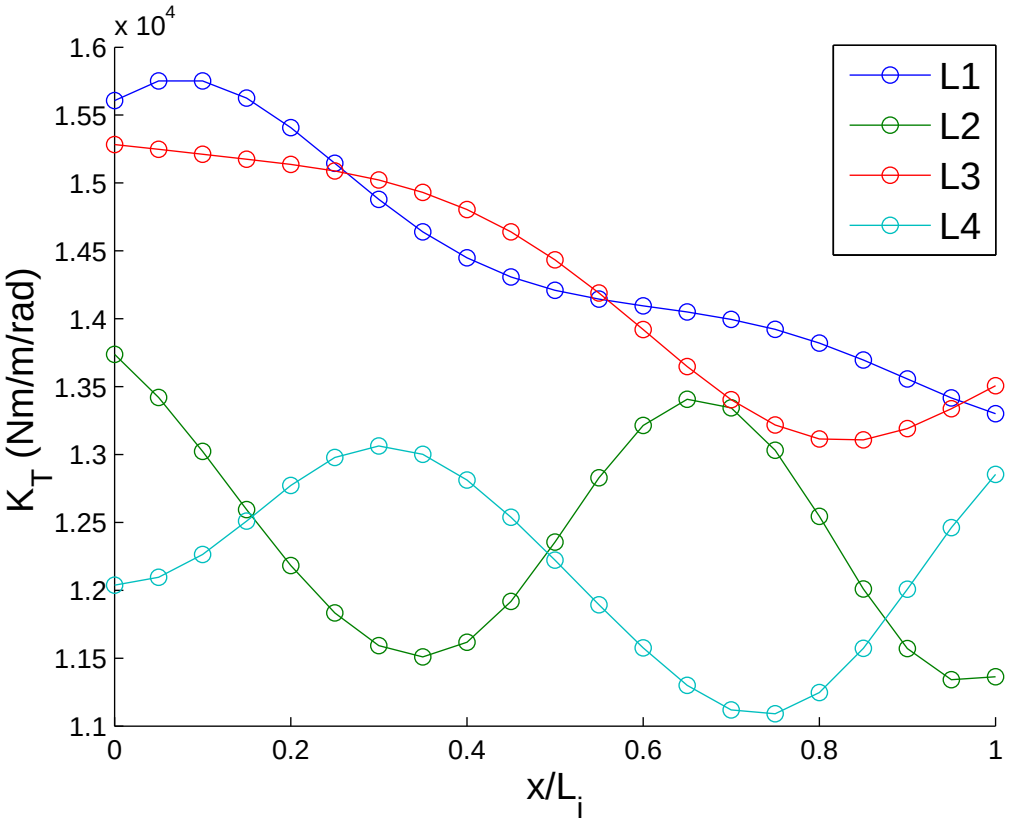

Figure 5.13: Random field of torsional stiffness used in Section 5.3.3 to generate the measurements. The values of the field are shown along the nondimensional length of each side of the plate. This field has correlation length $L_C = 0.4\,\ell_{\min}$ and standard-deviation $\sigma = 0.10\,K_{t,med}$, with mean value $K_{t,med} = 12.8 \times 10^3\,Nm/rad/m$.

5.3.3 Uncertain Stiffness Distribution

In this Section we consider the damage identification problem with uncertain stiffness distribution at the edges of the plate. The modeling error comes from the incorrect assumption that this distribution of stiffness is constant in all edges.

Figure 5.14 shows two realizations of the stiffness distribution field used to generate the synthetic measurements considered for the inverse problem.

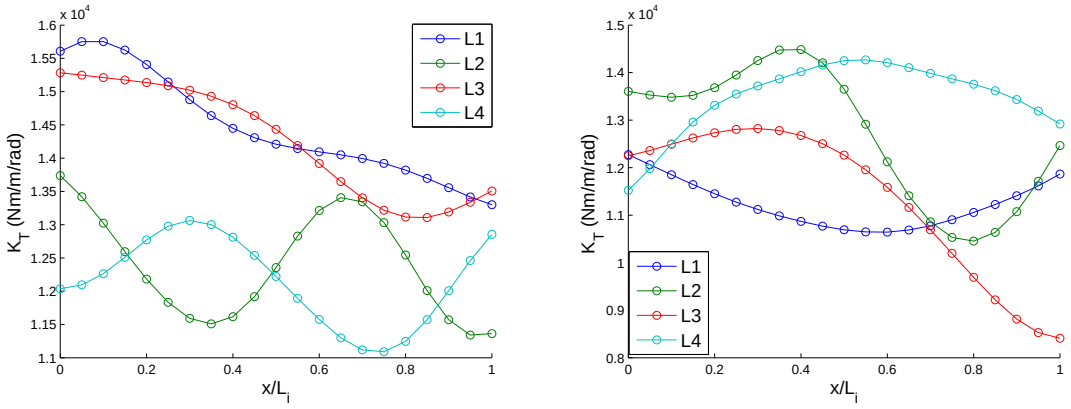

(a) K_t field 1 (b) K_t field 2

Figure 5.14: Two field realizations of the stiffness distribution used to generate the synthetic measurements.

Figure 5.15 shows the resulting estimated fields using both approaches.

Given the nature of the two step algorithm present in Section 5.1.2, the position can be identified with a good level of agreement, the (absolute) error in both cases not being greater than 2% of the true value with the AEA. The Traditional Approach resulted in erroneous estimation of the intensity (in as much as $\approx +100\%$).

The support of the field presented greater variation, the AEA resulted in a better estimation of the support's parameters corresponding to its extension (within an absolute error of $\approx 11\%$), however the AEA was unable to correct for the orientation of the damage field.

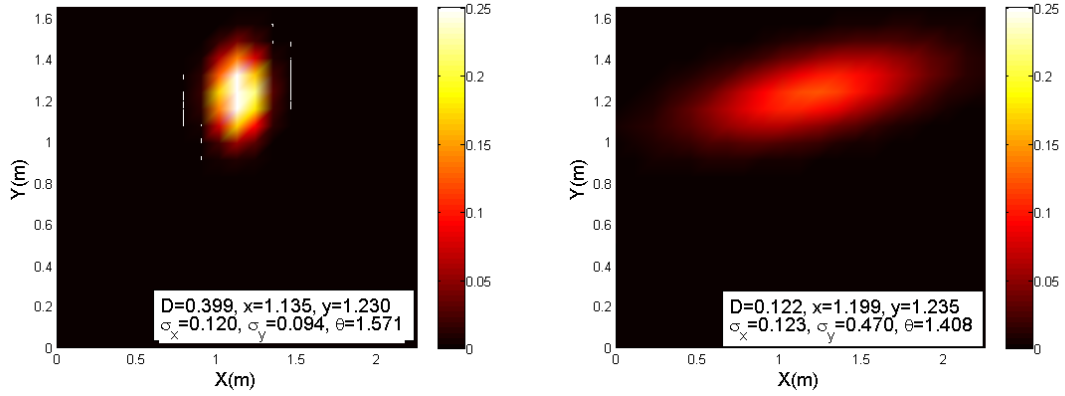

(a) Without AEA (b) Without AEA

(c) With AEA (d) With AEA

Figure 5.15: Comparison of estimated fields with uncertain K_t distribution using the Traditional (1st row) and AE (2nd row) approaches.

From Fig. 5.16, it can be seen that for very low frequencies, there is reasonable agreement between the predicted and true FRFs, this is due in part to the low sensitivity to damage at these frequencies and in part to low sensitivity to the *distribution* of K_t. However, at higher frequencies, the discrepancies become accentuated, leading to the conclusion that model response would be different from that of the actual system.

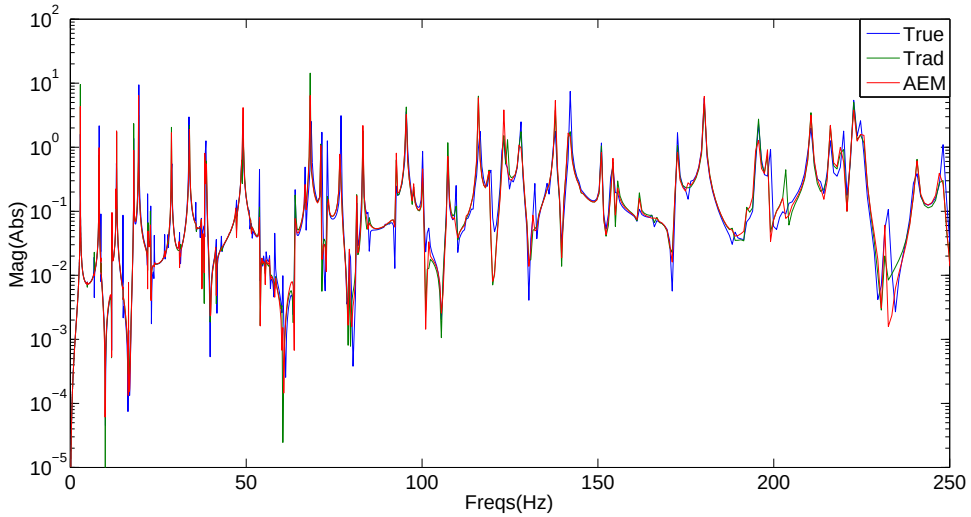

(a) FRF for K_t field 1

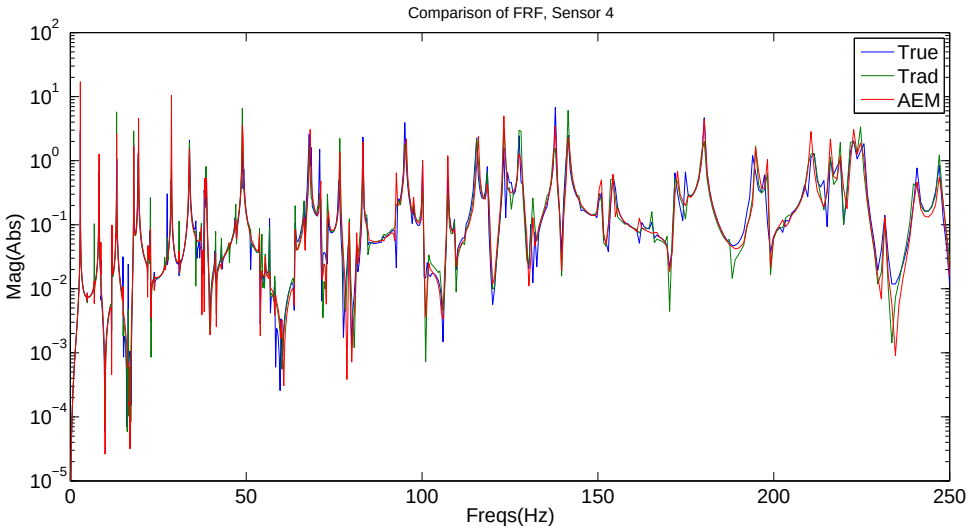

(b) FRF for K_t field 2

Figure 5.16: Comparison of predicted FRFs for K_t fields, at sensor 4.

5.3.4 Uncertain Mass Distribution

In this Section we consider the damage identification problem with uncertain mass distribution. The modeling error comes from the incorrect assumption that the specific mass is constant in the structure.

Figure 5.17 shows two realizations of the mass distribution field used to generate the synthetic measurements considered for the inverse problem.

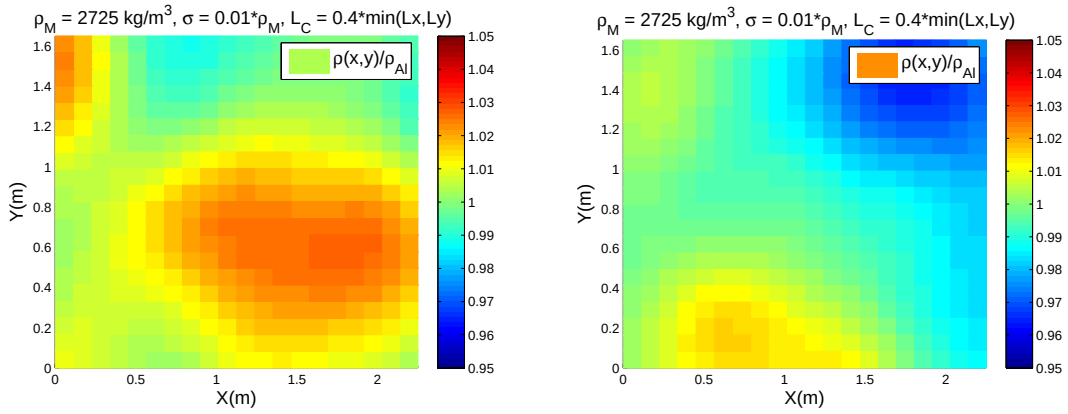

(a) ρ field 1 (b) ρ field 2

Figure 5.17: Two field realizations of mass distribution used to generate the synthetic measurements.

Figure 5.18 shows the estimated damage fields using both approaches. It can be observed that the traditional least squares fails to consistently identify the damage field. Although results with the AEA showed variation in the support, similarly to what is observed in the previous section, it was still able to satisfactorily identify intensity and location of the field in a consistent manner.

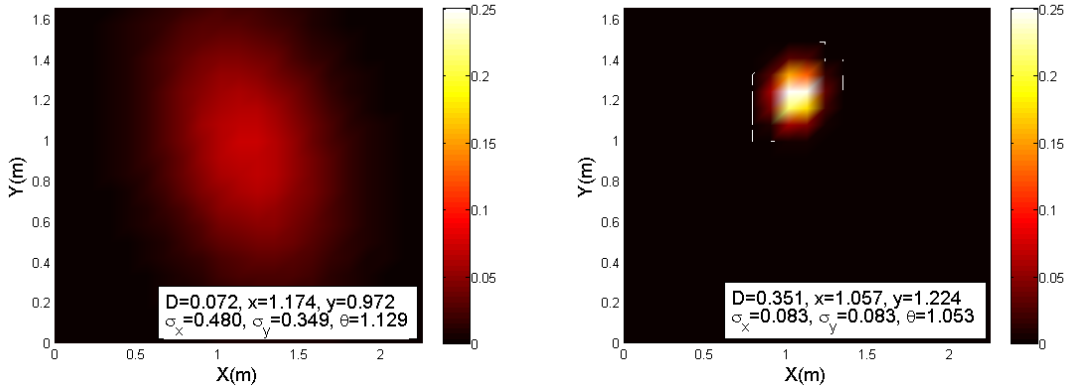

(a) Without AEA

(b) Without AEA

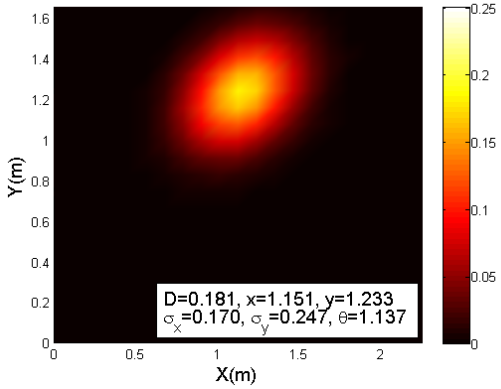

(c) With AEA

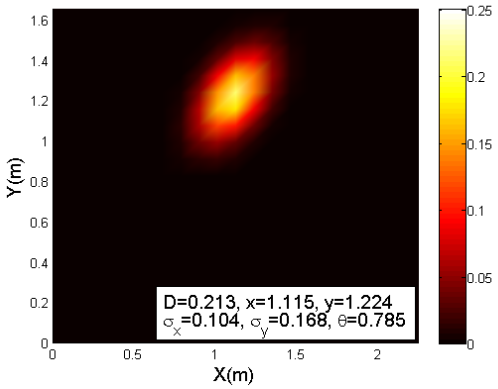

(d) With AEA

Figure 5.18: Comparison of estimated fields with uncertain ρ distribution using the Traditional (1st row) and AEA (2nd row) approaches.

Figure 5.19 shows a comparison between FRFs at sensor 4 for ρ fields 1 and 2. As with the results from the previous section, for low frequencies both approaches reproduced the system's response. Note that while the use of a model with constant ρ for damage identification *alone* may be successful when applying the AEA, this is not the case for model predictions. The AEA was introduced in order to *avoid* the estimation of undesired fields.

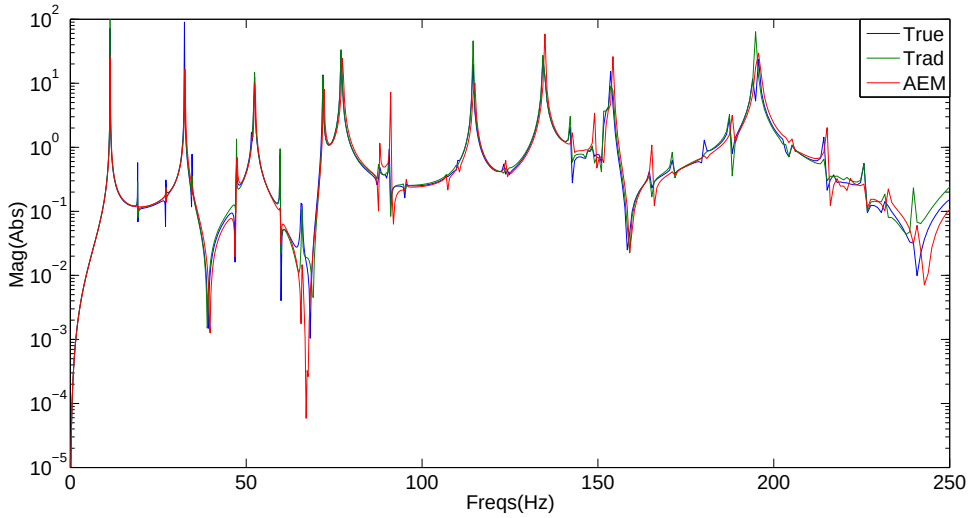

(a) ρ field 1

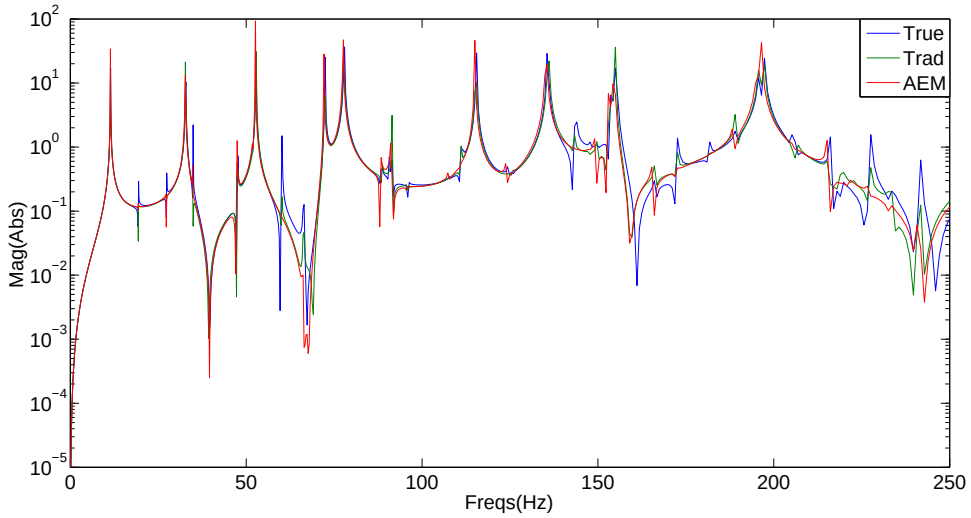

(b) ρ field 2

Figure 5.19: Comparison of predicted FRFs for ρ fields, at sensor 4.

Chapter 6

Numerical Experiment: Distributed Field

In this chapter we consider the damage identification problem of a non localized damage field. In this case, the proposed approach is to estimate the damage field at *each point* in the space defined by the structure. Also, in this Chapter, we ***do not consider*** any form of modeling errors.

The field to be estimated is presented in Fig. 6.1.

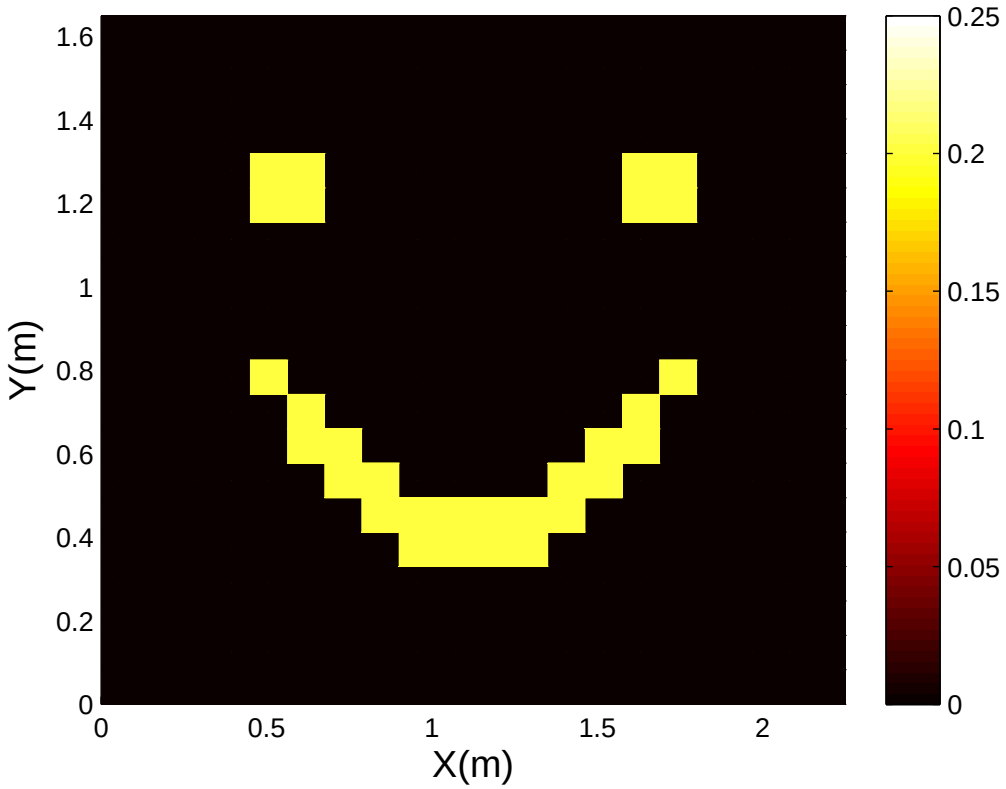

Figure 6.1: Non-localized damage field to be estimated.

6.1 Direct problem

This direct problem is similar to the one presented in Section 4.3: given an isotropic aluminum plate with properties and dimensions defined in Table 4.1, one wishes to find the acceleration response $\mathbf{y}$ at key locations over the plate, given an excitation $\mathbf{u}$, which corresponds to the two consecutive impacts, and auxiliary parameters $\boldsymbol{\theta}$, which correspond to the damage field $d(\mathbf{x})$.

Damage is assumed to be the cause of a local reduction in stiffness, this is modeled as a change in the elastic parameter, E_0, at some position $\mathbf{x}$ over the area of the plate [17, 24, 26, 29], as given by eq.(4.3.1).

6.2 Inverse problem

This inverse problem is similar to the one presented in Section 4.4. That is, given a set of acceleration measurements $\mathbf{y}$ and input variables $\mathbf{u}$, one seeks information about *unknown* parameters $\boldsymbol{\theta}$ corresponding to the structure's damage field $d(\mathcal{X})$ given by eq.(4.3.1) using the forward model previously described.

The proposed approach is to estimate a parameter α_i associated with the variation of a property P_i^*:

$$P_i = P_i^*(1 + \alpha_i)$$

where i is associated with each parameter in the parameter space. This could be, for example, the value of the damage functions proposed by TEUGHELS *et al.* [21] at each node of a mesh defined for these functions. In the case of [21, 22], these parameters *are not linked* to any particular discretization of the domain Ω in which eq.(4.2.1) is defined.

In this dissertation, the parameter to be estimated is a vector of damage values *per element* $\boldsymbol{\theta} = (d^1, \cdots, d^{N_e})^T$, where N_e is the number of elements in the FE discretization, such that:

$$E^e = E_0(1 - d^e) \tag{6.2.1}$$

is the value of the Young's modulus in each element e. Thus, the parameter space *is linked* to the discretization used, and in the case of the 20×20 mesh used in this section, there are $N_p = N_e = 400$ parameters to be identified.

The inverse problem is solved by finding the set of parameters $\boldsymbol{\theta}'$ that is the solution of a minimization problem similar to (3.3.2), here repeated for convenience:

$$\boldsymbol{\theta}' = arg\min_{\boldsymbol{\theta}\in\Omega_P} S(\boldsymbol{\theta}) \tag{6.2.2}$$

where $S(\boldsymbol{\theta})$ is some functional relating the parameters to the measurement data. The parameter space is the hypercube of unitary side $\Omega_P = [0,1]^{N_p} \subset \mathbb{R}^{N_p}$.

Consider the *Continuous Least Squares* functional [13, 30]

$$S(\boldsymbol{\theta}) = \int_T [\bar{\mathbf{y}}(t) - \mathbf{y}(t,\boldsymbol{\theta})]^T \boldsymbol{W} [\bar{\mathbf{y}}(t) - \mathbf{y}(t,\boldsymbol{\theta})]\, dt \tag{6.2.3}$$

where $\mathbf{y}(t,\boldsymbol{\theta}) = C_a \ddot{\mathbf{q}}(t,\boldsymbol{\theta})$ is the model response and $\bar{\mathbf{y}}(t)$ are the measured accelerations. $\ddot{\mathbf{q}}(t,\boldsymbol{\theta})$ is obtained from the forward problem $\mathbf{g}(\mathbf{q},\boldsymbol{\theta}) = \mathbf{0}$, eq.(6.2.4).

$$\mathbf{M}(\boldsymbol{\theta})\ddot{\mathbf{q}}(t,\boldsymbol{\theta}) + \mathbf{D}(\boldsymbol{\theta})\dot{\mathbf{q}}(t,\boldsymbol{\theta}) + \mathbf{K}(\boldsymbol{\theta})\mathbf{q}(t,\boldsymbol{\theta}) = \mathbf{f}(t,\boldsymbol{\theta}), \quad T = (t_0, t_f] \tag{6.2.4a}$$

$$\mathbf{q}(t_0,\boldsymbol{\theta}) = \mathbf{q}_0(\boldsymbol{\theta}), \quad \dot{\mathbf{q}}(t_0,\boldsymbol{\theta}) = \dot{\mathbf{q}}_0(\boldsymbol{\theta}) \tag{6.2.4b}$$

In eq.(6.2.3), model response $\mathbf{y}$ and measured data $\bar{\mathbf{y}}$ *are not* concatenated, they are instead regarded as functions of time. Thus $\mathbf{y}, \bar{\mathbf{y}} \in \mathbb{R}^{N_s}$, and $\mathbf{W} \in \mathbb{R}^{N_s \times N_s}$ is the *inverse* of the covariance matrix of measurements errors, $\boldsymbol{\Sigma}_e$. Alternatively $\mathbf{W}$ can be set as the identity matrix $\mathbf{W} = \mathbf{I}$, thus results from difference sensors have the same weights, and $[S] = [m^2/s^3]$. For a richer spatial information content, we consider the use of $N_s = 16$ uniformly spaced acceleration sensors placed over the plate.

In this chapter, we do not consider the application of any regularization technique. Instead, we consider a two step approach, restarting the optimization procedure maintaining only parameters that presented a variation that surpassed the threshold value of $d_T = 0.01$.

6.3 Adjoint Formulation

Generally speaking, the number of particles present in the search space increases with the increase of the dimensionality of said space [59, 61], thus the use of small populations sizes is desirable to reduce the computational cost of the algorithm (since, for each particle, an evaluation of the objective function must be made). However, the use of small population sizes restricts the PSO's ability to search a high dimensional space.

To counteract this problem present in population-based (global) optimization techniques, one may wish to make use of "traditional" gradient-based techniques, even though with such techniques one risks getting stuck in any of the possibly many local minima.

In addition, the use of such algorithms is faced with the same problem of global techniques for a large parameter space: the number of evaluations of the object function. In the general situation where the derivatives of the objective function cannot be analytically obtained, they must be computed numerically by finite differences or any other scheme, the problem with this approach being that if the number of parameter increases the number of functions evaluations is also increased. It also increases with increasing degree of precision.

An alternative to the use of finite differences is the *Adjoint Formulation* [14, 62–64]. Authors who applied the adjoint formulation to the damage identification problem include PEREIRA *et al.* [30], CASTELLO *et al.* [31]. For more details on the Adjoint Formulation, see Appendix D of this dissertation.

6.4 Conjugate Gradient with Adjoint Method

Problem (6.2.2-6.2.3) can be solved by means of the Conjugate Gradient (CG) Method [14, 15, 65]:

$$\mathbf{d}^k = \nabla S^k + \gamma^k \, \mathbf{d}^{k-1} \tag{6.4.1a}$$

$$\boldsymbol{\theta}^{k+1} = \boldsymbol{\theta}^k - \beta_k \, \mathbf{d}^k \tag{6.4.1b}$$

where $\boldsymbol{\theta}^k$ is the vector of parameters $\boldsymbol{\theta} = (p_1, \cdots, p_i, \cdots, p_{N_p})^T$ at iteration k, β_k is the step size in the search direction $\mathbf{d}^k$ and γ^k is the *conjugation coefficient*. Depending on the choice of γ^k, different versions of the algorithm can be obtained [15, 65]. The Polak-Ribière's version of the algorithm considers

$$\gamma^k = \frac{(\nabla S^k)^T(\nabla S^k - \nabla S^{k-1})}{\|\nabla S^{k-1}\|^2}, \quad k = 1, 2, ... \tag{6.4.2}$$

with $\gamma^0 = 0$, that is, the CG starts with the steepest descent direction.

The gradient ∇S is efficiently calculated at each iteration k using the Adjoint Method, eq.(6.4.3) (see Appendix E.4).

$$(\nabla S)_i = \boldsymbol{\alpha}^T \frac{\partial \boldsymbol{\varphi}}{\partial p_i} + \int_T \boldsymbol{\lambda}^T \left[\frac{\partial \mathbf{M}}{\partial p_i}\ddot{\mathbf{q}} + \frac{\partial \mathbf{D}}{\partial p_i}\dot{\mathbf{q}} + \frac{\partial \mathbf{K}}{\partial p_i}\mathbf{q} - \frac{\partial \mathbf{f}}{\partial p_i} \right] dt \tag{6.4.3}$$

The adjoint variable $\boldsymbol{\lambda}$ is obtained from the *Adjoint Problem* for acceleration measurements, eq.(6.4.4).

$$\begin{aligned} &\ddot{\boldsymbol{\lambda}}^T \mathbf{M} - \dot{\boldsymbol{\lambda}}^T \mathbf{D} + \boldsymbol{\lambda}^T \mathbf{K} = +2(\bar{\mathbf{y}} - \mathbf{y})^T \mathbf{W} C_a \\ &\dot{\boldsymbol{\lambda}}(t_f) = \boldsymbol{\lambda}(t_f) = \mathbf{0} \end{aligned} \tag{6.4.4}$$

The optimum step-size β_k is obtained from the 1D minimization problem in the search direction. This can be done efficiently by solving the *Sensitivity Problem*, eq.(6.4.5), for the variation $\delta\mathbf{y}^k$, using $\delta p_i = (\mathbf{d}^k)_i$, at each global iteration k of the optimization algorithm (see Appendix E.3).

$$\mathbf{M}\delta\ddot{\mathbf{q}} + \mathbf{D}\delta\dot{\mathbf{q}} + \mathbf{K}\delta\mathbf{q} = \sum_{i=1}^{N} \left(\frac{\partial \mathbf{f}}{\partial p_i} - \frac{\partial \mathbf{M}}{\partial p_i}\ddot{\mathbf{q}} - \frac{\partial \mathbf{D}}{\partial p_i}\dot{\mathbf{q}} - \frac{\partial \mathbf{K}}{\partial p_i}\mathbf{q} \right) \delta p_i \tag{6.4.5}$$

Thus

$$\beta_k \approx \frac{1}{2} \left(\frac{\boldsymbol{\alpha}^T \boldsymbol{\delta\varphi}^k + 2\int_T [\mathbf{y}^k - \bar{\mathbf{y}}]^T \boldsymbol{W} [\delta\mathbf{y}^k] dt}{\int_T [\delta\mathbf{y}^k]^T \boldsymbol{W} [\delta\mathbf{y}^k] \, dt} \right) \tag{6.4.6}$$

where $\delta\mathbf{y}^k$ is the variation of the measured accelerations $\delta\mathbf{y} = C_a\delta\ddot{\mathbf{q}}$ calculated at iteration k and $\mathbf{y}^k = \mathbf{y}(t, \boldsymbol{\theta}^k)$.

For the damage identification problem, iterations are started from an undamaged state, that is, $\boldsymbol{\theta}^0 = \mathbf{0}$.

The stopping criteria are the *limit number of iterations*, the *discrepancy principle* and *evolution of objective function*. If the discrepancy principle is used to stop the iterative procedure, the CG may gain a well-posed character [14, 15]. The principle states that iterations must be terminated when $S(\boldsymbol{\theta}) \approx \epsilon$, where:

- $\epsilon = \sum_m^M \sum_i^I \sigma_{im}^2$, for M sensors with I measurements each.
- $\epsilon = \Delta T \sum_m^M \sigma_m^2$, for continuous measurements of M sensors over time ΔT.

where σ_m and σ_{im} are the standard-deviations of uncorrelated measurements per sensor m. For the problem considered in this section, we set $\mathbf{W} = \mathbf{I}$, thus $\epsilon = 3.57 \times 10^{-3}\, m^2/s^3$.

However, the use of the discrepancy principle implies knowledge of the standard-deviation of measurement errors. In the case of *almost errorless* measurements, ϵ can be chosen sufficiently small, since the expected value of the functional is zero. However if this is not the case and σ is not known, a second stopping criterion based upon a separate measurement can be used [14].

This *separate measurement criterion* is similar to accompanying the evolution of the functional itself, that is, both criteria are based upon the divergence of the accompanied quantity. If the iterative procedure is stopped at the iteration whose value for either quantity is minimum, sufficiently stable solutions can be obtained for the inverse problem.

6.5 Benchmark Problem

In this section, the estimated damage field corresponding to the solution of minimization problem (6.2.2-6.2.3) is presented.

The two stage procedure used resulted in a correct estimation of the damage's geometric support, which is consistent with results found in literature [31, 64, 66]. It should be noted however that the intensity is not correctly identified everywhere, and that there is significant variation among close elements. The use of a regularization technique could positively impact the later.

In Fig. 6.3, the predicted responses in time and frequency of the estimated field (end of the second stage) are compared to the ones of the actual field in Fig. 6.1. Also, for comparison, the responses for an undamaged structure are shown. Due to the extension of the damage considered in this section, there is a much clearer difference between damaged and undamaged states.

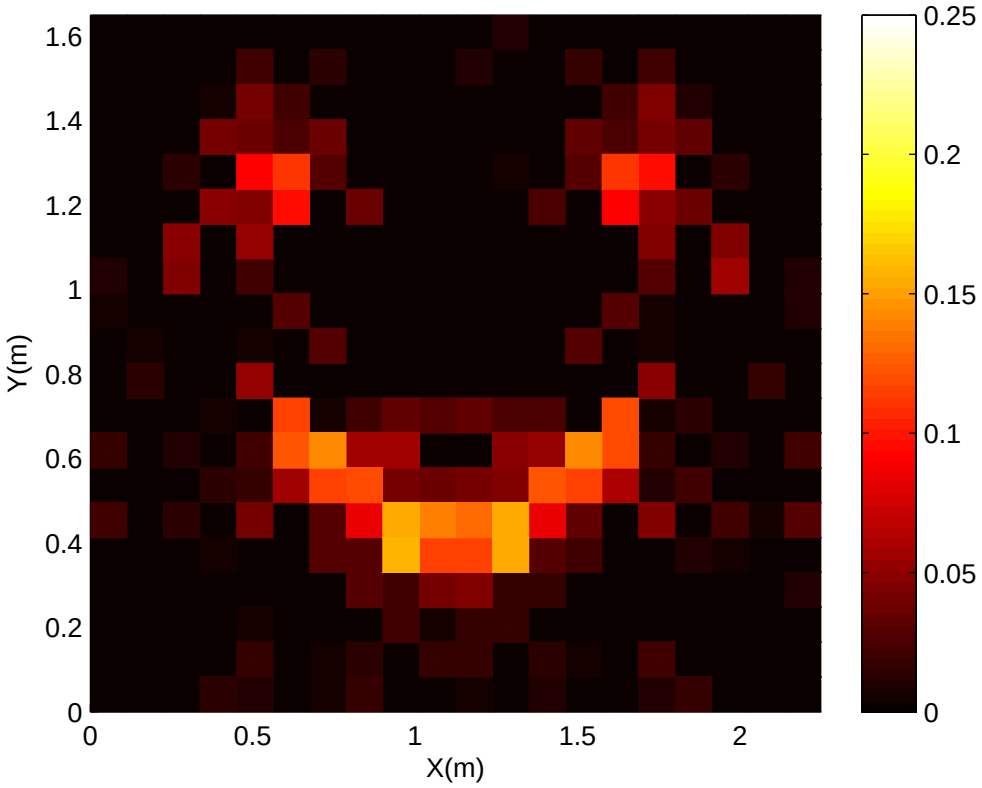

(a) Stage One: $k = 49$ iterations, $S = 3.96 \times 10^{-3}\, m^2/s^3$

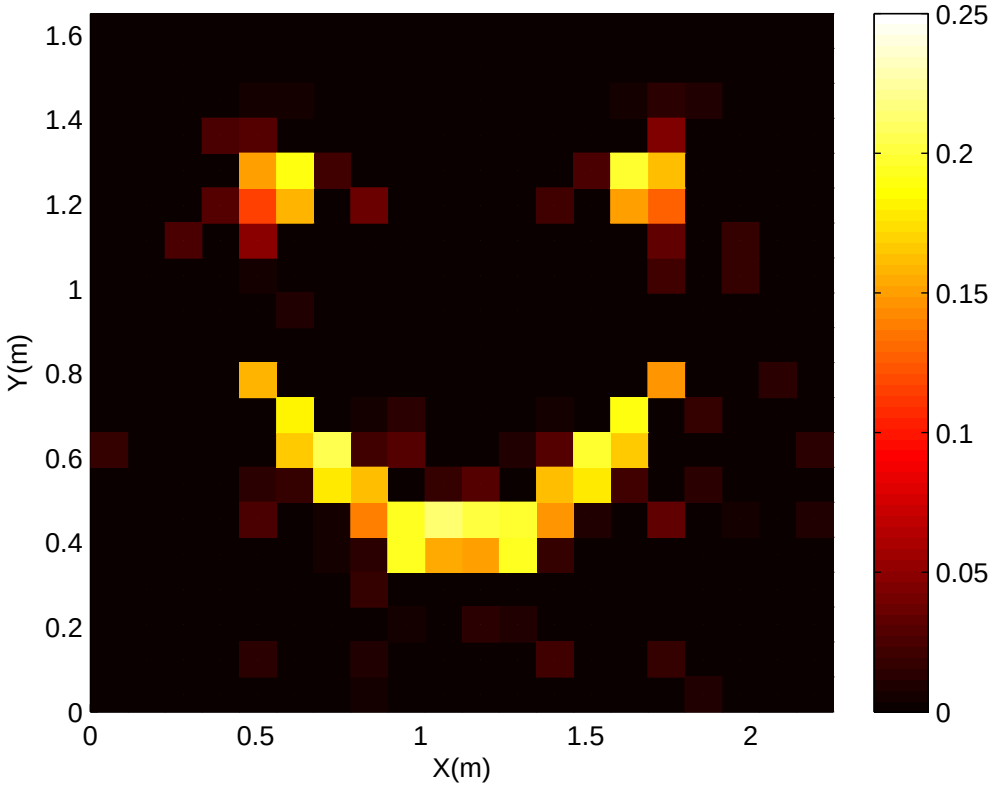

(b) Stage Two: $k = 27$ iterations, $S = 3.59 \times 10^{-3}\, m^2/s^3$

Figure 6.2: Non-localized estimated damage field obtained from the two stage procedure. Estimated field is shown for the final iterations of both stages.

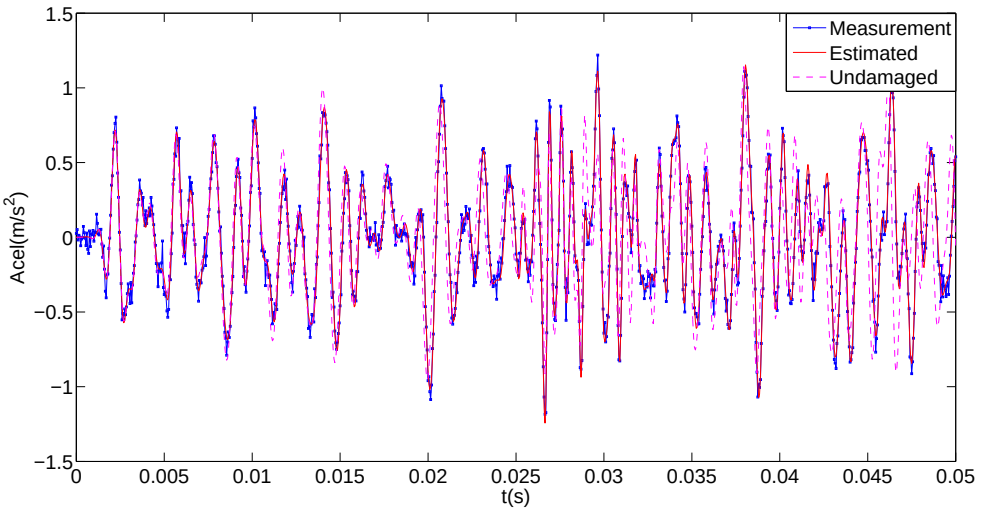

(a) Predicted Time Response

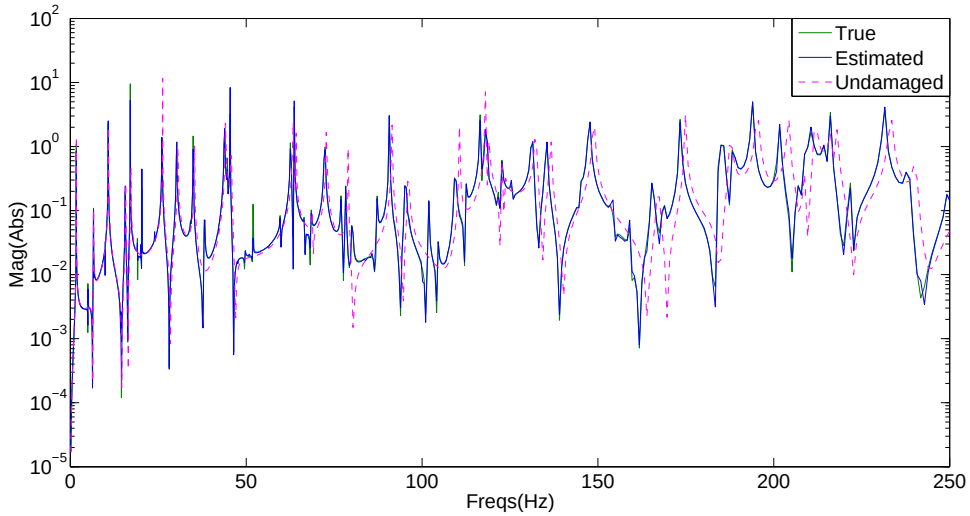

(b) Predicted FRF

Figure 6.3: Predicted responses of estimated field at final stage. (a) Time series comparison between predicted and measurements. (b) FRF comparison between predict and the actual FRF of the system. The actual responses of an undamaged structure is also show for comparison in both cases.

Chapter 7

Conclusions

The examples presented in Chapter 5 consider scenarios where the simplified models could be corrected if the variables corresponding to the uninteresting parameters where also updated, thus leading to models that would be capable of making predictions on the system's response outside the training scenarios. However, as its previous applications suggest, the AEA is better applied when knowledge of such uninteresting parameters is not required, or would introduce unnecessary complications to the solution of the inverse problem in the form of more sophisticated or simply completer models [39–44].

Results from both Sections 5.2 and 5.3 exemplify this idea: the simplified models are essentially wrong, but do still have purpose. In both chapters, within each section the same simplified model was used to solve the inverse problem of damage identification in different scenarios, where information that once was essential to the problem (with varying degrees of influence, given the sensitivity of the system's response) can now be "*marginalized*" thanks to the AEA.

This is one of the main advantages of the AEA, in comparison to traditional identification procedures that *do not* take into account modeling errors: the capacity of using simplified (or incomplete) models for the solution of the inverse problem, thus leading to the applicability of the AEA to essentially different, but "*similar*", inverse problems – similarity in this context means "within training scenarios". Particularly, the AEA is well suited to be applied in conjunction with standardized procedures, and its use implies the need for a *single* simplified model that can be used for all "*similar*" systems to which the inverse analysis is performed, in contrast to one complete model to each system.

The AEA results in a straightforward modification in the final statement of the inverse problem, the objective function of the minimization problem, thus lending itself to be readily applied in conjunction with available optimization techniques, without additional computational cost at this stage other than some additional matrix multiplications, which can be circumvented with the use of the *enhanced error model* (Section 2.3).

However, while the AEA allows for some variation between different experiments in scenarios where a certain procedure is to be followed, due to the way it is formulated, the AEA is not expected to succeed if one changes the excitation too much in comparison with the training scenarios (position, intensity or functional form – in the case where time domain data is considered), neither if the type of measured data is changed.

In hindsight, the use of modal data (such as mode shapes and resonance frequencies) gathered from *output only procedures* could be of great value in combination with the AEA, since model response could be obtained without the need to consider input variables.

With respect to an efficient implementation of the AEA for a large number of parameters, we were unable to construct an adjoint problem that maintained the autocorrelation structure of the measurements present in the AEA, since the covariance matrices for modeling error do not have, necessarily, off-diagonal entries that can be neglected.

For future work, consider the following:

- An investigation on how different sampling strategies affect the AEA.
- The application of the AEA to the inverse problem of damage identification considering modal data.
- The application of the AEA to real experimental data.
- The construction of an adjoint problem based for structural dynamics whose driving term accounts for the autocorrelation structure of the AEA.

Bibliography

[1] KAIPIO, J., SOMERSALO, E. "Statistical inverse problems: discretization, model reduction and inverse crimes", *Journal of computational and applied mathematics*, v. 198, n. 2, pp. 493–504, 2007.

[2] FRISWELL, M. I. "Damage identification using inverse methods", *Philosophical Transactions of the Royal Society of London A: Mathematical, Physical and Engineering Sciences*, v. 365, n. 1851, pp. 393–410, 2007. ISSN: 1364-503X.

[3] SIMOEN, E., ROECK, G. D., LOMBAERT, G. "Dealing with uncertainty in model updating for damage assessment: A review", *Mechanical Systems and Signal Processing*, v. 56–57, pp. 123 – 149, 2015. ISSN: 0888-3270.

[4] FARRAR, C. R., WORDEN, K. "An introduction to structural health monitoring", *Philosophical Transactions of the Royal Society of London A: Mathematical, Physical and Engineering Sciences*, v. 365, n. 1851, pp. 303–315, 2007. ISSN: 1364-503X.

[5] FARRAR, C. R., DOEBLING, S. W., NIX, D. A. "Vibration–based structural damage identification", *Philosophical Transactions of the Royal Society of London A: Mathematical, Physical and Engineering Sciences*, v. 359, n. 1778, pp. 131–149, 2001.

[6] CARDEN, E. P., FANNING, P. "Vibration based condition monitoring: a review", *Structural health monitoring*, v. 3, n. 4, pp. 355–377, 2004.

[7] MONTALVÃO, D., M. M. MAIA, N., RIBEIRO, A. "A Review of Vibration-based Structural Health Monitoring with Special Emphasis on Composite Materials", v. 38, pp. 295, 07 2006.

[8] DOEBLING, S. W., FARRAR, C. R., PRIME, M. B., et al. "A summary review of vibration-based damage identification methods", *Shock and vibration digest*, v. 30, n. 2, pp. 91–105, 1998.

[9] RYTTER, A. "Vibrational based inspection of civil engineering structures", *(PhD Thesis) Dept. of Building Technology and Structural Engineering. Aalborg University, Denmark*, 1993.

[10] FARRAR, C. R., LIEVEN, N. A. "Damage prognosis: the future of structural health monitoring", *Philosophical Transactions of the Royal Society of London A: Mathematical, Physical and Engineering Sciences*, v. 365, n. 1851, pp. 623–632, 2007.

[11] TARANTOLA, A. *Inverse Problem Theory and Methods for Model Parameter Estimation*. SIAM, 2004.

[12] KAIPIO, J., SOMERSALO, E. *Statistical and computational inverse problems*, v. 160. Springer Science & Business Media, 2006.

[13] BECK, J. V., ARNOLD, K. J. *Parameter estimation in engineering and science*. John Wiley and Sons, New York, 1977.

[14] OZISIK, M. N., ORLANDE, H. R. *Inverse Heat Transfer: Fundamentals and Applications*. CRC Press, New York, 2000.

[15] COLAÇO, M. J., ORLANDE, H. R. B., DULIKRAVICH, G. S. "Inverse and optimization problems in heat transfer", *Journal of the Brazilian Society of Mechanical Sciences and Engineering*, v. 28, pp. 1 – 24, 03 2006. ISSN: 1678-5878.

[16] MOTTERSHEAD, J. E., LINK, M., FRISWELL, M. I. "The sensitivity method in finite element model updating: A tutorial", *Mechanical Systems and Signal Processing*, v. 25, n. 7, pp. 2275 – 2296, 2011. ISSN: 0888-3270.

[17] CHOI, S., PARK, S., YOON, S., et al. "Nondestructive damage identification in plate structures using changes in modal compliance", *NDT & E International*, v. 38, n. 7, pp. 529 – 540, 2005.

[18] CORRÊA, R., STUTZ, L., TENENBAUM, R. "Identificação de danos estruturais em placas baseada em um modelo de dano contínuo", *Revista Internacional de Métodos Numéricos para Cálculo y Diseño en Ingeniería*, v. 32, n. 1, pp. 58–64, 2016.

[19] CASTELLO, D., STUTZ, L., ROCHINHA, F. "A structural defect identification approach based on a continuum damage model", *Computers and Structures*, v. 80, n. 5–6, pp. 417 – 436, 2002. ISSN: 0045-7949.

[20] STUTZ, L., CASTELLO, D., ROCHINHA, F. "A flexibility-based continuum damage identification approach", *Journal of Sound and Vibration*, v. 279, n. 3, pp. 641 – 667, 2005. ISSN: 0022-460X.

[21] TEUGHELS, A., MAECK, J., ROECK, G. D. "Damage assessment by FE model updating using damage functions", *Computers and Structures*, v. 80, n. 25, pp. 1869 – 1879, 2002. ISSN: 0045-7949.

[22] TEUGHELS, A., ROECK, G. D. "Structural damage identification of the highway bridge Z24 by FE model updating", *Journal of Sound and Vibration*, v. 278, n. 3, pp. 589 – 610, 2004. ISSN: 0022-460X.

[23] BECK, J. L., KATAFYGIOTIS, L. S. "Updating models and their uncertainties. I: Bayesian statistical framework", *Journal of Engineering Mechanics*, v. 124, n. 4, pp. 455–461, 1998.

[24] MOAVENI, B., BEHMANESH, I. "Effects of changing ambient temperature on finite element model updating of the Dowling Hall Footbridge", *Engineering Structures*, v. 43, pp. 58 – 68, 2012. ISSN: 0141-0296.

[25] CHANDRASHEKHAR, M., GANGULI, R. "Damage assessment of composite plate structures with material and measurement uncertainty", *Mechanical Systems and Signal Processing*, v. 75, n. Supplement C, pp. 75 – 93, 2016. ISSN: 0888-3270.

[26] LEE, U., SHIN, J. "A structural damage identification method for plate structures", *Engineering Structures*, v. 24, 2002. ISSN: 1177-1188.

[27] GRIP, N., SABOUROVA, N., TU, Y. "Sensitivity-based model updating for structural damage identification using total variation regularization", *Mechanical Systems and Signal Processing*, v. 84, pp. 365–383, 2017.

[28] LINK, M., WEILAND, M. "Damage identification by multi-model updating in the modal and in the time domain", *Mechanical Systems and Signal Processing*, v. 23, n. 6, pp. 1734 – 1746, 2009. ISSN: 0888-3270. Special Issue: Inverse Problems.

[29] FU, Y., LU, Z., LIU, J. "Damage identification in plates using finite element model updating in time domain", *Journal of Sound and Vibration*, v. 332, n. 26, pp. 7018 – 7032, 2013.

[30] PEREIRA, R. R. F. O., CASTELLO, D. A., ROCHINHA, F. A. "A time domain based mechanical system identification", *17th International Congress of Mechanical Engineering (COBEM 2003)*. São Paulo, São Paulo, Brazil, 2003.

[31] CASTELLO, D. A., STUTZ, L. T., ROCHINHA, F. A. "A time domain technique for defect identification based on a continuous damage model", *Proceedings of the 2002 ASME International Mechanical Engineering Congress & Exposition*. New Orleans, Louisiana, USA, 2002.

[32] BOLLER, C. "Next generation structural health monitoring and its integration into aircraft design", *International Journal of Systems Science*, v. 31, n. 11, pp. 1333–1349, 2000.

[33] VANIK, M. W., BECK, J. L., AU, S. "Bayesian probabilistic approach to structural health monitoring", *Journal of Engineering Mechanics*, v. 126, n. 7, pp. 738–745, 2000.

[34] BEHMANESH, I., MOAVENI, B. "Accounting for environmental variability, modeling errors, and parameter estimation uncertainties in structural identification", *Journal of Sound and Vibration*, v. 374, pp. 92 – 110, 2016. ISSN: 0022-460X.

[35] BEHMANESH, I., MOAVENI, B., LOMBAERT, G., et al. "Hierarchical Bayesian model updating for structural identification", *Mechanical Systems and Signal Processing*, v. 64–65, pp. 360 – 376, 2015. ISSN: 0888-3270.

[36] NANDAN, H., SINGH, M. P. "Effects of thermal environment on structural frequencies: Part I – A simulation study", *Engineering Structures*, v. 81, pp. 480 – 490, 2014. ISSN: 0141-0296.

[37] NANDAN, H., SINGH, M. P. "Effects of thermal environment on structural frequencies: Part II – A system identification model", *Engineering Structures*, v. 81, pp. 491 – 498, 2014. ISSN: 0141-0296.

[38] LEE, J. J., LEE, J. W., YI, J. H., et al. "Neural networks-based damage detection for bridges considering errors in baseline finite element models", *Journal of Sound and Vibration*, v. 280, n. 3–5, pp. 555 – 578, 2005. ISSN: 0022-460X.

[39] KOLEHMAINEN, V., TARVAINEN, T., ARRIDGE, S. R., et al. "Marginalization of uninteresting distributed parameters in inverse problems - application to diffuse optical tomography", *International Journal for Uncertainty Quantification*, v. 1, pp. 1–17, 2011. ISSN: 2152-5099.

[40] NISSINEN, A., KOLEHMAINEN, V. P., KAIPIO, J. P. "Compensation of Modelling Errors Due to Unknown Domain Boundary in Electrical Impedance Tomography", *IEEE Transactions on Medical Imaging*, v. 30, n. 2, pp. 231–242, Feb 2011. ISSN: 0278-0062.

[41] NISSINEN, A., HEIKKINEN, L. M., KOLEHMAINEN, V., et al. "Compensation of errors due to discretization, domain truncation and unknown contact impedances in electrical impedance tomography", *Measurement Science and Technology*, v. 20, n. 10, pp. 105504, 2009.

[42] MOZUMDER, M., TARVAINEN, T., KAIPIO, J. P., et al. "Compensation of modeling errors due to unknown domain boundary in diffuse optical tomography", *J. Opt. Soc. Am. A*, v. 31, n. 8, pp. 1847–1855, Aug 2014.

[43] KOULOURI, A., RIMPILÄINEN, V., BROOKES, M., et al. "Compensation of domain modelling errors in the inverse source problem of the Poisson equation: Application in electroencephalographic imaging", *Applied Numerical Mathematics*, v. 106, pp. 24 – 36, 2016. ISSN: 0168-9274.

[44] TARVAINEN, T., KOLEHMAINEN, V., PULKKINEN, A., et al. "An approximation error approach for compensating for modelling errors between the radiative transfer equation and the diffusion approximation in diffuse optical tomography", *Inverse Problems*, v. 26, n. 1, pp. 015005, 2010.

[45] COTTA, C. P. N. "Experimental-Theoretical Analysis of Biodiesel Synthesis in Micro-reactors with Inverse Problem Solution for Parameter Estimation", *Thematic Program on Parameter identification in mathematical models*. IMPA, Rio de Janeiro, Brazil, 2017.

[46] ORLANDE, H. R. B., DULIKRAVICH, G. S., NEUMAYER, M., et al. "Accelerated Bayesian Inference for the Estimation of Spatially Varying Heat Flux in a Heat Conduction Problem", *Numerical Heat Transfer, Part A: Applications*, v. 65, n. 1, pp. 1–25, 2014.

[47] LAMIEN, B., ORLANDE, H. R. B. "Approximation Error Model To Account For Convective Effects In Liquids Characterized By The Line Heat Source Probe", *4th Inverse Problems, Design and Optimization Symposium*. Albi, France, 2013.

[48] HUTTUNEN, J. M., KAIPIO, J. P., SOMERSALO, E. "Approximation errors in nonstationary inverse problems", *Inverse problems and imaging*, v. 1, n. 1, pp. 77, 2007.

[49] ROBERT, C., CASELLA, G. *Parameter estimation in engineering and science*, v. 2. Springer-Verlag New York, 2004.

[50] RITTO, T., SAMPAIO, R., AGUIAR, R. "Uncertain boundary condition Bayesian identification from experimental data: A case study on a cantilever beam", *Mechanical Systems and Signal Processing*, v. 68–69, pp. 176 – 188, 2016. ISSN: 0888-3270.

[51] CRANDALL, S. H., LARDNER, T. J., ARCHER, R. R., et al. "An introduction to the mechanics of solids", 1978.

[52] GÉRADIN, M., RIXEN, D. J. *Mechanical vibrations: theory and application to structural dynamics*. John Wiley & Sons, 2014.

[53] REDDY, J. N. *An introduction to the finite element method*, v. 2. McGraw-Hill New York, 1993.

[54] FISH, J., BELYTSCHKO, T. *A First Course in Finite Elements*. John Wiley & Sons, 2007.

[55] DA COSTA, M. M. A. "*Análise do Comportamento de estrutura utilizando. Múltiplos Sistemas Passivos de Absorção*", Dissertation (Masters degree in civil engineering). Universidade Federal do Rio de Janeiro, Rio de Janeiro, Brazil, 2014.

[56] REDDY, J. N. *Theory and Analysis of Elastic Plates and Shells*. CRC press, 2006.

[57] EBERHART, R. C., SHI, Y. "Particle swarm optimization: developments, applications and resources". In: *evolutionary computation, 2001. Proceedings of the 2001 Congress on*, v. 1, pp. 81–86. IEEE, 2001.

[58] NAPOLES, G., GRAU, I., BELLO, R. "Constricted Particle Swarm Optimization based Algorithm for Global Optimization", *Polibits*, pp. 05 – 11, 12 2012. ISSN: 1870-9044.

[59] PEDERSEN, M. E. H. "Good parameters for particle swarm optimization", *Hvass Lab., Copenhagen, Denmark, Tech. Rep. HL1001*, 2010.

[60] O'CALLAHAN, J. C. "Proceedings of the 6th International Modal Analysis Conference", *A procedure for an improved reduced system (IRS) model*. Las Vegas, United States, 1989.

[61] CHEN, S., MONTGOMERY, J., BOLUFÉ-RÖHLER, A. "Measuring the Curse of Dimensionality and Its Effects on Particle Swarm Optimization and Differential Evolution", *Applied Intelligence*, v. 42, n. 3, pp. 514–526, apr 2015. ISSN: 0924-669X.

[62] JARNY, Y., OZISIK, M., BARDON, J. "A general optimization method using adjoint equation for solving multidimensional inverse heat conduction", *International journal of heat and mass transfer*, v. 34, n. 11, pp. 2911–2919, 1991.

[63] FICHTNER, A., BUNGE, H.-P., IGEL, H. "The adjoint method in seismology: I. Theory", *Physics of the Earth and Planetary Interiors*, v. 157, n. 1, pp. 86 – 104, 2006. ISSN: 0031-9201.

[64] BONNET, M., CONSTANTINESCU, A. "Inverse problems in elasticity", *Inverse problems*, v. 21, n. 2, pp. R1, 2005.

[65] HAGER, W. W., ZHANG, H. "A survey of nonlinear conjugate gradient methods", *Pacific journal of Optimization*, v. 2, n. 1, pp. 35–58, 2006.

[66] BANERJEE, B., WALSH, T. F., AQUINO, W., et al. "Large scale parameter estimation problems in frequency-domain elastodynamics using an error in constitutive equation functional", *Computer methods in applied mechanics and engineering*, v. 253, pp. 60–72, 2013.

[67] LORD, G. J., POWELL, C. E., SHARDLOW, T. *An introduction to computational stochastic PDEs*. Cambridge University Press, 2014.

[68] KIM, H., SHIELDS, M. D. "Simulation of strongly non-Gaussian non-stationary stochastic processes utilizing Karhunen-Loeve expansion", *12th International Conference on Applications of Statistics and Probability in Civil Engineering*. Vancouver, Canada, 2015.

[69] VIO, R., ANDREANI, P., WAMSTEKER, W. "Numerical Simulation of Non-Gaussian Random Fields with Prescribed Correlation Structure", *Publications of the Astronomical Society of the Pacific*, v. 113, n. 786, pp. 1009, 2001.

[70] VIO, R., ANDREANI, P., TENORIO, L., et al. "Numerical simulation of non-Gaussian random fields with prescribed marginal distributions and cross-correlation structure. II. Multivariate random fields", *Publications of the Astronomical Society of the Pacific*, v. 114, n. 801, pp. 1281, 2002.

[71] TRANDAFIR, R., DEMETRIU, S. "Numerical Simulation of Non-Gaussian Random Fields", *7th Balkan Conference on Operational Research.* Constanta, Romania, 2005.

[72] LAI, K.-L., CRASSIDIS, J. L. *Generalizations of the complex-step derivative approximation.* State University of New York at Buffalo, 2006.

A Finite Element Model for FSDT

This appendix describes the finite element from REDDY [56] for plate bending. The element is a four node bilinear quadrilateral one, with 3 degrees of freedom per node, isoparametric with linear interpolation of geometry and material properties *constant* over the element.

The corresponding code was verified against analytical and numerical solutions presented in reference [56].

A.1 The Finite Element

In local element coordinates, the shape functions of a bilinear quadrilateral element are:

$$\begin{pmatrix}\psi_1\\ \psi_2\\ \psi_3\\ \psi_4\end{pmatrix} = \frac{1}{4}\begin{pmatrix}(1-r)(1-s)\\ (1-r)(1+s)\\ (1+r)(1+s)\\ (1+r)(1-s)\end{pmatrix}, \quad (r,s)\in[-1,1]\times[-1,1] \tag{A.1.1}$$

The following interpolation of degrees of freedom:

$$w_0(x,y,t) = \sum_{j=1}^{N} w_j(t)\psi_j(x,y) = \mathbf{N_v}\mathbf{v}, \quad \mathbf{N_v} = \begin{pmatrix}\psi_1 & \cdots & \psi_N\end{pmatrix}_{1\times N} \tag{A.1.2a}$$

$$\begin{pmatrix}\phi_x(x,x,t)\\ \phi_y(x,x,t)\end{pmatrix} = \sum_{j=1}^{N}\begin{pmatrix}S_j^x(t)\\ S_j^y(t)\end{pmatrix}\psi_j(x,y) = \mathbf{N_s}\mathbf{s}, \quad \mathbf{N_s} = \begin{pmatrix}\psi_1 & 0\cdots & \psi_N & 0\\ 0 & \psi_1\cdots & 0 & \psi_N\end{pmatrix} \tag{A.1.2b}$$

leads to equations of motion of the form:

$$\begin{pmatrix}\boldsymbol{M}_{\text{vv}} & \mathbf{0}\\ \mathbf{0} & \boldsymbol{M}_{\text{ss}}\end{pmatrix}\begin{pmatrix}\ddot{\mathbf{v}}\\ \ddot{\mathbf{s}}\end{pmatrix} + \begin{pmatrix}\boldsymbol{K}_{\text{vv}} & \boldsymbol{K}_{\text{vs}}\\ \boldsymbol{K}_{\text{vs}}^T & \boldsymbol{K}_{\text{ss}}\end{pmatrix}\begin{pmatrix}\mathbf{v}\\ \mathbf{s}\end{pmatrix} = \begin{pmatrix}\boldsymbol{F}_{\text{v}}\\ \boldsymbol{F}_{\text{s}}\end{pmatrix} \tag{A.1.3}$$

where $\mathbf{v} = (w_1, w_2, \cdots, w_N)^T$ are the displacements at each node *of the element* and $\mathbf{s} = (S_1^x, S_1^y, \cdots, S_N^x, S_N^y)^T$ are the rotations.

Letting

$$\mathbf{m} = \begin{pmatrix} T_x \\ T_y \end{pmatrix}, \quad \mathbf{A} = \begin{pmatrix} A_{55}K_s & 0 \\ 0 & A_{44}K_s \end{pmatrix}, \quad \mathbf{D} = \begin{pmatrix} D_{11} & D_{12} & 0 \\ D_{12} & D_{22} & 0 \\ 0 & 0 & D_{66} \end{pmatrix} \tag{A.1.4a}$$

$$T_x = M_{nn}n_x - M_{ns}n_y = M_{xx}n_x + M_{xy}n_y \tag{A.1.4b}$$

$$T_y = M_{ns}n_x + M_{nn}n_y = M_{xy}n_x + M_{yy}n_y \tag{A.1.4c}$$

The matrices $\mathbf{A}$ and $\mathbf{D}$ are defined in the constitutive equations (4.2.7-4.2.8). Define the differential operators

$$\mathbf{D_1} = \begin{pmatrix} \partial_x \\ \partial_y \end{pmatrix}, \quad \mathbf{D_2} = \begin{pmatrix} \partial_x & 0 \\ 0 & \partial_y \\ \partial_y & \partial_x \end{pmatrix} \tag{A.1.5}$$

Thus the derivatives of the shape functions can be calculate as:

$$\mathbf{D_1}\mathbf{N_v} = \mathbf{B_v} = \begin{pmatrix} \psi_{1,x} & \psi_{2,x} \cdots & \psi_{N,x} \\ \psi_{1,y} & \psi_{2,y} \cdots & \psi_{N,y} \end{pmatrix} \tag{A.1.6a}$$

$$\mathbf{D_2}(\mathbf{N_s})_i = (\mathbf{B_s})_i = \begin{pmatrix} \psi_{i,x} & 0 \\ 0 & \psi_{i,y} \\ \psi_{i,y} & \psi_{i,x} \end{pmatrix} \Rightarrow \mathbf{B_s} = \begin{pmatrix} \psi_{1,x} & 0 \cdots & \psi_{N,x} & 0 \\ 0 & \psi_{1,y} \cdots & 0 & \psi_{N,y} \\ \psi_{1,y} & \psi_{1,x} \cdots & \psi_{N,y} & \psi_{N,x} \end{pmatrix} \tag{A.1.6b}$$

Therefore the hole finite element model can be constructed by calculating:

$$\mathbf{M_{vv}} = \int_{\Omega^e} \mathbf{N_v}^T I_0 \mathbf{N_v} d\Omega^e, \quad \mathbf{M_{ss}} = \int_{\Omega^e} \mathbf{N_s}^T I_2 \mathbf{N_s} d\Omega^e \tag{A.1.7a}$$

$$\mathbf{K_{vv,1}} = \int_{\Omega^e} \mathbf{B_v}^T \mathbf{A} \mathbf{B_v} d\Omega^e, \quad \mathbf{K_{vv,2}} = \int_{\Omega^e} \mathbf{N_v}^T k \mathbf{N_v} d\Omega^e \tag{A.1.7b}$$

$$\mathbf{K_{ss,1}} = \int_{\Omega^e} \mathbf{N_s}^T \mathbf{A} \mathbf{N_s} d\Omega^e, \quad \mathbf{K_{ss,2}} = \int_{\Omega^e} \mathbf{B_s}^T \mathbf{D} \mathbf{B_s} d\Omega^e \tag{A.1.7c}$$

$$\mathbf{K_{vv}} = \sum_i \mathbf{K_{vv},i}, \quad \mathbf{K_{ss}} = \sum_j \mathbf{K_{ss},j}, \quad \mathbf{K_{vs}} = \int_{\Omega^e} \mathbf{B_v}^T \mathbf{A} \mathbf{N_s} d\Omega^e \tag{A.1.7d}$$

$$\mathbf{F_v} = \int_{\Omega^e} \mathbf{N_v}^T q d\Omega^e + \int_{\Gamma \cap \Gamma^e} \mathbf{N_v}^T Q_n dS, \quad \mathbf{F_s} = \int_{\Gamma \cap \Gamma^e} \mathbf{N_s}^T \mathbf{m}\, dS \tag{A.1.7e}$$

Where k is the stiffness coefficient of a possible elastic bedding and q is a distributed load.

NOTE: The contour integrals $\int_\Gamma(\cdot)dS$ of adjacent elements are canceled out, thus only elements in the boundary actually contribute, leading to the notation $\int_{\Gamma\cap\Gamma^e}(\cdot)dS$, which can be further restricted to $\int_{\Gamma_t\cap\Gamma^e}(\cdot)dS$.

A.2 Shear Locking and Numerical Integration

Lower-order (quadratic or less) interpolations are plagued with shear locking, that is, when lower order equal interpolations of the transverse deflection and rotations are used, the elements become excessively stiff in the thin plate limit, yielding displacements that are too small compared to the true solution.

A commonly used technique is to under-integrate the transverse shear stiffness terms (i.e., coefficients in K_{ij} that contain A_{44} and A_{55}).

For a 4 node bilinear quadrilateral element with gauss rule 2×2, the terms of $\mathbf{A}$ should be evaluated with a 1×1 rule [53]. This is the quadrature rule implemented.

As an example, consider the evaluation of the integral:

$$\mathbf{K_{vs}} = \int_{\Omega^e} \mathbf{B_v}^T \mathbf{A} \mathbf{N_s} d\Omega^e$$

Two steps are required: first, the necessary change of variables from Ω^e to a standard domain $\mathcal{D}$.

$$\mathbf{K_{vs}} = \int_{\mathcal{D}} \mathbf{B_v}^T(r,s)\, \mathbf{A}(r,s)\, \mathbf{N_s}(r,s) \det(J_e(r,s))\, d\mathcal{D}$$

Followed by the quadrature in both directions for a quadrilateral element:

$$\mathbf{K_{vs}} \approx \sum_{i=1}^{N_i}\sum_{j=1}^{N_j} w_i w_j\, \mathbf{B_v}^T(g_i,g_j)\, \mathbf{A}(g_i,g_j)\, \mathbf{N_s}(g_i,g_j) \det(J_e(g_i,g_j))$$

Where w_i are the weights of the quadrature procedure, and g_i the Gauss points in which to evaluate the function.

A.3 Elastic Boundaries

In order to add effects of elastic boundaries (Neumann boundary condition), consider the presence of torsion springs distributed over a region Γ_t:

$$\begin{pmatrix} T_x \\ T_y \end{pmatrix} = \mathbb{R} \begin{pmatrix} M_{nn} \\ M_{ns} \end{pmatrix}, \quad \begin{pmatrix} M_{nn} \\ M_{ns} \end{pmatrix} = -\Bbbk \begin{pmatrix} \phi_n \\ \phi_s \end{pmatrix}, \quad \begin{pmatrix} \phi_n \\ \phi_s \end{pmatrix} = \mathbb{R}^{-1} \begin{pmatrix} \phi_x \\ \phi_y \end{pmatrix} \tag{A.3.1}$$

Where

$$\Bbbk = \begin{pmatrix} k_n & 0 \\ 0 & k_s \end{pmatrix}, \quad \mathbb{R} = \begin{pmatrix} n_x & -n_y \\ n_y & n_x \end{pmatrix}, \quad \|\mathbf{n}\| = 1 \tag{A.3.2}$$

$\Bbbk$ being the stiffness matrix related to rotation, with k_n the distributed torsional constant in the normal direction and k_s the distributed torsional constant in the tangent direction, and $\mathbb{R}$ a rotation between physical and element coordinate frames.

Define a new stiffness matrix $\mathbf{K_{ss,3}}$ as:

$$\mathbf{F_s} = \int_{\Gamma_t \cap \Gamma^e} \mathbf{N_s}^T \mathbf{m}\, dS = -\int_{\Gamma_t \cap \Gamma^e} \mathbf{N_s}^T \mathbb{R}\, \Bbbk\, \mathbb{R}^{-1} \mathbf{N_s}\, dS \equiv -\mathbf{K_{ss,3}} \tag{A.3.3}$$

To proceed with a systematical numerical evaluation of this integral, consider a geometry interpolation given by n points, $\mathbf{x} = (x, y)^T = \sum_{j=1}^{n} \mathbf{x}_j^e \phi_j(r, s)$. The Jacobian matrix of the map $T : \Omega^e(\mathbf{x}) \mapsto \mathcal{D}(\boldsymbol{\xi})$ is given by:

$$J_{ij} = \frac{\partial \mathbf{x}_i}{\partial \boldsymbol{\xi}_j} \Leftrightarrow J_e(r, s) = \begin{pmatrix} x_{,r} & y_{,r} \\ x_{,s} & y_{,s} \end{pmatrix} = \begin{pmatrix} \partial_r \phi_1 & \cdots & \partial_r \phi_n \\ \partial_s \phi_1 & \cdots & \partial_s \phi_n \end{pmatrix} \begin{pmatrix} x_1^e & y_1^e \\ \vdots & \vdots \\ x_n^e & y_n^e \end{pmatrix} \tag{A.3.4}$$

where $\mathbf{x}_j^e = (x_j^e, y_j^e)$ and ϕ_j are the element's node coordinates and shape functions at these nodes, respectively.

Therefore

$$\mathbf{A}(x, y) = \mathbf{A}(x(r, s), y(r, s)) \equiv \mathbf{A}(r, s), \text{ etc...}$$

and with respect to the shape functions:

$$\psi(x, y) = \psi(x(r, s), y(r, s)) \equiv \psi(r, s)$$

$$\begin{pmatrix} \psi_{i,x}(x, y) \\ \psi_{i,y}(x, y) \end{pmatrix} = J_e^{-1} \begin{pmatrix} \psi_{i,r}(r, s) \\ \psi_{i,s}(r, s) \end{pmatrix}$$

With *isoparametric* elements, $\psi_i = \phi_i$.

For boundary integrals, consider the following:

$$dS = \sqrt{dx^2 + dy^2} \tag{A.3.5a}$$

$$dx = x_{,r}dr + x_{,s}ds = J_{11}dr + J_{21}ds \tag{A.3.5b}$$

$$dy = y_{,r}dr + y_{,s}ds = J_{12}dr + J_{22}ds \tag{A.3.5c}$$

The Jacobian takes care of the change of variables to the standard element.

The tangent coordinate $t^{'}$ is related to t in local coordinates through the same change of variables. Thus a line connecting $(x_0, y_0) = T(r_0, s_0)$ to $(x, y) = T(r, s)$ in physical coordinates can be written in local coordinates as (because T is linear):

$$r = r_0 + \Delta r \cdot t, \quad t \in [0, 1] \tag{A.3.6a}$$

$$s = s_0 + \Delta s \cdot t, \quad t \in [0, 1] \tag{A.3.6b}$$

Therefore

$$dr = \Delta r dt, \quad ds = \Delta s dt \tag{A.3.7a}$$

$$dx(r, s) = (J_{11}(r, s)\Delta r + J_{21}(r, s)\Delta s)dt \tag{A.3.7b}$$

$$dy(r, s) = (J_{12}(r, s)\Delta r + J_{22}(r, s)\Delta s)dt \tag{A.3.7c}$$

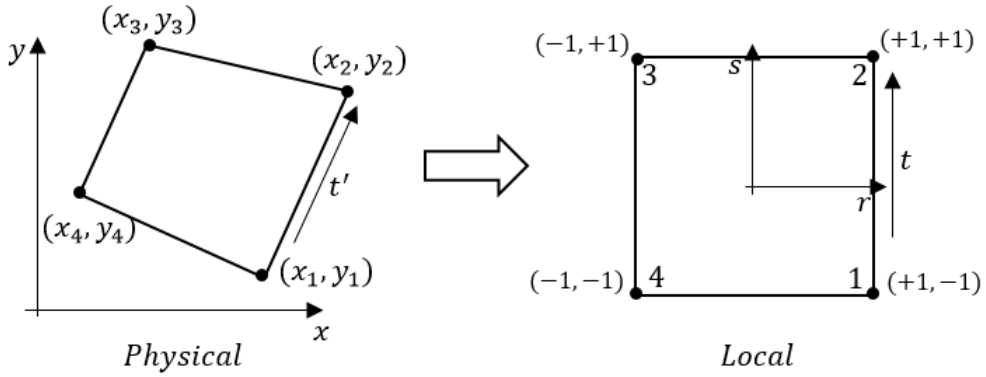

Figure A.1: Tangent coordinate $t^{'}$ in physical coordinates and change of variables.

And thus any line integral can be calculated as:

$$\begin{aligned}\int_\Gamma f(\mathbf{x})dS &= \int_0^t f(r(t),s(t))\sqrt{(J_{11}\Delta r + J_{21}\Delta s)^2 + (J_{12}\Delta r + J_{22}\Delta s)^2}dt \\ &= \int_{-1}^{1} f(r(\xi),s(\xi))\, d\Gamma(\xi)\frac{1}{2}d\xi, \quad t = \frac{\xi+1}{2} \\ &\approx \sum_{i=1}^{N_i} \frac{1}{2} w_i f(r(\xi_i),s(\xi_i))d\Gamma(\xi_i)\end{aligned}$$

Where

$$\begin{aligned}d\Gamma(\xi)^2 = [J_{11}(r(\xi),s(\xi))\Delta r + J_{21}(r(\xi),s(\xi))\Delta s]^2 + \\ + [J_{12}(r(\xi),s(\xi))\Delta r + J_{22}(r(\xi),s(\xi))\Delta s]^2\end{aligned}$$

As a concrete example, consider the addition of torsion sprigs distributed along the boundaries 1 ($x = 0$,y) and 3 ($x = L_X$,y). For boundary 1: $n_x = -1$, $n_y = 0$. For boundary 3: $n_x = +1$, $n_y = 0$.

The linear Hooke Law for the torsion springs and chance of coordinates between the local and global frames are given by equations (A.3.1-A.3.2). Thus

$$\begin{aligned}\mathbf{K_{ss,3}} &= \int_{\Gamma_t \cap \Gamma^e} \mathbf{N_s}^T \mathbb{R}\,\mathbb{k}\,\mathbb{R}^{-1}\mathbf{N_s}\, dS \\ &= \int_{\Gamma_t \cap \Gamma^e} \mathbf{N_s}^T \begin{pmatrix} n_x & -n_y \\ n_y & n_x \end{pmatrix} \begin{pmatrix} k_n & 0 \\ 0 & k_s \end{pmatrix} \begin{pmatrix} n_x & n_y \\ -n_y & n_x \end{pmatrix} \mathbf{N_s}\, dS \\ &= \int_0^1 \mathbf{N_s}^T \begin{pmatrix} k_n n_x^2 + k_s n_y^2 & k_n n_x n_y - k_s n_x n_y \\ k_n n_x n_y - k_s n_x n_y & k_s n_x^2 + k_n n_y^2 \end{pmatrix} \mathbf{N_s} \left\| J_e^T \begin{pmatrix} \Delta r \\ \Delta s \end{pmatrix} \right\|_2 dt\end{aligned} \tag{A.3.8}$$

Where $k_\alpha = k_{\alpha,1}(1-t) + k_{\alpha,2}$, $k_{\alpha,1}$ is the value at the local node with $t = 0$. In this work, the stiffness constants of the distributed springs are given at the nodes and linearly interpolated at the faces of the corresponding elements. However $k_s = 0$, always.

B Improved Reduce System

O'CALLAHAN [60] improved on the Static Reduction by Guyan (see [52]) by introducing the technique known as the Improved Reduced System (IRS) method. The IRS method perturbs the Static Reduction by including the inertia terms as pseudo-static forces. Obviously, it is impossible to emulate the behavior of a full system with a reduced model and every reduction transformation sacrifices accuracy for speed in some way. The IRS results in a reduced system which matches the low frequency resonances of the full system better than static reduction.

Consider the system of ODEs without damping of a system subjected to sinusoidal damping. This system is rearranged in such as in eq.(B.1).

$$\begin{pmatrix} M_{pp} & M_{ps} \\ M_{sp} & M_{ss} \end{pmatrix} \begin{pmatrix} \ddot{\mathbf{q}}_\mathbf{p} \\ \ddot{\mathbf{q}}_\mathbf{s} \end{pmatrix} + \begin{pmatrix} K_{pp} & K_{ps} \\ K_{sp} & K_{ss} \end{pmatrix} \begin{pmatrix} \mathbf{q}_\mathbf{p} \\ \mathbf{q}_\mathbf{s} \end{pmatrix} = \begin{pmatrix} \mathbf{f}_\mathbf{p} \\ \mathbf{0} \end{pmatrix} \tag{B.1}$$

Or

$$\mathbf{M}^\star \ddot{\mathbf{q}}^\star + \mathbf{K}^\star \mathbf{q}^\star = (\mathbf{f}_\mathbf{p}, \mathbf{0})^T$$

where $(\cdot)_p$ denotes the primary degrees of freedom (the ones that remain after reduction) and $(\cdot)_s$ denotes the secondary degrees of freedom (the ones "enslaved"). The secondary degrees of freedom (dof) are chosen to have $\mathbf{f}_s = \mathbf{0}$, they are rewritten in terms of the primary degrees of freedom:

$$\mathbf{q}_\mathbf{s} = -(K_{ss} - \omega^2 M_{ss})^{-1}(K_{sp} - \omega^2 M_{sp})\mathbf{q}_\mathbf{p} \tag{B.2}$$

$$= -K_{ss}^{-1}\left[K_{sp} + \omega^2(M_{ss}K_{ss}^{-1}K_{sp} - M_{sp}) + \mathcal{O}(\omega^4)\right]\mathbf{q}_\mathbf{p} \tag{B.3}$$

The reduced model based on Static Condensation satisfies:

$$\omega^2 \mathbf{M}_R = \mathbf{K}_R \mathbf{q}_\mathbf{p} \tag{B.4}$$

Where $(\cdot)_R$ are the reduced matrices obtained from static reduction, ω and $\mathbf{q}_\mathbf{p}$ are the natural frequency and correspondent (reduced) eigenvector. Substituting this relation and ignoring higher order terms:

$$\mathbf{q}_\mathbf{s} \approx \left[-K_{ss}^{-1}K_{sp} - K_{ss}^{-1}(M_{ss}K_{ss}^{-1}K_{sp} - M_{sp})\mathbf{M}_R\mathbf{K}_R\right]\mathbf{q}_\mathbf{p} \tag{B.5}$$

Although only strictly correct when the coordinate vector is a mode shape, equation (B.5) may be applied as a general transformation, $\mathbb{T}_I$:

$$\mathbb{T}_I = \mathbb{T}_g + \mathbf{S}\mathbf{M}\mathbb{T}_g(\mathbf{M}_R)^{-1}\mathbf{K}_R, \quad \mathbf{S} = \begin{pmatrix} \mathbf{0} & \mathbf{0} \\ \mathbf{0} & -K_{ss}^{-1} \end{pmatrix} \tag{B.6}$$

The transformation can be rewritten as:

$$\mathbb{T}_I = \begin{pmatrix} \mathbb{1} \\ -K_{ss}^{-1}K_{sp} + K_{ss}^{-1}\mathbf{S}\mathbf{M}_R^{-1}\mathbf{K}_R \end{pmatrix}, \quad \mathbf{S} = M_{sp} - M_{ss}K_{ss}^{-1}K_{sp} \tag{B.7}$$

Where $\mathbb{T}_g$ is the Static Condensation Transformation matrix.

$$\mathbb{T}_g = \begin{pmatrix} \mathbb{1} \\ -K_{ss}^{-1}K_{sp} \end{pmatrix} \tag{B.8}$$

Therefore the reduced matrices can be obtained from eq.(B.6) and eq.(B.9):

$$\overline{\mathbf{K}} = \mathbb{T}_I^T\mathbf{K}^\star\mathbb{T}_I, \quad \overline{\mathbf{M}} = \mathbb{T}_I^T\mathbf{M}^\star\mathbb{T}_I, \quad \mathbf{q}^\star = \mathbb{T}_I\,\mathbf{q_p}, \quad \text{etc.} \tag{B.9}$$

Since IRS method is constructed upon the Static Condensation, its algorithm is presented in conjunction with that of IRS in Fig.B.1. Both algorithms are is based upon a rearrangement of the dof such as the one in eq.(B.1).

The same recommendations that apply to the Static Condensation also apply to the IRS:

- Use dof $q_i \in \mathbf{q_s}$ such that the ratio K_{ii}/M_{ii} is elevated.
- Better results can be obtained if the primary dof are uniformly distributed over the physical domain: consider uniformly distributed nodes
- Consider nodes with both displacement and rotation degrees of freedom associated with them.

Given how the primary and secondary dof were chosen, $\mathbf{f_p} = \mathbb{T}^T\mathbf{f}^\star$ is automatically satisfied for both transformations.

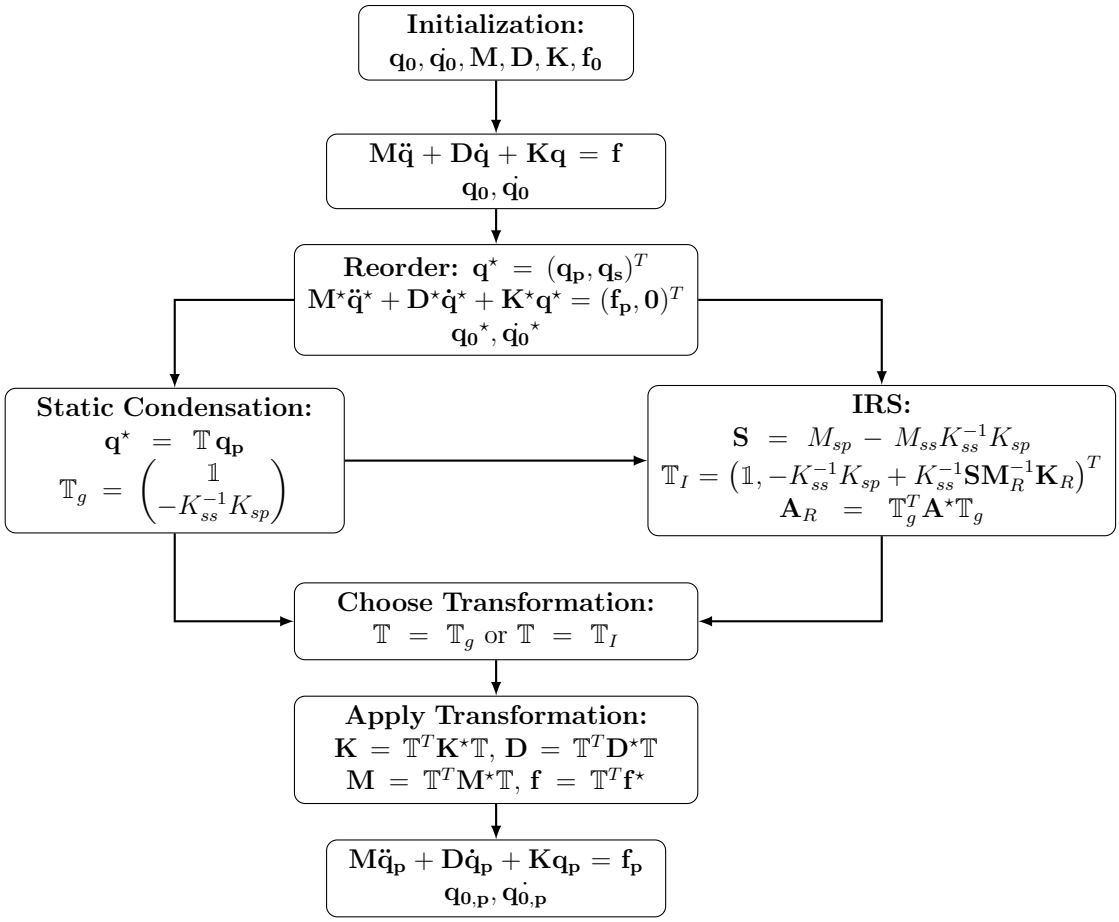

Figure B.1: Static Condensation algorithm and how it relates to the and Improved Reduced System to construct a reduced model.

C Random Fields

In order to generate the statics of the AEA, as describe in Section 2.4, one must consider the problem of generating random numbers, in particular, the generation of random correlated fields is of importance if one wishes to study the effects of uncertain distributed quantities, such as material properties.

The generation of random fields is not the main subject of this dissertation, however. Thus this chapter presents only the basic concepts necessary for the understanding of the situations presented in Chapter 5.3, as well as two relatively simple methods for the generation of random fields. Detailed information about this subject may be found in the reference books [49, 67].

C.1 Gaussian Random Fields

Let $u(\mathbf{x}) : \mathbf{x} \in \mathcal{D} \subset \mathbb{R}^n \mapsto \mathbb{R}$ be a *random field*. A *gaussian random field* $u(\mathbf{x})$ is a field such that $\mathbf{U} = (u(\mathbf{x}_1), \cdots, u(\mathbf{x}_N))^T$ follows the N-dimensional multivariate gaussian distribution, $\mathbf{U} \sim \mathcal{N}(\boldsymbol{\mu}, \mathbf{C})$, with expected value $\boldsymbol{\mu} = \mathbb{E}[\mathbf{U}]$ and covariance matrix $\mathbf{C}_{ij} = c(\mathbf{x_i}, \mathbf{x_j}) = \mathbb{E}[(u(\mathbf{x_i}) - \mu(\mathbf{x_i}))(u(\mathbf{x_j}) - \mu(\mathbf{x_j}))]$, where $\mathbf{x_i}, \mathbf{x_j} \in \mathcal{D}$ [67].

The function $c(\mathbf{x}, \mathbf{y})$ defines the basic characteristics of the field. Random fields are said to be *isotropic* if they are invariant to rotation

$$c(\mathbf{x}, \mathbf{y}) = c(\|\mathbf{x} - \mathbf{y}\|) \tag{C.1.1}$$

and *stationary* if they are invariant to translation

$$c(\mathbf{x}, \mathbf{y}) = c(\mathbf{x} - \mathbf{y}) \tag{C.1.2}$$

In both cases, the mean is independent of position, that is, $\mathbb{E}[u(\mathbf{x})] = \boldsymbol{\mu}$.

Equation (C.1.3) is a *Gaussian covariance function*, where $\mathbf{A}$ is a symmetric positive-definite $n \times n$ matrix, σ is the standard-deviation and $\ell_c > 0$ is the correlation length[1].

$$c(\mathbf{x}, \mathbf{y}) = \sigma^2 \exp\left\{ -\frac{(\mathbf{x} - \mathbf{y})^T \mathbf{A} (\mathbf{x} - \mathbf{y})}{\ell_c^2} \right\} \tag{C.1.3}$$

[1] $\mathbf{A}$ and ℓ_c^2 are multiplied, thus there are infinitely many combinations of $\mathbf{A}$ and ℓ_c^2 that produce the same correlation function.

where ℓ_c is a parameter that indicates the degree of correlation between the values of a random field u at two different locations, that is, if $\mathbf{x}$ and $\mathbf{y}$ are two points in space, their respective field values $u(\mathbf{x})$ and $u(\mathbf{y})$ are highly correlated if $\|\mathbf{y} - \mathbf{x}\| \ll \ell_c$ and effectively uncorrelated if $\|\mathbf{y} - \mathbf{x}\| \gg \ell_c$. While σ is simply a measure of the deviation between different realizations of the field $u(\mathbf{x})$ at the same location $\mathbf{x}_0$, that is, $\sigma^2 = \mathrm{Var}[u(\mathbf{x}_0)]$. This can be seen in one dimension, as shown in Fig. C.1, which also shows the intervals corresponding to $\mu \pm \sigma$, $\mu \pm 2\,\sigma$ and $\mu \pm 3\,\sigma$.

Figure C.2 shows that the effect of ℓ_c in isotropic two dimensional fields is analogous of that in one dimensional fields.

Whenever $\mathbf{A}$ is *not proportional* to the identity matrix of the $\mathbb{R}^n$ space, the field is *anisotropic*. Figure C.3 shows realizations of a random field with $\boldsymbol{\mu} = \mathbf{0}$ and different "signature" matrices $\mathbf{A}$, with $\ell_c = 0.1$ and $\sigma = 1$.

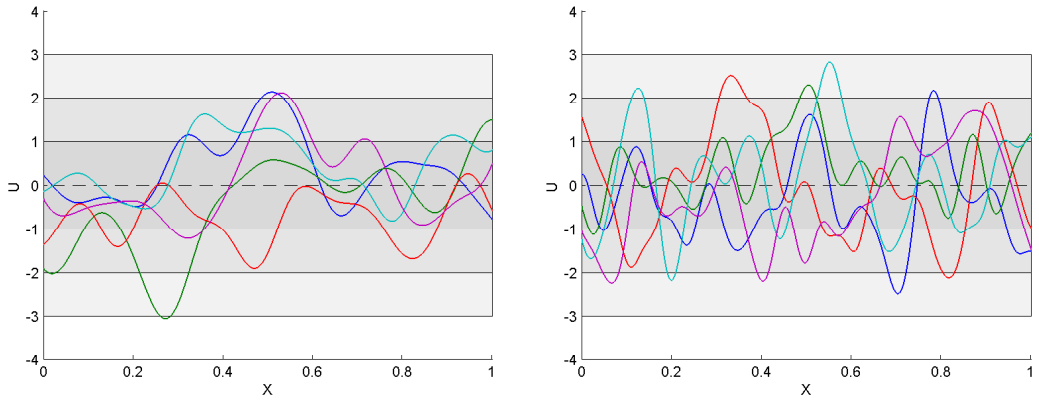

(a) $\ell_c = 0.10,\ \sigma = 1$ (b) $\ell_c = 0.05,\ \sigma = 1$

Figure C.1: Realizations of a Gaussian correlated 1D random field.

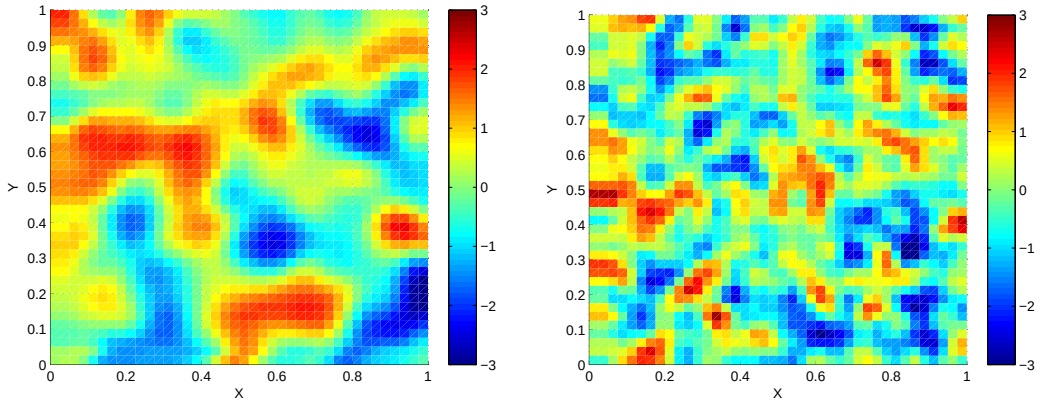

(a) $\ell_c = 0.10,\ \sigma = 1$ (b) $\ell_c = 0.05,\ \sigma = 1$

Figure C.2: Realizations of a Gaussian correlated Isotropic 2D random fields, $A = \mathbf{I}$.

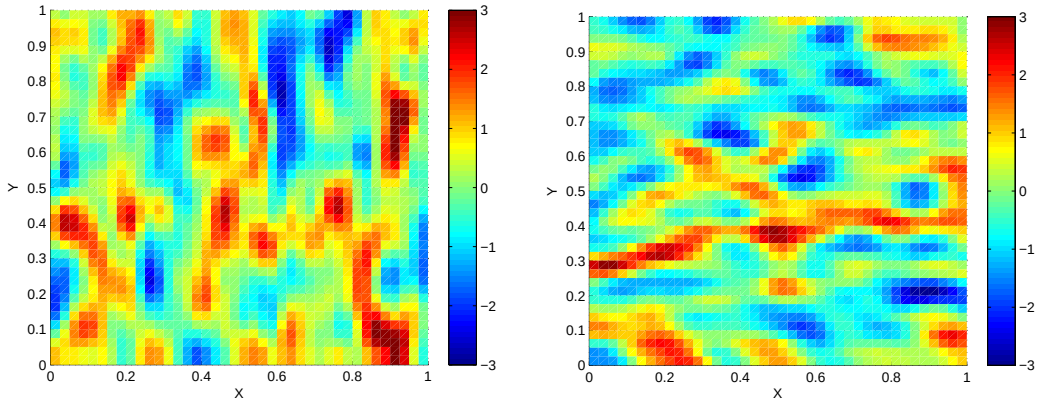

(a) $A = (+4.0,\ 0.0,\ 0.0,\ +1.0)$ (b) $A = (+1.0,\ 0.0,\ 0.0,\ +4.0)$

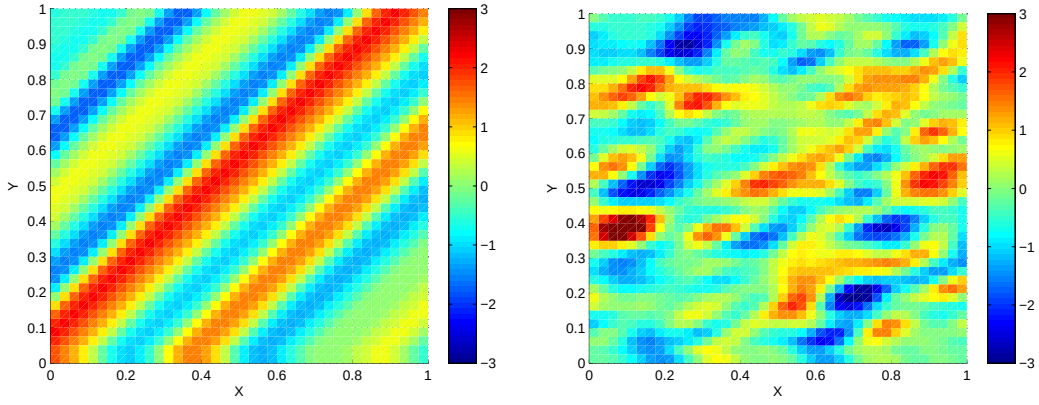

(c) $A = (+1.0,\ -1.0,\ -1.0,\ +1.0)$ (d) $A = (+1.0,\ -1.0,\ -1.0,\ +4.0)$

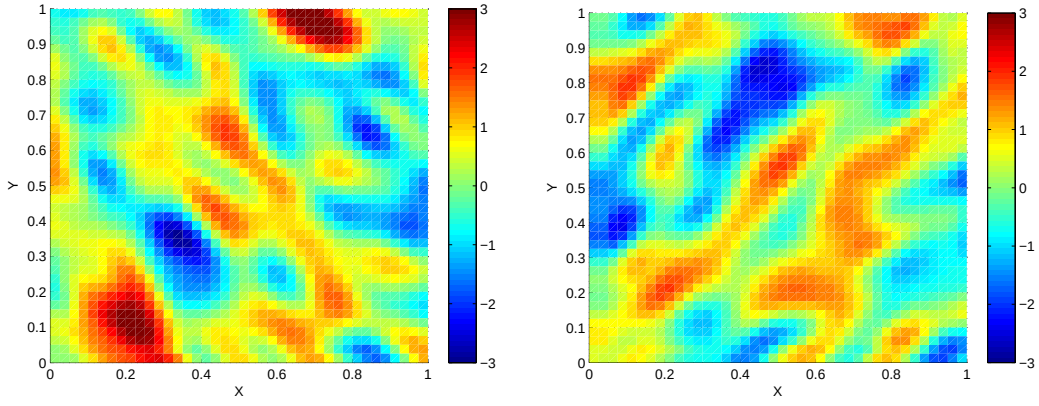

(e) $A = (+1.0,\ 0.5,\ 0.5,\ +1.0)$ (f) $A = (+1.0,\ -0.5,\ -0.5, +1.0)$

Figure C.3: Gaussian correlated anisotropic 2D random fields with $\ell_c = 0.1$ and $\sigma = 1$: different realizations of correlated fields are obtained when modifying the correlation structure $A = (A_{11},\ A_{12},\ A_{21},\ A_{22})$.

For one dimension, eq.(C.1.3) reduces to

$$c(x_1, x_2) = \sigma^2 \exp\left\{-\frac{\|(x_1 - x_2)\|_2^2}{\ell_c^2}\right\} \tag{C.1.4}$$

In order to generate a realization $\mathbf{U}$ of the random field $u(\mathbf{x})$, we use the *discrete Karhunen–Loève expansion*:

$$\mathbf{U} = \boldsymbol{\mu} + \sum_{j=1}^{N} \sqrt{\lambda_j}\mathbf{v}_j\xi_j \tag{C.1.5}$$

where λ_j and $\mathbf{v}_j$ are respectively the eigenvalues and eigenvectors of $\mathbf{C}$, and $\xi_j \sim \mathcal{N}(0,1)$ are *independent and identically distributed* (iid) realizations of a gaussian random variable. N is the dimension of the vector space corresponding to the discretization.

Eq.(C.1.5) can be rewritten in vector form as

$$\mathbf{U} = \boldsymbol{\mu} + \mathbf{V}\boldsymbol{\Lambda}^{1/2}\boldsymbol{\xi},\ \boldsymbol{\xi} \sim \mathcal{N}(\mathbf{0}, \mathbb{1}_{N\times N}) \tag{C.1.6}$$

In equations (C.1.5) and (C.1.6), $\boldsymbol{\mu}$ is the expected value of the field such that $\boldsymbol{\mu}_i = \mathbb{E}[u(\mathbf{x_i})]$ and $\boldsymbol{\Lambda}$ and $\mathbf{V}$ are respectively the diagonal matrix of eigenvalues and correspondent matrix of eigenvectors of $\mathbf{C}$. $\boldsymbol{\Lambda}$ and $\mathbf{V}$ are such that $\mathbf{L}^T = \mathbf{V}\boldsymbol{\Lambda}^{1/2}$, $\mathbf{C} = \mathbf{L}^T\mathbf{L}$. The covariance matrix $\mathbf{C}$ is calculated using a function $c(\mathbf{x}, \mathbf{y})$ such that $\mathbf{C}_{ij} = c(\mathbf{x_i}, \mathbf{x_j})$ gives the covariance structure between points $\mathbf{x_i}$ and $\mathbf{x_j}$, that is, eq.(C.1.3) or eq.(C.1.4) [67].

In Chapter 5.3, the fields were generated considering the *centroid* of the mesh's elements as the points $\mathbf{x_i}$ and $\mathbf{x_j}$ at which to calculate the covariance.

C.2 Non-gaussian Random Fields

Algorithms to generate non-gaussian correlated random fields are of practical interest, and while algorithms for generation of gaussian processes are well established, this cannot be said about non-gaussian ones [68]. For more on this subject, see the works by KIM and SHIELDS [68], VIO *et al.* [69, 70] and TRANDAFIR and DEMETRIU [71] and references therein.

This is not, however, the focus of this work, thus we consider the application of the *change of variables method* [11, 49] to generate a field $\mathbf{Z}$ with PDF $f(\mathbf{Z})$ and marginal $F_Z(\mathbf{Z})$ from a Gaussian correlated random field $\mathbf{U}$. We accomplish this by applying the transformation $g = F_Z^{-1} \circ F_U$:

$$\mathbf{Z} = g(\mathbf{U}) = F_Z^{-1}(F_U(\mathbf{U})) \tag{C.2.1}$$

where F_U is the marginal cumulative function of the Gaussian distribution.

In this work, we require realizations of a random field $d \in [0, 1]$. For the purpose of generating samples of this field, we consider a Beta distributed random variable $w \sim \mathcal{B}(\alpha, \beta)$, whose support is the interval $[0, 1]$. If we define a variable $z \in [z_{min}, z_{max}]$ it is possible to construct $z \sim \mathcal{B}(\alpha, \beta)$ with support $[z_{min}, z_{max}]$ [71]:

$$z = z_{min} + (z_{max} - z_{min})\, w \equiv z_{min} + \Delta z\, w \tag{C.2.2}$$

Thus z has PDF given by

$$f(z, \alpha, \beta) = \begin{cases} \dfrac{1}{B(\alpha, \beta)} \dfrac{(z - z_{min})^{\alpha-1}(z_{max} - z)^2}{(z_{max} - z_{min})^{\alpha+\beta+1}}, & z_{min} \leq z \leq z_{max} \\ 0, & \text{otherwise} \end{cases} \tag{C.2.3}$$

where $B(\alpha, \beta)$ is the beta function. Whose marginal is

$$F_Z(z) = \frac{B_u(\alpha, \beta)}{B(\alpha, \beta)} = \frac{1}{B(\alpha, \beta)} \int_0^u t^{\alpha-1}(1 - t)^{\beta-1} dt, \quad u = \frac{z - z_{min}}{z_{max} - z_{min}} \tag{C.2.4}$$

where $B_u(\alpha, \beta)$ is the incomplete beta function. Since F_Z is monotonically increasing, it has an inverse.

The mean and variance of z are related to those of w by

$$\mathbb{E}[z] = z_{min} + (\Delta z)\mathbb{E}[w] = z_{min} + (\Delta z)\frac{\alpha}{\alpha + \beta} \tag{C.2.5}$$

$$\mathrm{Var}[z] = \mathrm{Var}[z_{min} + (\Delta z)w] = (\Delta z)^2\, \mathrm{Var}[w] = \frac{\alpha\beta(\Delta z)^2}{(\alpha + \beta)^2(\alpha + \beta + 1)} \tag{C.2.6}$$

Figure C.4 shows a parametric study of the beta distribution. In order to simulate the damage field, we chose $\alpha = 0.2$, and further analysis lead us to choose $\beta = 5$, which produces less severe damage spikes.

Figure C.5 shows one-dimensional beta fields obtained for $\beta = 2$ and $\beta = 5$, the produced effect is an increase in the field. Also, a realization of a gaussian random field is shown and by its side the correspondent beta field obtained from change of variables (C.2.1).

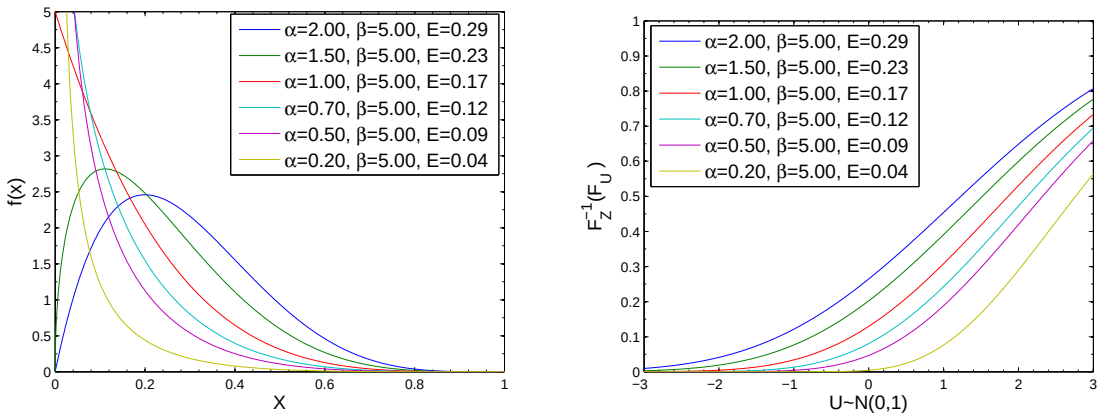

(a) $B(\alpha, \beta)$ (b) $g(u) = F_Z^{-1}(F_U(u))$

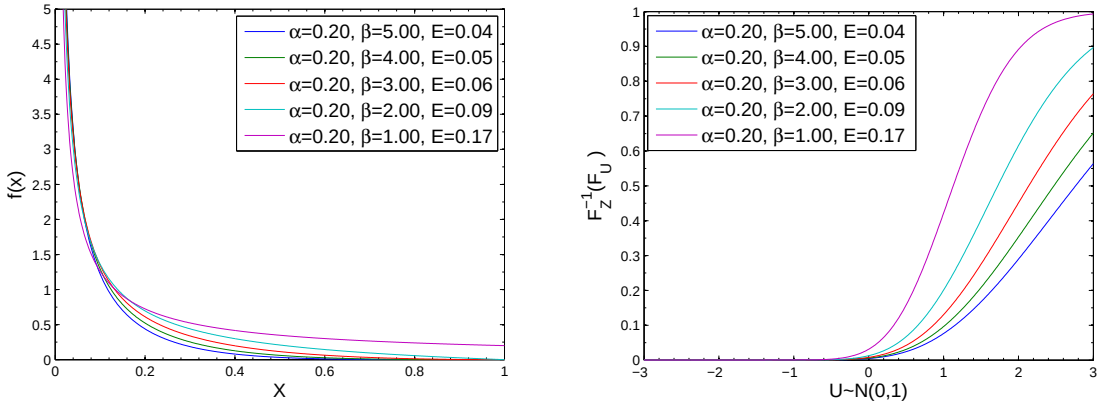

(c) $B(\alpha, \beta)$ (d) $g(u) = F_Z^{-1}(F_U(u))$

Figure C.4: Parametric Study of the Beta and composite functions. (a) and (c) various pdf of beta distributed variables with their respective expected values. (b) and (d) show the result of the composition $F_Z^{-1} \circ F_U$, it can be seen that for all proposed parameters, there is a vast linear region.

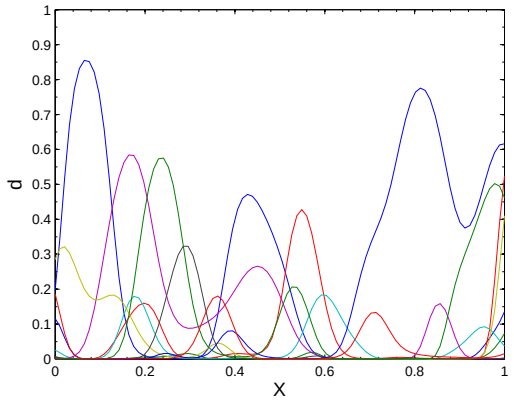

(a) $\alpha = 0.2, \beta = 2$

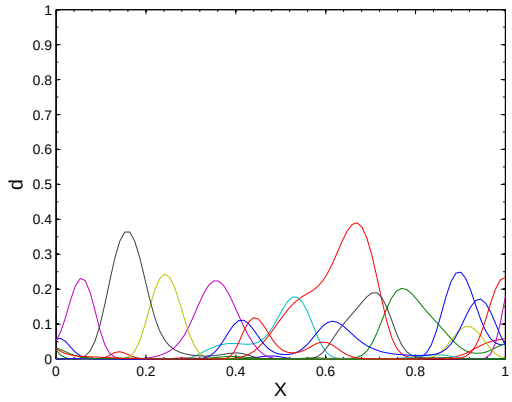

(b) $\alpha = 0.2, \beta = 5$

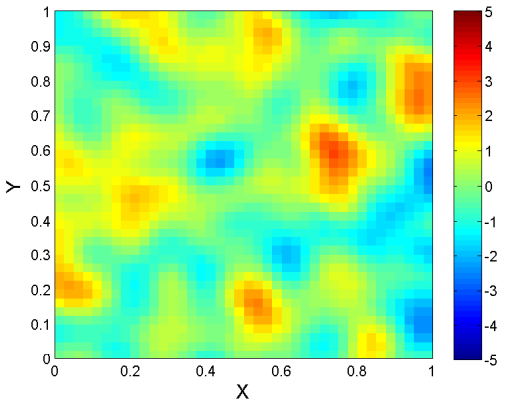

(c) Gaussian RF: $\boldsymbol{\mu} = \mathbf{0}, \sigma = 1, \ell_c = 0.1$

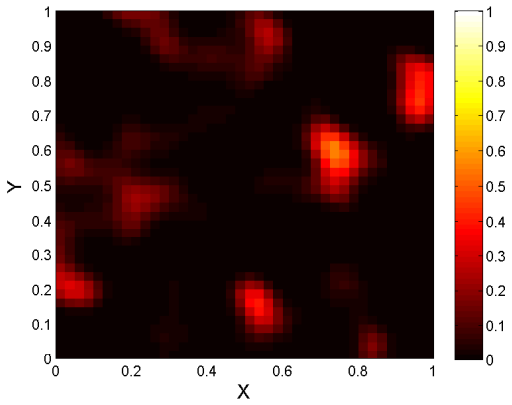

(d) Beta RF: $\alpha = 0.2, \beta = 5$

Figure C.5: Generation of Beta correlated random fields. (a) and (b) show the effects of the shape parameter β on a 1D field. (c) realization of a 2D gaussian correlated random field (d) correspondent 2D beta field obtained from change of variables.

D Approximation of the Posterior

The optimization problem for the traditional least squares is:

$$\boldsymbol{\theta}' = arg\min_{\boldsymbol{\theta}} \|\boldsymbol{\Gamma}_{\mathrm{e}}(\mathbf{y} - A(\boldsymbol{\theta}))\|^2 \tag{D.1}$$

where $\boldsymbol{\Gamma}_{\mathrm{e}}^T\boldsymbol{\Gamma}_{\mathrm{e}} = \boldsymbol{\Sigma}_{\mathrm{ee}}^{-1}$ and $\mathbf{e}_* = \mathbf{0}$.

Assuming $\pi(\boldsymbol{\theta}|\mathbf{y})$ is gaussian, it is possible to rewrite it around the estimated value $\boldsymbol{\theta}'$ leads to the following approximation:

$$\boldsymbol{\theta} \sim \mathcal{N}(\boldsymbol{\theta}', \boldsymbol{\Sigma}_{\boldsymbol{N}}) \tag{D.2a}$$

$$\boldsymbol{\Sigma}_N = \left(\mathbf{J}^T\boldsymbol{\Sigma}_{\mathrm{ee}}^{-1}\mathbf{J}\right)^{-1}, \quad \mathbf{J} = \left.\frac{\partial A}{\partial \boldsymbol{\theta}}\right|_{\boldsymbol{\theta}'} \tag{D.2b}$$

as described by TARANTOLA [11].

The optimization problem with Approximation Error is

$$\boldsymbol{\theta}' = arg\min_{\boldsymbol{\theta}} V(\boldsymbol{\theta}) \tag{D.3a}$$

$$V(\boldsymbol{\theta}) = \|\boldsymbol{\Gamma}_{\nu|\boldsymbol{\theta}}(\mathbf{y} - A(\boldsymbol{\theta}, \mathbf{z}_0, \xi_0) - \boldsymbol{\nu}_{*|\boldsymbol{\theta}})\|^2 + \|\boldsymbol{\Gamma}_{\boldsymbol{\theta}}(\boldsymbol{\theta} - \boldsymbol{\theta}_*)\|^2 \tag{D.3b}$$

$$\boldsymbol{\nu}_{*|\boldsymbol{\theta}} = \mathbf{e}_* + \boldsymbol{\epsilon}_* + \boldsymbol{\Sigma}_{\epsilon\boldsymbol{\theta}}\boldsymbol{\Sigma}_{\boldsymbol{\theta}\boldsymbol{\theta}}^{-1}(\boldsymbol{\theta} - \boldsymbol{\theta}_*) \tag{D.3c}$$

$$\boldsymbol{\Sigma}_{\nu|\boldsymbol{\theta}} = \boldsymbol{\Sigma}_e + \boldsymbol{\Sigma}_{\epsilon\epsilon} - \boldsymbol{\Sigma}_{\epsilon\boldsymbol{\theta}}\boldsymbol{\Sigma}_{\boldsymbol{\theta}\boldsymbol{\theta}}^{-1}\boldsymbol{\Sigma}_{\boldsymbol{\theta}\epsilon} \tag{D.3d}$$

Therefore if one assumes $\pi(\boldsymbol{\theta}|\mathbf{y})$ to be gaussian, it is possible to rewrite the posterior around the estimated value $\boldsymbol{\theta}'$:

$$\boldsymbol{\theta} \sim \mathcal{N}(\boldsymbol{\mu}, \boldsymbol{\Sigma}_{\boldsymbol{N}}) \tag{D.4a}$$

$$\boldsymbol{\mu} = \boldsymbol{\theta}' + \boldsymbol{\Sigma}_N\mathbf{J}^T\boldsymbol{\Sigma}_{\nu|\boldsymbol{\theta}}^{-1}(\mathbf{y} - f(\boldsymbol{\theta}')) \tag{D.4b}$$

$$\boldsymbol{\Sigma}_N = \left(\mathbf{J}^T\boldsymbol{\Sigma}_{\nu|\boldsymbol{\theta}}^{-1}\mathbf{J} + \boldsymbol{\Sigma}_{\boldsymbol{\theta}\boldsymbol{\theta}}^{-1}\right)^{-1}, \quad \mathbf{J} = \left.\frac{\partial f}{\partial \boldsymbol{\theta}}\right|_{\boldsymbol{\theta}'} \tag{D.4c}$$

$$\boldsymbol{\Sigma}_{\nu|\boldsymbol{\theta}} = \boldsymbol{\Sigma}_e + \boldsymbol{\Sigma}_{\epsilon\epsilon} - \boldsymbol{\Sigma}_{\epsilon\boldsymbol{\theta}}\boldsymbol{\Sigma}_{\boldsymbol{\theta}\boldsymbol{\theta}}^{-1}\boldsymbol{\Sigma}_{\boldsymbol{\theta}\epsilon} \tag{D.4d}$$

$$f(\boldsymbol{\theta}) = A(\boldsymbol{\theta}, \mathbf{z}_0, \boldsymbol{\xi}_0) + \mathbf{e}_* + \boldsymbol{\epsilon}_* + \boldsymbol{\Sigma}_{\epsilon\boldsymbol{\theta}}\boldsymbol{\Sigma}_{\boldsymbol{\theta}\boldsymbol{\theta}}^{-1}(\boldsymbol{\theta} - \boldsymbol{\theta}_*) \tag{D.4e}$$

Equations (D.2) and eq.(D.4) are used in Chapter 5.2 to construct the 98% confidence envelope of the estimates. This is not, however, used in Chapter 5.3 in order to maintain the figures comprehensible.

E Adjoint Formulation

E.1 Adjoint Formulation: Introduction

Consider the inverse problem of identifying the parameters $\mathbf{p}$ written as a minimization problem of a **continuous functional**

$$\min_{\mathbf{p}} J(\mathbf{p}) \tag{E.1.1a}$$

$$J(\mathbf{p}) = \int_T \left[\bar{\mathbf{y}}(t) - \mathbf{y}(t,\mathbf{p})\right]^T \mathbf{W} \left[\bar{\mathbf{y}}(t) - \mathbf{y}(t,\mathbf{p})\right] dt + \boldsymbol{\alpha}^T \boldsymbol{\varphi}(\mathbf{p}) \tag{E.1.1b}$$

where $\bar{\mathbf{y}}(t) \in \mathbb{R}^{N_s}$ is a vector containing the measurements collected at times t and $\mathbf{y}(t,\mathbf{p}) \in \mathbb{R}^{N_s}$ is a vector of model responses, which is some function of the forward problem's solution. The forward problem being represented by an equation of the form $\mathbf{g}(t,\mathbf{x},\mathbf{p}) = \mathbf{0}$. $\mathbf{p} \in \mathbb{R}^N$ is the vector of model parameters. The term $\boldsymbol{\alpha}^T\boldsymbol{\varphi}(\mathbf{p})$ is related to a regularization technique, with regularization parameter $\boldsymbol{\alpha}$.

Alternatively, the condition that the forward problem must be satisfied can be incorporated to construct a *constrained* minimization problem:

$$\begin{aligned} \min_{\mathbf{p}} \quad & J(\mathbf{p}) \\ \text{subject to} \quad & \mathbf{g}(\mathbf{p}) = 0. \end{aligned} \tag{E.1.2}$$

If the calculations corresponding to the direct problem $\mathbf{y}(t,\mathbf{p})$ are computationally expansive, calculating the gradient of the functional for a large number of parameters $\mathbf{p}$ using finite differences becomes prohibitive. Furthermore, the use of heuristic methods for solving the minimization problem would very quickly become prohibitive for the same reason.

To counteract these problems, one can make use of a technique known as *Adjoint Varibles Formulation* [14, 62–64]. This technique basically uses an *extension of the functional*, called the *Lagrangian*, to construct an auxiliary problem for the **Lagrangian multipliers**. Using these multipliers, it is possible to obtain the gradient of the original functional *without* calculating the derivatives through (at least) $N+1$ finite differences of the forward problem, instead using *one* auxiliary problem.

To solve either problem (E.1.1) or (E.1.2), consider the Lagrangian:

$$\mathcal{L}(\mathbf{p},\boldsymbol{\lambda}) = \boldsymbol{\alpha}^T\boldsymbol{\varphi}(\mathbf{p}) + \int_T \left[\bar{\mathbf{y}}(t) - \mathbf{y}(t,\mathbf{p})\right]^T \mathbf{W} \left[\bar{\mathbf{y}}(t) - \mathbf{y}(t,\mathbf{p})\right] dt + \int_\Omega \boldsymbol{\lambda}^T \mathbf{g}(t,\mathbf{x},\mathbf{p}) d\Omega \tag{E.1.3}$$

Where $\boldsymbol{\lambda}$ are the Lagrange multipliers and $\mathbf{g}(t, \mathbf{x}, \mathbf{p}) = \mathbf{0}$ is the governing equation of the *direct problem*[2] with parameters $\mathbf{p}$ and variables $\mathbf{x} \in \Omega$.

Using this functional, we can construct an *Adjoint Problem* in Ω, with boundary conditions and/or initial conditions, for $\boldsymbol{\lambda}$. For instance, if $\mathbf{g}(t, \mathbf{x}, \mathbf{p}) = \mathbf{0}$ is the strong formulation of a problem defined in $\Omega = [T_i, T_f] \times \mathbb{R}^n$, the problem for $\boldsymbol{\lambda}$ is defined in this domain.

In the case of spatially discretized linear model, one gets a *linear time invariant system of ODEs*

$$\mathbf{M}(\mathbf{p})\ddot{\mathbf{q}}(t, \mathbf{p}) + \mathbf{D}(\mathbf{p})\dot{\mathbf{q}}(t, \mathbf{p}) + \mathbf{K}(\mathbf{p})\mathbf{q}(t, \mathbf{p}) = \mathbf{f}(t, \mathbf{p}), \quad T = (t_0, t_f] \tag{E.1.4a}$$

$$\mathbf{q}(t_0, \mathbf{p}) = \mathbf{q}_0(\mathbf{p}), \quad \dot{\mathbf{q}}(t_0, \mathbf{p}) = \dot{\mathbf{q}}_0(\mathbf{p}) \tag{E.1.4b}$$

Therefore the Lagrangian (written in a concise manner) is:

$$\mathcal{L}(\mathbf{p}, \boldsymbol{\lambda}) = \boldsymbol{\alpha}^T \boldsymbol{\varphi} + \int_T \mathbf{e}^T \mathbf{W} \mathbf{e}\, dt + \int_T \boldsymbol{\lambda}^T \left(\mathbf{M}\ddot{\mathbf{q}} + \mathbf{D}\dot{\mathbf{q}} + \mathbf{K}\mathbf{q} - \mathbf{f}\right) dt \tag{E.1.5}$$

where $\mathbf{e} = \bar{\mathbf{y}}(t) - \mathbf{y}(t, \mathbf{p})$.

E.2 Conjugate Gradient Method

Consider the objective function defined by:

$$S(\mathbf{p}) = \int_T [\bar{\mathbf{y}}(t) - \mathbf{y}(t, \mathbf{p})]^T \boldsymbol{W} [\bar{\mathbf{y}}(t) - \mathbf{y}(t, \mathbf{p})]\, dt + \boldsymbol{\alpha}^T \boldsymbol{\varphi}(\mathbf{p}) \tag{E.2.1}$$

Using the *Conjugate Gradient* (CG) Method [14, 15, 65]

$$\begin{aligned} \mathbf{d}^k &= \nabla S^k + \gamma^k \mathbf{d}^{k-1} \\ \mathbf{p}^{k+1} &= \mathbf{p}^k - \beta_k \mathbf{d}^k \end{aligned} \tag{E.2.2}$$

Where β_k is the step size in the search direction $\mathbf{d}_k$ and γ^k is the *conjugation coefficient*. Depending on the choice of γ^k, different versions of the algorithm can be obtained [15, 65]. In this text we consider the Polak-Ribière version, eq.(E.2.3), due to reasons explained in [14].

$$\gamma^k = \frac{(\nabla S^k)^T (\nabla S^k - \nabla S^{k-1})}{\|\nabla S^{k-1}\|^2}, \quad k = 1, 2, ... \tag{E.2.3}$$

with $\gamma^0 = 0$, that is, the CG starts with the steepest descent direction.

[2] The parallel with constrained optimization should be clear.

The gradient is calculated using the Adjoint Method, eq.(E.4.19):

$$(\nabla S)_i = \boldsymbol{\alpha}^T \frac{\partial \boldsymbol{\varphi}}{\partial p_i} + \underbrace{\int_T \boldsymbol{\lambda}^T \left[\frac{\partial \mathbf{M}}{\partial p_i}\ddot{\mathbf{q}} + \frac{\partial \mathbf{D}}{\partial p_i}\dot{\mathbf{q}} + \frac{\partial \mathbf{K}}{\partial p_i}\mathbf{q} - \frac{\partial \mathbf{f}}{\partial p_i} \right] dt}_{\equiv \int_T f(t)\, dt \approx \frac{1}{2}\sum_n (t_{n+1}-t_n)[f(t_n)+f(t_{n+1})]}$$

with a trapezoidal rule approximation for the integral term. Where $\boldsymbol{\lambda}$ is obtained from the *Adjoint Problem*.

The objective function evaluated at $\mathbf{p}^{k+1}$ is

$$\begin{aligned} S(\mathbf{p}^{k+1}) &= \int_T [\bar{\mathbf{y}}(t) - \mathbf{y}(t, \mathbf{p}^{k+1})]^T \boldsymbol{W} [\bar{\mathbf{y}}(t) - \mathbf{y}(t, \mathbf{p}^{k+1})]\, dt + \boldsymbol{\alpha}^T \boldsymbol{\varphi}(\mathbf{p}^{k+1}) \\ &= \int_T [\bar{\mathbf{y}}(t) - \mathbf{y}(t, \mathbf{p}^{k} - \beta_k \mathbf{d}^k)]^T \boldsymbol{W} [\bar{\mathbf{y}}(t) - \mathbf{y}(t, \mathbf{p}^{k} - \beta_k \mathbf{d}^k)]\, dt + \boldsymbol{\alpha}^T \boldsymbol{\varphi}(\mathbf{p}^{k} - \beta_k \mathbf{d}^k) \\ \rightarrow S^{k+1} &\equiv \int_T [\bar{\mathbf{y}} - \mathbf{y}^{k+1}]^T \boldsymbol{W} [\bar{\mathbf{y}} - \mathbf{y}^{k+1}]\, dt + \boldsymbol{\alpha}^T \boldsymbol{\varphi}^{k+1} \end{aligned}$$

Thus the optimum step-size β_k can be obtained from the 1D minimization problem of S^{k+1}.

$$\beta_k = arg\min S(\mathbf{p}^{k+1}) \tag{E.2.4}$$

However, traditional optimization algorithms would required additional evaluations of the objective function, and that *can be* costly due to the forward problem[3]. One alternative to exactly solving the minimization problem is to allow for an approximation, this leads us to the *Sensitivity Problem*.

E.3 Sensitivity Problem

If we allow for an approximation, it is possible to construct the so called *Sensitivity Problem* [14, 15, 30, 62]. Starting by a Taylor expansion in the search direction:

$$\begin{aligned} \mathbf{y}^{k+1} &= \mathbf{y}(t, \mathbf{p}^k - \beta_k \mathbf{d}^k) \equiv \mathbf{y}^k(\mathbf{p}^k + \Delta \mathbf{p}^k) \\ &\approx \mathbf{y}^k(\mathbf{p}^k) + \left.\frac{\partial \mathbf{y}^k}{\partial \mathbf{p}^k}\right|_{\mathbf{p}^k} \Delta \mathbf{p}^k \\ &= \mathbf{y}^k - \beta_k \left.\frac{\partial \mathbf{y}^k}{\partial \mathbf{p}^k}\right|_{\mathbf{p}^k} \mathbf{d}^k = \mathbf{y}^k - \beta_k \delta \mathbf{y}^k \end{aligned} \tag{E.3.1}$$

[3] In this case, it isn't. The use of a reduced model allows for an exact linear search to be conducted in appropriate time, however, for consistency, we use the sensitivity problem.

Where

$$\delta \mathbf{y}^k = \sum_{i=1}^{N} \left. \frac{\partial \mathbf{y}^k}{\partial p_i^k} \right|_{\mathbf{p}^k} (\mathbf{d}^k)_i \tag{E.3.2}$$

For a continuous functional, the proposed approximation leads to

$$\begin{aligned} S^{k+1} &\equiv \int_T [\bar{\mathbf{y}} - \mathbf{y}^{k+1}]^T \boldsymbol{W} [\bar{\mathbf{y}} - \mathbf{y}^{k+1}] \, dt + \boldsymbol{\alpha}^T \boldsymbol{\varphi}^{k+1} \\ &\approx \int_T [\bar{\mathbf{y}} - (\mathbf{y}^k - \beta_k \delta \mathbf{y}^k)]^T \boldsymbol{W} [\bar{\mathbf{y}} - (\mathbf{y}^k - \beta_k \delta \mathbf{y}^k)] \, dt + \boldsymbol{\alpha}^T (\boldsymbol{\varphi}^k - \beta_k \delta \boldsymbol{\varphi}^k) \\ &= \int_T [\bar{\mathbf{y}} - \mathbf{y}^k]^T \boldsymbol{W} [\bar{\mathbf{y}} - \mathbf{y}^k] + \beta_k^2 [\delta \mathbf{y}^k]^T \boldsymbol{W} [\delta \mathbf{y}^k] \, dt + \boldsymbol{\alpha}^T (\boldsymbol{\varphi}^k - \beta_k \delta \boldsymbol{\varphi}^k) \\ &+ \int_T \underbrace{\beta_k [\bar{\mathbf{y}} - \mathbf{y}^k]^T \boldsymbol{W} [\delta \mathbf{y}^k] + \beta_k [\delta \mathbf{y}^k]^T \boldsymbol{W} [\bar{\mathbf{y}} - \mathbf{y}^k]}_{= 2\beta_k [\bar{\mathbf{y}} - \mathbf{y}^k]^T \boldsymbol{W} \delta \mathbf{y}^k, \text{ since } \boldsymbol{W} = \boldsymbol{W}^T} dt \end{aligned} \tag{E.3.3}$$

Taking the derivative with respect to β_k in order to search for extreme points:

$$\frac{\partial S^{k+1}}{\partial \beta_k} \approx \int_T 2[\bar{\mathbf{y}} - \mathbf{y}^k]^T \boldsymbol{W} [\delta \mathbf{y}^k] + 2\beta_k [\delta \mathbf{y}^k]^T \boldsymbol{W} [\delta \mathbf{y}^k] \, dt - \boldsymbol{\alpha}^T \boldsymbol{\delta} \boldsymbol{\varphi}^k \tag{E.3.4}$$

$$\frac{\partial S^{k+1}}{\partial \beta_k} = 0 \Rightarrow \beta_k = \frac{1}{2} \left(\frac{\boldsymbol{\alpha}^T \boldsymbol{\delta} \boldsymbol{\varphi}^k + 2 \int_T [\mathbf{y}^k - \bar{\mathbf{y}}]^T \boldsymbol{W} [\delta \mathbf{y}^k] dt}{\int_T [\delta \mathbf{y}^k]^T \boldsymbol{W} [\delta \mathbf{y}^k] \, dt} \right) \tag{E.3.5}$$

which, in the absence of regularization, reduces to what is found in reference [14].

The variation $\delta\mathbf{y}^k$ is obtained from the solution of the *Sensitivity Problem*, eq.(E.3.6), at each global iteration k of the optimization algorithm.

The sensitivity problem is constructed from the governing equations of the direct problem. In this case:

$$\mathbf{M}\ddot{\mathbf{q}} + \mathbf{D}\dot{\mathbf{q}} + \mathbf{K}\mathbf{q} = \mathbf{f}(t)$$

Introducing a variation δp_i to each parameter leads to

$$\begin{aligned}\mathbf{M}\delta\ddot{\mathbf{q}} + \mathbf{D}\delta\dot{\mathbf{q}} + \mathbf{K}\delta\mathbf{q} &= \delta\mathbf{f} - (\delta\mathbf{M}\ddot{\mathbf{q}} + \delta\mathbf{D}\dot{\mathbf{q}} + \delta\mathbf{K}\mathbf{q}) \\ &= \sum_{i=1}^{N}\left(\frac{\partial\mathbf{f}}{\partial p_i} - \frac{\partial\mathbf{M}}{\partial p_i}\ddot{\mathbf{q}} - \frac{\partial\mathbf{D}}{\partial p_i}\dot{\mathbf{q}} - \frac{\partial\mathbf{K}}{\partial p_i}\mathbf{q}\right)\delta p_i \\ &\equiv \mathbf{F}(t)\end{aligned} \tag{E.3.6}$$

Therefore, using $\delta p_i = (\mathbf{d}^k)_i$ for each iteration k, and solving eq.(E.3.6), it is possible to calculate the *approximate* ideal step-size β_k [14].

Given that acceleration measurements are considered, it follows that:

$$\delta\mathbf{y} = C_a\delta\ddot{\mathbf{q}} \tag{E.3.7}$$

E.4 Adjoint Problem

A more abstract approach to the construction of the adjoint problem is presented by FICHTNER *et al.* [63], in this section, however, we consider a more explicit approach to the derivation of the adjoint problem for damage identification such as presented by PEREIRA *et al.* [30].

Starting from the extended functional eq.(E.1.5)

$$\mathcal{L}(\mathbf{p},\boldsymbol{\lambda}) = \boldsymbol{\alpha}^T\boldsymbol{\varphi}(\mathbf{p}) + \int_T \mathbf{e}^T\mathbf{W}\mathbf{e}\,dt + \int_T \boldsymbol{\lambda}^T\left(\mathbf{M}\ddot{\mathbf{q}} + \mathbf{D}\dot{\mathbf{q}} + \mathbf{K}\mathbf{q} - \mathbf{f}\right)\,dt$$

Introducing a variation $\delta\mathbf{p}$ on the parameters, which in turn produces variations of the predict response, model and observation:

$$\mathbf{p} \to \mathbf{p} + \delta\mathbf{p} \Rightarrow \mathcal{L}(\mathbf{p},\boldsymbol{\lambda}) \to \mathcal{L}(\mathbf{p}+\delta\mathbf{p},\boldsymbol{\lambda}) \tag{E.4.1}$$

Thus

$$\begin{aligned}\mathcal{L}(\mathbf{p}+\delta\mathbf{p},\boldsymbol{\lambda}) = \boldsymbol{\alpha}^T(\boldsymbol{\varphi}+\delta\boldsymbol{\varphi}) &+ \int_T (\mathbf{e}+\delta\mathbf{e})^T\mathbf{W}(\mathbf{e}+\delta\mathbf{e})\,dt + \\ &+ \int_T \boldsymbol{\lambda}^T[(\mathbf{M}+\boldsymbol{\Delta}\mathbf{M})(\ddot{\mathbf{q}}+\delta\ddot{\mathbf{q}}) + (\mathbf{D}+\boldsymbol{\Delta}\mathbf{D})(\dot{\mathbf{q}}+\delta\dot{\mathbf{q}}) + \\ &+ (\mathbf{K}+\boldsymbol{\Delta}\mathbf{K})(\mathbf{q}+\delta\mathbf{q}) - (\mathbf{f}+\delta\mathbf{f})]\,dt\end{aligned}$$

Expanding and dropping out second order terms:

$$\begin{aligned}\mathcal{L}(\mathbf{p}+\delta\mathbf{p},\boldsymbol{\lambda}) = \boldsymbol{\alpha}^T(\boldsymbol{\varphi}+\delta\boldsymbol{\varphi}) &+ \int_T \underbrace{\delta\mathbf{e}^T\mathbf{W}\delta\mathbf{e}}_{\approx 0} + \underbrace{\mathbf{e}^T\mathbf{W}\delta\mathbf{e} + \delta\mathbf{e}^T\mathbf{W}\mathbf{e}}_{=2\mathbf{e}^T\mathbf{W}\delta\mathbf{e}} + \mathbf{e}^T\mathbf{W}\mathbf{e}\,dt + \\ &+ \int_T \boldsymbol{\lambda}^T\left\{[\mathbf{M}\ddot{\mathbf{q}} + \mathbf{D}\dot{\mathbf{q}} + \mathbf{K}\mathbf{q} - \mathbf{f}] + [\mathbf{M}\delta\ddot{\mathbf{q}} + \mathbf{D}\delta\dot{\mathbf{q}} + \mathbf{K}\delta\mathbf{q} - \delta\mathbf{f}]\right\}\,dt + \\ &+ \int_T \boldsymbol{\lambda}^T\left[\boldsymbol{\Delta}\mathbf{M}\ddot{\mathbf{q}} + \boldsymbol{\Delta}\mathbf{D}\dot{\mathbf{q}} + \boldsymbol{\Delta}\mathbf{K}\mathbf{q} + \underbrace{\boldsymbol{\Delta}\mathbf{M}\delta\ddot{\mathbf{q}}}_{\approx 0} + \underbrace{\boldsymbol{\Delta}\mathbf{D}\delta\dot{\mathbf{q}}}_{\approx 0} + \underbrace{\boldsymbol{\Delta}\mathbf{K}\delta\mathbf{q}}_{\approx 0}\right]\,dt\end{aligned}$$

Define $\delta\mathcal{L} \equiv \mathcal{L}(\mathbf{p}+\delta\mathbf{p}, \boldsymbol{\lambda}) - \mathcal{L}(\mathbf{p}, \boldsymbol{\lambda})$, thus

$$\begin{aligned}\delta\mathcal{L}(\mathbf{p}, \boldsymbol{\lambda}) = \boldsymbol{\alpha}^T \delta\boldsymbol{\varphi} + \int_T 2\mathbf{e}^T \mathbf{W} \delta\mathbf{e}\, dt + \\ + \int_T \boldsymbol{\lambda}^T \left\{ [\Delta\mathbf{M}\ddot{\mathbf{q}} + \Delta\mathbf{D}\dot{\mathbf{q}} + \Delta\mathbf{K}\mathbf{q} - \delta\mathbf{f}] + [\mathbf{M}\delta\ddot{\mathbf{q}} + \mathbf{D}\delta\dot{\mathbf{q}} + \mathbf{K}\delta\mathbf{q}] \right\} dt\end{aligned} \tag{E.4.2}$$

Consider measurements $\mathbf{y}(t, \mathbf{p})$ linear combinations of the responses in acceleration, velocity and displacement of the system such as:

$$\mathbf{y}(t, \mathbf{p}) = C_a \ddot{\mathbf{q}}(t, \mathbf{p}) + C_v \dot{\mathbf{q}}(t, \mathbf{p}) + C_d \mathbf{q}(t, \mathbf{p}) \tag{E.4.3}$$

It follows directly that:

$$\delta\mathbf{e} = \delta\left(\bar{\mathbf{y}}(t) - \mathbf{y}(t, \mathbf{p})\right) = -\delta\mathbf{y}(t, \mathbf{p}) = -[C_a \delta\ddot{\mathbf{q}}(t, \mathbf{p}) + C_v \delta\dot{\mathbf{q}}(t, \mathbf{p}) + C_d \delta\mathbf{q}(t, \mathbf{p})] \tag{E.4.4}$$

Introducing the following decomposition for $\boldsymbol{\lambda}$ [30]:

$$\boldsymbol{\lambda} = \ddot{\boldsymbol{\lambda}}_a + \dot{\boldsymbol{\lambda}}_v + \boldsymbol{\lambda}_d \tag{E.4.5}$$

We arrive at

$$\begin{aligned}\delta\mathcal{L}(\mathbf{p}, \boldsymbol{\lambda}) = \boldsymbol{\alpha}^T \delta\boldsymbol{\varphi} - \int_T 2\mathbf{e}^T \mathbf{W} (C_a \delta\ddot{\mathbf{q}} + C_v \delta\dot{\mathbf{q}} + C_d \delta\mathbf{q})\, dt + \\ + \int_T \boldsymbol{\lambda}_d^T \left\{ [\Delta\mathbf{M}\ddot{\mathbf{q}} + \Delta\mathbf{D}\dot{\mathbf{q}} + \Delta\mathbf{K}\mathbf{q} - \delta\mathbf{f}] + [\mathbf{M}\delta\ddot{\mathbf{q}} + \mathbf{D}\delta\dot{\mathbf{q}} + \mathbf{K}\delta\mathbf{q}] \right\} dt \\ + \int_T \dot{\boldsymbol{\lambda}}_v^T \left\{ [\Delta\mathbf{M}\ddot{\mathbf{q}} + \Delta\mathbf{D}\dot{\mathbf{q}} + \Delta\mathbf{K}\mathbf{q} - \delta\mathbf{f}] + [\mathbf{M}\delta\ddot{\mathbf{q}} + \mathbf{D}\delta\dot{\mathbf{q}} + \mathbf{K}\delta\mathbf{q}] \right\} dt \\ + \int_T \ddot{\boldsymbol{\lambda}}_a^T \left\{ [\Delta\mathbf{M}\ddot{\mathbf{q}} + \Delta\mathbf{D}\dot{\mathbf{q}} + \Delta\mathbf{K}\mathbf{q} - \delta\mathbf{f}] + [\mathbf{M}\delta\ddot{\mathbf{q}} + \mathbf{D}\delta\dot{\mathbf{q}} + \mathbf{K}\delta\mathbf{q}] \right\} dt\end{aligned} \tag{E.4.6}$$

Integrating by parts the terms associated with displacements:

$$\begin{aligned}\int_T \underbrace{\boldsymbol{\lambda}_d^T}_{u}\mathbf{D}\underbrace{\delta\dot{\mathbf{q}}}_{dv}\,dt &= \boldsymbol{\lambda}_d^T\mathbf{D}\delta\mathbf{q}\Big|_T - \int_T \underbrace{\dot{\boldsymbol{\lambda}}_d^{\,T}}_{du}\mathbf{D}\underbrace{\delta\mathbf{q}}_{v}\,dt\\ \int_T \boldsymbol{\lambda}_d^T\mathbf{M}\ddot{\mathbf{q}}\,dt &= \boldsymbol{\lambda}_d^T\mathbf{M}\delta\dot{\mathbf{q}}\Big|_T - \int_T \dot{\boldsymbol{\lambda}}_d^{\,T}\mathbf{M}\delta\dot{\mathbf{q}}\,dt\\ &= \boldsymbol{\lambda}_d^T\mathbf{M}\delta\dot{\mathbf{q}}\Big|_T - \dot{\boldsymbol{\lambda}}_d^{\,T}\mathbf{M}\delta\mathbf{q}\Big|_T + \int_T \ddot{\boldsymbol{\lambda}}_d^{\,T}\mathbf{M}\delta\mathbf{q}\,dt\end{aligned}$$

Integrating by parts the terms associated with velocities:

$$\begin{aligned}\int_T \dot{\boldsymbol{\lambda}}_v^{\,T}\mathbf{M}\delta\ddot{\mathbf{q}}\,dt &= \dot{\boldsymbol{\lambda}}_v^{\,T}\mathbf{M}\delta\dot{\mathbf{q}}\Big|_T - \int_T \ddot{\boldsymbol{\lambda}}_v^{\,T}\mathbf{M}\delta\dot{\mathbf{q}}\,dt\\ \int_T \dot{\boldsymbol{\lambda}}_v^{\,T}\mathbf{K}\delta\mathbf{q}\,dt &= \boldsymbol{\lambda}_v^T\mathbf{K}\delta\mathbf{q}\Big|_T - \int_T \boldsymbol{\lambda}_v^T\mathbf{K}\delta\dot{\mathbf{q}}\,dt\end{aligned}$$

Integrating by parts the terms associated with accelerations:

$$\begin{aligned}\int_T \ddot{\boldsymbol{\lambda}}_a^{\,T}\mathbf{D}\delta\dot{\mathbf{q}}\,dt &= \dot{\boldsymbol{\lambda}}_a^{\,T}\mathbf{D}\delta\dot{\mathbf{q}}\Big|_T - \int_T \dot{\boldsymbol{\lambda}}_a^{\,T}\mathbf{D}\delta\ddot{\mathbf{q}}\,dt\\ \int_T \ddot{\boldsymbol{\lambda}}_a^{\,T}\mathbf{K}\delta\mathbf{q}\,dt &= \dot{\boldsymbol{\lambda}}_a^{\,T}\mathbf{K}\delta\mathbf{q}\Big|_T - \int_T \dot{\boldsymbol{\lambda}}_a^{\,T}\mathbf{K}\delta\dot{\mathbf{q}}\,dt\\ &= \dot{\boldsymbol{\lambda}}_a^{\,T}\mathbf{K}\delta\mathbf{q}\Big|_T - \boldsymbol{\lambda}_a^T\mathbf{K}\delta\dot{\mathbf{q}}\Big|_T + \int_T \boldsymbol{\lambda}_a^T\mathbf{K}\delta\ddot{\mathbf{q}}\,dt\end{aligned}$$

Since the variations must respect the boundary conditions $\delta\mathbf{q}_0 = \delta\dot{\mathbf{q}}_0 = \mathbf{0}$:

$$\begin{aligned}\delta\mathcal{L} = &\left[\boldsymbol{\lambda}_d^T\mathbf{M}\delta\dot{\mathbf{q}} - \dot{\boldsymbol{\lambda}}_d^{\,T}\mathbf{M}\delta\mathbf{q} + \boldsymbol{\lambda}_d^T\mathbf{D}\delta\mathbf{q}\right]\Big|_{t_f} + \int_T (\ddot{\boldsymbol{\lambda}}_d^{\,T}\mathbf{M} - \dot{\boldsymbol{\lambda}}_d^{\,T}\mathbf{D} + \boldsymbol{\lambda}_d^T\mathbf{K} - 2\mathbf{e}^T\mathbf{W}C_d)\delta\mathbf{q}\,dt\\ &+ \left[\boldsymbol{\lambda}_v^T\mathbf{K}\delta\mathbf{q} + \dot{\boldsymbol{\lambda}}_v^{\,T}\mathbf{M}\delta\dot{\mathbf{q}}\right]\Big|_{t_f} + \int_T (-\ddot{\boldsymbol{\lambda}}_v^{\,T}\mathbf{M} + \dot{\boldsymbol{\lambda}}_v^{\,T}\mathbf{D} - \boldsymbol{\lambda}_v^T\mathbf{K} - 2\mathbf{e}^T\mathbf{W}C_v)\delta\dot{\mathbf{q}}\,dt\\ &+ \left[\dot{\boldsymbol{\lambda}}_a^{\,T}\mathbf{D}\delta\dot{\mathbf{q}} + \dot{\boldsymbol{\lambda}}_a^{\,T}\mathbf{K}\delta\mathbf{q} - \boldsymbol{\lambda}_a^T\mathbf{K}\delta\dot{\mathbf{q}}\right]\Big|_{t_f} + \int_T (\ddot{\boldsymbol{\lambda}}_a^{\,T}\mathbf{M} - \dot{\boldsymbol{\lambda}}_a^{\,T}\mathbf{D} + \boldsymbol{\lambda}_a^T\mathbf{K} - 2\mathbf{e}^T\mathbf{W}C_a)\delta\ddot{\mathbf{q}}\,dt\\ &+ \boldsymbol{\alpha}^T\boldsymbol{\varphi} + \int_T \boldsymbol{\lambda}^T(\Delta\mathbf{M}\ddot{\mathbf{q}} + \Delta\mathbf{D}\dot{\mathbf{q}} + \Delta\mathbf{K}\mathbf{q})\,dt\end{aligned} \tag{E.4.7}$$

In order to eliminate the contributions of $\delta\mathbf{q}$ and $\delta\mathbf{q}(t_f)$:

$$\ddot{\boldsymbol{\lambda}}_d^T\mathbf{M} - \dot{\boldsymbol{\lambda}}_d^T\mathbf{D} + \boldsymbol{\lambda}_d^T\mathbf{K} = +2\mathbf{e}^T\mathbf{W}C_d \tag{E.4.8a}$$

$$\boldsymbol{\lambda}_d^T(t_f)\mathbf{D} - \dot{\boldsymbol{\lambda}}_d(t_f)^T\mathbf{M} = \mathbf{0} \tag{E.4.8b}$$

$$\boldsymbol{\lambda}_d^T(t_f)\mathbf{M} = \mathbf{0} \tag{E.4.8c}$$

In order to eliminate the contributions of $\delta\dot{\mathbf{q}}$ and $\delta\dot{\mathbf{q}}(t_f)$:

$$\ddot{\boldsymbol{\lambda}}_v^T\mathbf{M} - \dot{\boldsymbol{\lambda}}_v^T\mathbf{D} + \boldsymbol{\lambda}_v^T\mathbf{K} = -2\mathbf{e}^T\mathbf{W}C_v \tag{E.4.9a}$$

$$\boldsymbol{\lambda}_v^T(t_f)\mathbf{K} = \mathbf{0} \tag{E.4.9b}$$

$$\dot{\boldsymbol{\lambda}}_v^T(t_f)\mathbf{M} = \mathbf{0} \tag{E.4.9c}$$

In order to eliminate the contributions of $\delta\ddot{\mathbf{q}}$ and $\delta\ddot{\mathbf{q}}(t_f)$:

$$\ddot{\boldsymbol{\lambda}}_a^T\mathbf{M} - \dot{\boldsymbol{\lambda}}_a^T\mathbf{D} + \boldsymbol{\lambda}_a^T\mathbf{K} = +2\mathbf{e}^T\mathbf{W}C_a \tag{E.4.10a}$$

$$\dot{\boldsymbol{\lambda}}_a^T(t_f)\mathbf{D} - \boldsymbol{\lambda}_a^T(t_f)\mathbf{K} = \mathbf{0} \tag{E.4.10b}$$

$$\dot{\boldsymbol{\lambda}}_a^T(t_f)\mathbf{K} = \mathbf{0} \tag{E.4.10c}$$

Problems E.4.8, E.4.9 and E.4.10 are the *Adjoint Problems*, in their natural *final value problem* form.

They can be rewritten in a transposed manner, with zero boundary conditions. For example:

$$\mathbf{M}^T\ddot{\boldsymbol{\lambda}}_a - \mathbf{D}^T\dot{\boldsymbol{\lambda}}_a + \mathbf{K}^T\boldsymbol{\lambda}_a = +2C_a^T\mathbf{W}^T\mathbf{e} \tag{E.4.11a}$$

$$\mathbf{D}^T\dot{\boldsymbol{\lambda}}_a(t_f) - \mathbf{K}^T\boldsymbol{\lambda}_a(t_f) = \mathbf{0} \tag{E.4.11b}$$

$$\mathbf{K}^T\dot{\boldsymbol{\lambda}}_a(t_f) = \mathbf{0} \tag{E.4.11c}$$

Since $\mathbf{W}$ is the covariance matrix, $\mathbf{W} = \mathbf{W}^T$. And since the system is **not singular**, the matrices $\mathbf{M}$, $\mathbf{D}$ and $\mathbf{K}$ have inverses, and these inverses have their respective transposes $\mathbf{M}^{-T}$, $\mathbf{D}^{-T}$ and $\mathbf{K}^{-T}$. Therefore it follows that

$$\dot{\boldsymbol{\lambda}}_a(t_f) = \boldsymbol{\lambda}_a(t_f) = \mathbf{0} \tag{E.4.12}$$

In order to solve these equations, we rewrite them as Initial Value Problems – this way, the same algorithms that were applied to the system's ODEs can be applied to the adjoint equations.

Define the new time coordinate τ such that $t = t_f - \tau$. For convenience, $t_0 = 0$.

$$t = t_f - \tau \rightarrow \frac{d}{d\tau} = -\frac{d}{dt} \tag{E.4.13}$$

Therefore problem E.4.11 can be cast as an *initial value problem* (IVP).

$$\begin{aligned}
&\mathbf{M}^T\ddot{\boldsymbol{\lambda}}_a + \mathbf{D}^T\dot{\boldsymbol{\lambda}}_a + \mathbf{K}^T\boldsymbol{\lambda}_a = +2C_a^T\mathbf{W}^T\mathbf{e}(t_f - \tau), \quad \tau > 0 \\
&\dot{\boldsymbol{\lambda}}_a(\tau = 0) = \boldsymbol{\lambda}_a(\tau = 0) = \mathbf{0}
\end{aligned}$$

Where $\mathbf{e}(t_f - \tau)$ is the error vector evaluated backwards in time.

In practical terms, one reverses the order of $\mathbf{e}$ and uses it to drive the pertinent FVP rewritten as a IVP. Once the adjoint variables $\boldsymbol{\lambda}$ are calculated, these are reversed in order to be in accordance with the governing equations of the problem, which are, in the case of structural dynamics, the equations of motion.

Finally, we rewrite the Adjoint Problems as:

$$\mathbf{M}^T\ddot{\boldsymbol{\lambda}}_d + \mathbf{D}^T\dot{\boldsymbol{\lambda}}_d + \mathbf{K}^T\boldsymbol{\lambda}_d = +2C_d^T\mathbf{W}^T\mathbf{e}(t_f - \tau), \quad \dot{\boldsymbol{\lambda}}_d(0) = \boldsymbol{\lambda}_d(0) = \mathbf{0} \tag{E.4.14}$$

$$\mathbf{M}^T\ddot{\boldsymbol{\lambda}}_v + \mathbf{D}^T\dot{\boldsymbol{\lambda}}_v + \mathbf{K}^T\boldsymbol{\lambda}_v = -2C_v^T\mathbf{W}^T\mathbf{e}(t_f - \tau), \quad \dot{\boldsymbol{\lambda}}_v(0) = \boldsymbol{\lambda}_v(0) = \mathbf{0} \tag{E.4.15}$$

$$\mathbf{M}^T\ddot{\boldsymbol{\lambda}}_a + \mathbf{D}^T\dot{\boldsymbol{\lambda}}_a + \mathbf{K}^T\boldsymbol{\lambda}_a = +2C_a^T\mathbf{W}^T\mathbf{e}(t_f - \tau), \quad \dot{\boldsymbol{\lambda}}_a(0) = \boldsymbol{\lambda}_a(0) = \mathbf{0} \tag{E.4.16}$$

It is blatantly obvious that if one does not measure a particular quantity, for instance displacement, it follows that the corresponding C is the **zero matrix** and therefore $\boldsymbol{\lambda} = \mathbf{0}$.

The Lagrangian $\mathcal{L}$ and the original functional J are **equal by construction**, and thus have the **same gradient**. If $\boldsymbol{\lambda}$ satisfies the adjoint problem, however, the gradient can be calculated through the variation of $\mathcal{L}$

$$\delta\mathcal{L}(\mathbf{p},\boldsymbol{\lambda}) = \boldsymbol{\alpha}^T\delta\boldsymbol{\varphi} + \int_T \boldsymbol{\lambda}^T\left[\Delta\mathbf{M}\ddot{\mathbf{q}} + \Delta\mathbf{D}\dot{\mathbf{q}} + \Delta\mathbf{K}\mathbf{q} - \delta\mathbf{f}\right]\,dt = \delta J \tag{E.4.17}$$

Using the definition of first variation of a function:

$$\begin{aligned}
\delta\mathcal{L}(\mathbf{p},\boldsymbol{\lambda}) &= \sum_{i=1}^{N}\frac{\partial\mathcal{L}}{\partial p_i}\delta p_i \\
&= \sum_{i=1}^{N}\left[\boldsymbol{\alpha}^T\frac{\partial\boldsymbol{\varphi}}{\partial p_i}\delta p_i + \int_T \boldsymbol{\lambda}^T\left(\frac{\partial\mathbf{M}}{\partial p_i}\delta p_i\ddot{\mathbf{q}} + \frac{\partial\mathbf{D}}{\partial p_i}\delta p_i\dot{\mathbf{q}} + \frac{\partial\mathbf{K}}{\partial p_i}\delta p_i\mathbf{q} - \frac{\partial\mathbf{f}}{\partial p_i}\delta p_i\right)\,dt\right] \\
&= \sum_{i=1}^{N}\left[\boldsymbol{\alpha}^T\frac{\partial\boldsymbol{\varphi}}{\partial p_i} + \int_T \boldsymbol{\lambda}^T\left(\frac{\partial\mathbf{M}}{\partial p_i}\ddot{\mathbf{q}} + \frac{\partial\mathbf{D}}{\partial p_i}\dot{\mathbf{q}} + \frac{\partial\mathbf{K}}{\partial p_i}\mathbf{q} - \frac{\partial\mathbf{f}}{\partial p_i}\right)\,dt\right]\delta p_i \\
&\equiv \sum_{i=1}^{N}(\nabla\mathcal{L})_i\,\delta p_i
\end{aligned} \tag{E.4.18}$$

The response of the system – $\ddot{\mathbf{q}}, \dot{\mathbf{q}}, \mathbf{q}$ – was previously obtained. Thus to calculate the gradient, it is only necessary to perform the pertinent matrix multiplications and *integration over the domain* T.

To summarize

$$(\nabla\mathcal{L})_i = \left[\boldsymbol{\alpha}^T\frac{\partial\boldsymbol{\varphi}}{\partial p_i} + \int_T \boldsymbol{\lambda}^T\left(\frac{\partial\mathbf{M}}{\partial p_i}\ddot{\mathbf{q}} + \frac{\partial\mathbf{D}}{\partial p_i}\dot{\mathbf{q}} + \frac{\partial\mathbf{K}}{\partial p_i}\mathbf{q} - \frac{\partial\mathbf{f}}{\partial p_i}\right)\,dt\right] = (\nabla J)_i \tag{E.4.19}$$

where $\boldsymbol{\lambda}$ is obtained from eq.(E.4.5) and one or all of the problems E.4.14, E.4.15 and E.4.16.

The derivatives of $\mathbf{M}, \mathbf{D}$ and $\mathbf{K}$ are obtained as described in the Section E.6.

E.5 Derivatives of the Constitutive Equations

In this section, a example of how to obtain the derivatives of the finite element model is shown.

We start by taking the derivatives of the constitutive matrices.

$$A_{11} = \frac{E_1 h}{1 - \nu_{12}\nu_{21}}, \quad A_{22} = \frac{E_2 h}{1 - \nu_{12}\nu_{21}}, \quad A_{12} = A_{21} = \nu_{12} A_{22} \tag{E.5.1}$$

$$D_{11} = A_{11}\frac{h^2}{12}, \quad D_{22} = A_{22}\frac{h^2}{12}, \quad D_{12} = D_{21} = A_{12}\frac{h^2}{12} \tag{E.5.2}$$

$$A_{66} = G_{12}h, \quad A_{55} = G_{13}h, \quad A_{44} = G_{23}h, \quad D_{66} = A_{66}\frac{h^2}{12} \tag{E.5.3}$$

$$D = \begin{pmatrix} D_{11} & D_{12} & 0 \\ D_{12} & D_{22} & 0 \\ 0 & 0 & D_{66} \end{pmatrix} \quad A = \begin{pmatrix} A_{11} & A_{12} & 0 \\ A_{12} & A_{22} & 0 \\ 0 & 0 & A_{66} \end{pmatrix} \tag{E.5.4}$$

$$\frac{\partial}{\partial p_i} D = \begin{pmatrix} \frac{\partial D_{11}}{\partial p_i} & \frac{\partial D_{12}}{\partial p_i} & 0 \\ \frac{\partial D_{12}}{\partial p_i} & \frac{\partial D_{22}}{\partial p_i} & 0 \\ 0 & 0 & \frac{\partial D_{66}}{\partial p_i} \end{pmatrix} \quad \frac{\partial}{\partial p_i} A = \begin{pmatrix} \frac{\partial A_{11}}{\partial p_i} & \frac{\partial A_{12}}{\partial p_i} & 0 \\ \frac{\partial A_{12}}{\partial p_i} & \frac{\partial A_{22}}{\partial p_i} & 0 \\ 0 & 0 & \frac{\partial A_{66}}{\partial p_i} \end{pmatrix} \tag{E.5.5}$$

Given the following properties for an isotropic plate:

- $E_0 = E_{1,0} = E_{2,0} = E_{3,0} = 69\,GPa$
- $\nu = \nu_{12} = \nu_{21} = 0.33$
- $G = G_{12} = G_{23} = G_{13} = \dfrac{E}{2(1+\nu)}$
- $\rho = 2725\,kg/m^3$
- $L_x = 2.25\,m,\ L_y = 1.6\,m, h = 5\,mm$

The derivative of an entry of D with respect to some parameter p_i is

$$\frac{\partial D_{11}}{\partial p_i} = \frac{\partial}{\partial p_i}\left(\frac{Eh^3}{1 - \nu_{12}\nu_{21}}\right)$$

If $p_i = E$, then

$$\left.\frac{\partial D_{11}}{\partial p_i}\right|_{E=69\,GPa} = \left.\frac{h^3}{1-\nu_{12}\nu_{21}}\right|_{E=69\,GPa} = 1.168967194104665 \times 10^{-8}$$

If $p_i = h$, then

$$\left.\frac{\partial D_{11}}{\partial p_i}\right|_{h=0.005\,m} = \left.\frac{3Eh^2}{1-\nu_{12}\nu_{21}}\right|_{h=0.005\,m} = 4.839524183593312 \times 10^{5}$$

From isotropy considerations, the derivatives of D with respect to E and h are:

$$\left.\frac{\partial D}{\partial E}\right|_{E=69\,GPa} = \begin{pmatrix} 0.116897 \times 10^{-7} & 0.038576 \times 10^{-7} & 0 \\ 0.038576 \times 10^{-7} & 0.116897 \times 10^{-7} & 0 \\ 0 & 0 & 0.039160 \times 10^{-7} \end{pmatrix}$$

$$\left.\frac{\partial D}{\partial h}\right|_{h=0.005\,m} = \begin{pmatrix} 4.83952 \times 10^{5} & 1.59704 \times 10^{5} & 0 \\ 1.59704 \times 10^{5} & 4.83952 \times 10^{5} & 0 \\ 0 & 0 & 1.62124 \times 10^{5} \end{pmatrix}$$

For an anisotropic material, consider the derivative with respect to E_1 at $E_1 = 69\,GPa$:

$$\left.\frac{\partial D}{\partial E_1}\right|_{E=69\,GPa} = \begin{pmatrix} 0.116897 \times 10^{-7} & 0 & 0 \\ 0 & 0 & 0 \\ 0 & 0 & 0 \end{pmatrix}$$

And the derivative with respect to h at $h = 0.005\,m$ is unchanged:

$$\left.\frac{\partial D}{\partial h}\right|_{h=0.005\,m} = \begin{pmatrix} 4.83952 \times 10^{5} & 1.59704 \times 10^{5} & 0 \\ 1.59704 \times 10^{5} & 4.83952 \times 10^{5} & 0 \\ 0 & 0 & 1.62124 \times 10^{5} \end{pmatrix}$$

Notice the great disparity in orders of magnitude between both cases.

Consider now that the parameter p_i is a deviation α_i from a reference value P_i^* for a given property P_i:

$$P_i = P_i^*(1 + \alpha_i) \tag{E.5.6}$$

Therefore

$$\frac{\partial D_{11}}{\partial \alpha_i} = \frac{\partial}{\partial P_i}\left(\frac{Eh^3}{1 - \nu_{12}\nu_{21}}\right)\frac{\partial P_i}{\partial \alpha_i} \tag{E.5.7}$$

To calculate these same derivatives, let $P_i = E$, with $E_i^* = 69\,GPa$, then

$$\left.\frac{\partial D_{11}}{\partial \alpha_i}\right|_{\alpha=0} = \frac{h^3}{1 - \nu_{12}\nu_{21}}E_i^* = 1.16896 \times 10^{-8} \times 69 \times 10^9 = 8.06587 \times 10^2$$

and $P_i = h$, with $h_i^* = 0.005\,m$, then

$$\left.\frac{\partial D_{11}}{\partial \alpha_i}\right|_{\alpha=0} = \frac{3E[h_i(\alpha_i)]^2}{1 - \nu_{12}\nu_{21}}h_i^* = 4.83952 \times 10^5 \times 0.005 = 2.41976 \times 10^3$$

Where $h_i(\alpha_i) = h_i^*(1 + \alpha_i)$.

And from isotropy considerations, we have:

$$\left.\frac{\partial D}{\partial \alpha_E}\right|_{\alpha=0} = \begin{pmatrix} 8.06587 \times 10^2 & 2.66174 \times 10^2 & 0 \\ 2.66174 \times 10^2 & 8.06587 \times 10^2 & 0 \\ 0 & 0 & 2.70207 \times 10^2 \end{pmatrix}$$

$$\left.\frac{\partial D}{\partial \alpha_h}\right|_{\alpha=0} = \begin{pmatrix} 2.41976 \times 10^3 & 0.79852 \times 10^3 & 0 \\ 0.79852 \times 10^3 & 2.41976 \times 10^3 & 0 \\ 0 & 0 & 0.81062 \times 10^3 \end{pmatrix}$$

For an anisotropic material, the extension is direct.

These derivatives were obtained using complex step differentiation [72] using a forward difference scheme, eq.(E.5.8). The truncation error is of order $\mathcal{O}(h^2)$, h being the step-size.

$$\left.\frac{\partial f}{\partial x}\right|_{\mathcal{X}} = \mathbb{I}\mathrm{m}\left[\frac{f(\mathcal{X} + ih)}{h}\right] + \mathcal{O}(h^2) \tag{E.5.8}$$

There is good agreement with analytic results up to machine precision when an appropriate step-size is used. General aspects of this technique's implementation can be found in the work by LAI e CRASSIDIS [72].

E.6 Derivatives of the FE Matrices

Consider the Finite Element Model (here repeated for convenience)

$$\begin{pmatrix} \boldsymbol{M}_{\mathrm{vv}} & \mathbf{0} \\ \mathbf{0} & \boldsymbol{M}_{\mathrm{ss}} \end{pmatrix} \begin{pmatrix} \ddot{\mathbf{v}} \\ \ddot{\mathbf{s}} \end{pmatrix} + \begin{pmatrix} \boldsymbol{K}_{\mathrm{vv}} & \boldsymbol{K}_{\mathrm{vs}} \\ \boldsymbol{K}_{\mathrm{vs}}^T & \boldsymbol{K}_{\mathrm{ss}} \end{pmatrix} \begin{pmatrix} \mathbf{v} \\ \mathbf{s} \end{pmatrix} = \begin{pmatrix} \boldsymbol{F}_{\mathrm{v}} \\ \boldsymbol{F}_{\mathrm{s}} \end{pmatrix} \tag{E.6.1}$$

where the mass matrix $\mathbf{M}^e$ and stiffness matrix $\mathbf{K}^e$ are obtained from

$$\mathbf{M_{vv}} = \int_{\Omega^e} {\mathbf{N_v}}^T I_0 \mathbf{N_v} d\Omega^e, \quad \mathbf{M_{ss}} = \int_{\Omega^e} {\mathbf{N_s}}^T I_2 \mathbf{N_s} d\Omega^e \tag{E.6.2}$$

$$\mathbf{K_{vv,1}} = \int_{\Omega^e} {\mathbf{B_v}}^T \mathbf{A} \mathbf{B_v} d\Omega^e, \quad \mathbf{K_{vv,2}} = \int_{\Omega^e} {\mathbf{N_v}}^T k \mathbf{N_v} d\Omega^e \tag{E.6.3}$$

$$\mathbf{K_{ss,1}} = \int_{\Omega^e} {\mathbf{N_s}}^T \mathbf{A} \mathbf{N_s} d\Omega^e, \quad \mathbf{K_{ss,2}} = \int_{\Omega^e} {\mathbf{B_s}}^T \mathbf{D} \mathbf{B_s} d\Omega^e \tag{E.6.4}$$

$$\mathbf{K_{vv}} = \sum_i \mathbf{K_{vv,i}}, \quad \mathbf{K_{ss}} = \sum_j \mathbf{K_{ss,j}}, \quad \mathbf{K_{vs}} = \int_{\Omega^e} {\mathbf{B_v}}^T \mathbf{A} \mathbf{N_s} d\Omega^e \tag{E.6.5}$$

Differentiation of matrices is done term by term, for example consider the element stiffness matrix:

$$\boldsymbol{K}^e = \begin{pmatrix} \boldsymbol{K}_{\mathrm{vv}} & \boldsymbol{K}_{\mathrm{vs}} \\ \boldsymbol{K}_{\mathrm{vs}}^T & \boldsymbol{K}_{\mathrm{ss}} \end{pmatrix} \rightarrow \frac{\partial \boldsymbol{K}^e}{\partial p_i} = \begin{pmatrix} \dfrac{\partial \boldsymbol{K}_{\mathrm{vv}}}{\partial p_i} & \dfrac{\partial \boldsymbol{K}_{\mathrm{vs}}}{\partial p_i} \\ \left(\dfrac{\partial \boldsymbol{K}_{\mathrm{vs}}}{\partial p_i} \right)^T & \dfrac{\partial \boldsymbol{K}_{\mathrm{ss}}}{\partial p_i} \end{pmatrix}$$

Further consider the derivative of $\mathbf{K_{vv,1}}$

$$\mathbf{K_{vv,1}} = \int_{\Omega^e} {\mathbf{B_v}}^T \mathbf{A} \mathbf{B_v} d\Omega^e \rightarrow \frac{\partial \mathbf{K_{vv,1}}}{\partial p_i} = \frac{\partial}{\partial p_i} \int_{\Omega^e} {\mathbf{B_v}}^T \mathbf{A} \mathbf{B_v} d\Omega^e$$

Since the interpolation functions do not dependent on the parameters, one obtains

$$\begin{aligned} \frac{\partial}{\partial p_i} \int_{\Omega^e} {\mathbf{B_v}}^T \mathbf{A} \mathbf{B_v} d\Omega^e &= \int_{\Omega^e} \frac{\partial}{\partial p_i} \left({\mathbf{B_v}}^T \mathbf{A} \mathbf{B_v} \right) d\Omega^e \\ &= \int_{\Omega^e} \frac{\partial {\mathbf{B_v}}^T}{\partial p_i} \mathbf{A} \mathbf{B_v} + {\mathbf{B_v}}^T \frac{\partial \mathbf{A}}{\partial p_i} \mathbf{B_v} + {\mathbf{B_v}}^T \mathbf{A} \frac{\partial \mathbf{B_v}}{\partial p_i} d\Omega^e \\ &= \int_{\Omega^e} {\mathbf{B_v}}^T \frac{\partial \mathbf{A}}{\partial p_i} \mathbf{B_v} d\Omega^e \end{aligned}$$

Repeating this procedure to all elemental matrices leads to:

$$\frac{\partial \mathbf{K_{vv,1}}}{\partial p_i} = \int_{\Omega^e} \mathbf{B_v}^T \frac{\partial \mathbf{A}}{\partial p_i} \mathbf{B_v} d\Omega^e, \quad \frac{\partial \mathbf{K_{vv,2}}}{\partial p_i} = \int_{\Omega^e} \mathbf{N_v}^T \frac{\partial k}{\partial p_i} \mathbf{N_v} d\Omega^e \tag{E.6.6}$$

$$\frac{\partial \mathbf{K_{ss,1}}}{\partial p_i} = \int_{\Omega^e} \mathbf{N_s}^T \frac{\partial \mathbf{A}}{\partial p_i} \mathbf{N_s} d\Omega^e, \quad \frac{\partial \mathbf{K_{ss,2}}}{\partial p_i} = \int_{\Omega^e} \mathbf{B_s}^T \frac{\partial \mathbf{D}}{\partial p_i} \mathbf{B_s} d\Omega^e \tag{E.6.7}$$

$$\frac{\partial \mathbf{K_{vv}}}{\partial p_i} = \sum_k \frac{\partial \mathbf{K_{vv,k}}}{\partial p_i}, \quad \frac{\partial \mathbf{K_{ss}}}{\partial p_i} = \sum_j \frac{\partial \mathbf{K_{ss,j}}}{\partial p_i}, \quad \frac{\partial \mathbf{K_{vs}}}{\partial p_i} = \int_{\Omega^e} \mathbf{B_v}^T \frac{\partial \mathbf{A}}{\partial p_i} \mathbf{N_s} d\Omega^e \tag{E.6.8}$$

$$\frac{\partial \mathbf{M_{vv}}}{\partial p_i} = \int_{\Omega^e} \mathbf{N_v}^T \frac{\partial I_0}{\partial p_i} \mathbf{N_v} d\Omega^e, \quad \frac{\partial \mathbf{M_{ss}}}{\partial p_i} = \int_{\Omega^e} \mathbf{N_s}^T \frac{\partial I_2}{\partial p_i} \mathbf{N_s} d\Omega^e \tag{E.6.9}$$

The derivatives of the global matrices $\mathbf{K}$ and $\mathbf{M}$ are the result of the assembly of the derivatives of the elemental matrices, followed by the pertinent transformations (application of boundary conditions and model reduction with transformation matrix $\mathbb{T}$ given by the **original system transformation matrix**). Let $\mathbf{A}$ be a matrix standing for either $\mathbf{K}$, $\mathbf{D}$ or $\mathbf{M}$. Then:

$$[\mathbf{A}^e] \xrightarrow[\text{elements}]{\text{Assemble}} [\mathbf{A}_G] \xrightarrow[\text{Boundary Conditions}]{\text{Apply}} [\mathbf{A}] \xrightarrow[\mathbb{T}=\text{f}(\mathbf{M},\mathbf{K})]{\text{Model Reduction}} [\bar{\mathbf{A}}] = \mathbb{T}^T \mathbf{A} \mathbb{T}$$

Therefore

$$\left[\frac{\partial \mathbf{A}^e}{\partial p_i}\right] \xrightarrow[\textbf{correct} \text{ elements}]{\text{Assemble}} \left[\frac{\partial \mathbf{A}_G}{\partial p_i}\right] \xrightarrow[\text{Conditions}]{\text{Boundary}} \left[\frac{\partial \mathbf{A}}{\partial p_i}\right] \xrightarrow[\text{Reduction}]{\text{Model}} \left[\frac{\partial \bar{\mathbf{A}}}{\partial p_i}\right] \approx \mathbb{T}^T \frac{\partial \mathbf{A}}{\partial p_i} \mathbb{T}$$

Here, an approximation was considered in regards to the reduced model obtained from IRS. When considering the inversion with the use of a complete or reduced model, no substantial difference between models was noted, other than the amount of computational time. Therefore, for this case, this approximation seems acceptable.

Regardless of this, it should be noted that, if the parameters are somehow related to a spatial distribution of properties, the derivatives of the FE global matrices usually require assembly over a much smaller number of elements than the original matrices. In the case of this thesis, each element is associate with a parameter α_i, thus leading to derivatives of global matrices with all zero entries except for the entries associated with the derivatives of such elements.

Since, in this case, $\mathbf{D} = a\mathbf{K} + b\mathbf{M}$, it follows directly that:

$$\frac{\partial \mathbf{D}}{\partial p_i} = a\frac{\partial \mathbf{K}}{\partial p_i} + b\frac{\partial \mathbf{M}}{\partial p_i} \tag{E.6.10}$$

The dynamics of the system studied in this thesis is linear, given that the applied forces do not depend on the current configuration, they do not depend, therefore, on the parameters p_i. Generally speaking

$$\mathbf{f}(t, \mathbf{p}) = \mathbf{f}(t) \rightarrow \frac{\partial \mathbf{f}}{\partial p_i} = 0 \tag{E.6.11}$$

The field estimated is that of the Young Modulus E, defined element-wise. For the isotropic case, **isotropy is enforced** by setting G_e of an element e as:

$$G_e = \frac{E_e}{2(1+\nu)} \tag{E.6.12}$$